Investigation and Optimisation of a Discrete Fluid Power PTO-system for Wave Energy Converters

Hansen, Anders Hedegaard

Publication date:
2014

Document Version
Publisher's PDF, also known as Version of record

DEPARTMENT OF ENERGY TECHNOLOGY
AALBORG UNIVERSITY

Investigation and Optimisation of a Discrete Fluid Power PTO-system for Wave Energy Converters

by
Anders Hedegaard Hansen

June, 2014

Submitted to the Faculty of Engineering & Science at Aalborg University for the degree of Doctor of Phiosophy in Energy Technology

Investigation and Optimisation of a Discrete Fluid Power PTO-system for Wave Energy Converters

AALORG UNIVERSITY
Institute of Energy Technology
Ponstoppidanstraede 101 DK-9220 Aalborg East
Denmark
http://www.et.aau.dk

Printed in Denmark by Uniprint, 2014

ISBN 978-87-92846-44-0

PUBLIC DEFENCE OF PHD DISSERTATION

Thesis Title:
Investigation and Optimisation of a Discrete Fluid Power PTO-System for Wave Energy Converters

Ph.D. Defendant:
Anders Hedegaard Hansen

Supervisor:
Associate Professor Henrik C. Pedersen

Moderator:
Associate Professor Michael Møller Bech

Assessment Committee:
Associate Professor Søren Juhl Andreasen (chairman)
Department of Energy Technology
Aalborg University
Pontoppidanstræde 101
9220 Aalborg East, Denmark

Professor Takao Nishiumi
Department of Mechanical Systems Engineering
National Defense Academy of Japan
1-10-20 Hashirimizu
Yokosuka
Kanagawa, 239-8686, Japan

Dr.Ing. Matthias Liermann
American University of Beirut
Faculty of Engineering and Architecture
P.O. Box 11-0236
Riad El Solh
Beirut 1107-2020, Lebanon

Defence Date and Place:
Monday, June 16, 2014
Pontoppidanstræde 101, Room 23, Aalborg University

COPYRIGHT STATEMENTS

Preface

This dissertation has been submitted to the Faculty of Engineering and Science at Aalborg University in partial fulfilment of the requirements for the Ph.D. degree in Energy Technology. The work has been carried out at the Department of Energy Technology at Aalborg University. The work has been funded via the ForskEL research project No. 2011-1-10705 through the PSO resources administrated by Energynet.dk. The research project has been carried out in corporation with Wave Star A/S.

This project is based on the Wavestar wave energy converter, why I thanks Wave Star A/S for the good corporation, sharing of data and knowledge. A special thanks go to Ph.D. Rico Hjerm Hansen, Wave Star A/S for the productive and enlightening discussions and the helpfulness in modelling of the Wavestar.

Special thanks go to my supervisor, Asc. Prof. Henrik C. Pedersen, for an enthusiastic and thorough involvement in the project; and for his support in creating a comfortable research environment. Likewise, I would like to place a thanks to Prof. Torben O. Andersen and Asc. Prof. Michael M. Bech for aid in an enthusiastic and pleasant work environment.

I would also like to thank Prof. Dr. Rudolf Schiedl for the invitation to spend four inspiring months at Johannes Kepler University and the enthusiastic involvement in my project. Likewise I like to show my gratitude to Dr. Winkler and DI. Plöckinger from LCM for the relevant and enlightening discussion on my work. Lastly I thank the staff at Institute of Machine Design and Hydraulic Drives at Johannes Kepler University and LCM (Hydraulische Antriebssysteme) for the delightful hours on and off work.

Further, thanks to my office mates Rico, Søren, Lasse, Per and Daniel for the enthusiastic, fun and educational discussions emerging at the office from the pronounced hunger for knowledge.

Finally, my deep felt gratitude goes to Malene and my family for supporting me in my work and demonstrating the art of patience when the Ph.D. project conquered time.

Aalborg, January 2014
Anders Hedegaard Hansen

Contents

Abstract

Patents on ocean wave energy dates back to 1799, however no wave energy converter (WEC) concept has a commercialised device. The cost of energy produced with wave energy converters is very high compared to traditional energy sources. Even when compared to energy from wind turbines wave energy needs cost reductions. Hence, next to political will, the main obstacle for a commercial break through of wave energy technology is the high cost of energy. Initiatives to lower costs are made in areas of minimising structural costs and increasing the energy production per device.

Wave Star A/S has recently focused research on improving the power take off (PTO) system converting the mechanical motion of the floats into electricity. This has brought attention to discrete fluid power (DFP) technology, especially secondary controlled common pressure rail systems. A novel discrete PTO-system has been proposed and found feasible for the Wavestar WEC. However, with a technology shift from a continuous to a discrete fluid power PTO-system new challenges emerge.

The current project investigates and optimises the novel discrete fluid power PTO-system proposed for the Wavestar WEC. Initiating from an investigation of energy extraction by WECs utilising a discrete PTO force, an investigation of the system configuration is conducted. Hence, the configuration of the multi-chamber cylinder and the common pressure rails are investigated for the discrete fluid power force system. A method for choosing the system configuration for a given wave climate is demonstrated. From the energy extraction by WECs employing a discrete PTO force it is seen that a discrete system with relative few applicable forces may yield energy extraction levels close to that of a continuous PTO force system. The system configuration investigation shows how the wave climate naturally influences the optimal system configuration yielding maximal energy output, and how one may choose the system configuration based on the installation site.

The switching manifold is the control element of the secondary controlled force system. The force is controlled by connecting each of the cylinder chambers to one of the common pressure lines. Bidirectional check valves are proposed as a possible improvement of the energy conversion efficiency, since these enable passive valve shifts at a favourable low pressure difference across the switching valves. A model based feasibility study shows promising energy results for the bidirectional check valves, however, a minor increase in the force steps applied may be induced.

Due to the lack of cheap and commercial large fast on/off valves and especially bidirectional check valves, the current project further includes a conceptual design of a multi-poppet on/off valve and a multi-poppet bidirectional check valve. The conceptual design is based on a theoretical investigation of valve switching time dependency on various design parameters. Finally a set of parameters are given based on dynamical simulations of the designed valves. The valves are designed with a rated flow of 1000 L/min@5bar and the active switching time for the designed valves is seen to be less than 10 ms. A combination of on/off and bidirectional check valve are proposed for the switching manifold when designed for use in wave energy converters.

Involvement in designing, installation and control of a full scale PTO test-bench has been under-taken parallel to the theoretical work. Preliminary force switching tests have been conducted to investigate the influence of valve switching time on the dynamic behaviour of the PTO-system. The results of these tests show that the pressure dynamic in the cylinder chambers and the transmission lines connecting the switching manifold and the cylinder chambers are highly influenced by the valve switching time.

Resumé

Forskning i bølgeenergi teknologi kan føres tilbage til 1799 hvor Girard & Son var de først til at udnytte havbølger til energigenerering. Selv med Girard & Sons tidlige start og de mere end 340 britiske patenter i årene 1855 til 1973 er bølgeenergi langt fra et kommercielt gennembrud. Det manglende gennembrud for bølgeenergi skyldes til dels de meget høje omkostninger knyttet til energi produktion med bølgeenergimaskiner. De høje omkostninger skyldes i høj grad at bølgeenergimaskiner skal designes til de barske vejrforhold og medfølgende belastninger der kendetegner off shore konstruktioner.

Wave Star A/S forsøger at forbedre rentabiliteten af bølge energi ved at øge mængden af energi produceret pr. maskine, sideløbende med at sænke størrelse og pris af den strukturelle del af maskinen. Målsætningen om at øge energi produktionen har medført en teknologi opgradering fra det nuværende kontinuerte hydrauliske power take off (PTO) system til et diskret hydraulisk PTO-system. Dette teknologi skifte ventes at medføre en signifikant forbedring af maskines energi konverterings effektivitet. Formålet med forskningen præsenteret i denne afhandling er at understøtte udviklingen og implementeringen af et diskret hydraulisk PTO-system i Wavestar bølge energi maskinen.

Med udgangs punkt i en simpel model af en point absorber bølgeenergimaskine undersøges antallet af diskrete kraft niveauers indflydelse på den potentielle energiproduktion. For at muligøre en analytisk undersøgelse benyttes regulære bølger som input til modellen. Det vises at et diskret PTO-system med relativt få kraftniveauer potentiellet kan producere næsten tilsvarende mængder energier som et PTO-system med kontinuerlig kraftstyring. Denne analytiske fremgangs metode er dog kun valid under regulære bølgeforhold, hvorfor tidssimuleringer benyttes til at analysere diskrete PTO-systems energiproduktions potentiale under irregulære bølgeforhold. En generisk model af det diskrete hydrauliske PTO-system benyttes til at undersøge hvorledes konfigurationen af den hydrauliske flerkammercylinder og de fælles tryklinerne påvirker energiproduktionen og energikonverteringseffektiviteten. Der gives desuden en metode til udvælgelse af system konfiguration der tager højde for bølge klimaet på en given installationsplacering.

Kraftstyringen udføres med ventilmanifolden, der forbinder de forskellige tryk liner med hvert cylinderkammer alt efter den ønskede kraft. Således ændres kraften ved at ventilerne ændre forbindelsen mellem et given cylinderkammer og tilsvarende trykliner. Ved hvert tryk skifte i et cylinderkammer forekommer et kompressionstab, hvilket er afhængig af trykændringens og kammervoluminets størrelse. En model baseret undersøgelse af mulighed for at benyttet bidirektionelle kontra ventiler i ventilmanifolden foretages da dette ses som en mulighed for at nedsætte kompressionstabet.

Projektet indeholder endvidere konceptuelle designs af en multi-poppet on/off ventil og en multi-poppet bidirektional kontra ventil. Design parametrenes indflydelse på ventil skifte tiderne anskueliggøres gennem en teoretisk undersøgelse. Det konceptuelle ventil design valideres med simuleringsresultater der viser ventilskiftetider under 10 ms for ventiler med et nominelt flow på 1000 L/min@5bar. Med de designede ventiler som baggrund beskrives en mulig ventilmanifoldskonfiguration hvor on/off og bidirektionelle kontra ventiler kombineres.

Sideløbende med de teoretiske undersøgelser er der taget del i design og installering af en fuld størrelse PTO-system testopstilling. Hvilket bevirker at indledende test resultater kan indgår i den afhandling. Under kraftskift med det diskrete PTO-system er ventilskiftetidens betydning for tryk og system dynamikken fundet signifikant.

List of Publications

List of published and submitted papers:

[A] Optimal Discrete PTO Force for Point Absorber Wave Energy Converters in Regular Waves. Hansen, Anders Hedegaard; Pedersen, Henrik C. *In Proceedings of the 10th European Wave and Tidal Energy Conference. 2013*

[B] Optimal Number of Pressure Lines in a Discrete Hydraulic Force System for the PTO-system in Wave Energy Converters. Hansen, Anders Hedegaard; Hansen, Rico Hjerm; Pedersen, Henrik C. *In Proceedings of the 7th FPNI PhD symposium on Fluid Power. 2012*

[C] Optimisation of Working Areas in Discrete Hydraulic Power Take Off-system for Wave Energy Converters. Hansen, Anders Hedegaard; Hansen, Rico Hjerm; Pedersen, Henrik C. *In Proceedings of the fifth Workshop on Digital Fluid Power. 2012*

[D] Optimal Configuration of Discrete Fluid Power System Utilised in the PTO for WECs. Anders Hedegaard Hansen; Henrik C. Pedersen. *Submitted to Ocean Engineering - An International Journal of Research and Development*

[E] Model Based Feasibility Study on Bidirectional Check Valves in WECs. Anders H Hansen; Henrik C Pedersen; Torben O Andersen. *In International Journal of Marine Energy (2014), pp. 1-23 DOI information: 10.1016/j.ijome.2014.03.001*

[F] Design of Bidirectional Check Valve for Discrete Fluid Power Force System for Wave Energy Converters. Hansen, Anders Hedegaard; Pedersen, Henrik C.; Andersen, Torben Ole. *In Proceedings of Symposium on Fluid Power & Motion Control, ASME/BATH 2013. 2013*

[G] Design of a Multi-Poppet On-Off Valve for Wave Energy Converters. Hansen, Anders Hedegaard; Pedersen, Henrik C.; Andersen, Torben Ole. *In Proceedings of 2013 IEEE International Conference on Mechatronics and Automation. 2013*

[H] On/Off Multi-poppet Valve for Switching Manifold in Discrete Fluid Power Force System PTO in Wave Energy Converters. Hansen, Anders Hedegaard; Pedersen, Henrik C.; Andersen, Torben Ole. *In Int. J. Mechatronics and Automation, Vol. 4, No 2, 2014. Inderscience Enterprises Ltd.*

[I] Design and Control of Full Scale Wave Energy Simulator System. Pedersen, Henrik C.; Hansen, Anders Hedegaard; Hansen, Rico Hjerm; Andersen, Torben Ole; Bech, Michael Møller. *In Proceeding of Fluid power and Motion Control, FPMC2012. 2012*

* Influence and Utilisation of Pressure Propagation in Pipelines for Secondary Controlled Discrete Displacement Cylinders. Hansen, Rico Hjerm; Hansen, Anders Hedegaard; Andersen, Torben Ole. *Applied Mechanics and Materials, Vol. 233, 29.11.2012, s. 72-75.*

* Simulation of Utilisation of Pressure Propagation for Increased Efficiency of Secondary Controlled Discrete Displacement Cylinders. Hansen, Rico Hjerm; Hansen, Anders Hedegaard; Andersen, Torben Ole. *Applied Mechanics and Materials, Vol. 233, 29.11.2012, s. 3-6.*

This thesis has been submitted for assessment in partial fulfillment of the PhD degree. The thesis is based on the submitted or published scientific papers which are listed above. Parts of the papers are used directly or indirectly in the extended summary of the thesis. As part of the assessment, co-author statements have been made available to the assessment committee and are also available at the Faculty. The thesis is not in its present form acceptable for open publication but only in limited and closed circulation as copyright may not be ensured.

The papers marked with * are included in this dissertation for completeness, however, are not part of the appended papers included in partial fulfilment of the requirements for the Ph.D. degree in Energy Technology. The discussion of the topic in these papers serves as a basis for part of the work in the dissertation.

Abbreviation

BCV	Bidirectional check valves
DFP	Discrete fluid power
DFPF	Discrete fluid power force
DFCU	Digital flow control units
HP	High pressure line
LP	Low pressure line
PTO	Power take off
PWM	Pulse width modulation
SSI	Sea state I
SSII	Sea state II
SSIII	Sea state III
V_{PS}	Valve connected to supply pressure
V_{PT}	Valve connected to tank pressure
V_{CVPS}	Check valve connected to supply pressure
V_{CVPT}	check valve connected to tank pressure
WEC	Wave energy converter

Nomenclature

α		[]
β	Bulk modulus	[Pa]
β_{oil}	Bulk modulus of oil	[Pa]
β_{eff}	Effective bulk modulus	[Pa]
Δp_{Nom}	Nominal pressure drop	[Pa]
ΔV_{pilot}	Change in pilot volume	[cm^3]
ΔQ_{pilot}	Pilot volume flow	[L/min]
$\Delta Q_{\text{leakage}}$	Leakage volume flow	[L/min]
η	Free surface elevation/wave height	[m]
ε	leakage gap height	[m]
ε_{air}	Air content in oil at pressure p	[%]
$\varepsilon_{\text{air.0}}$	Content in oil at atmospheric pressure p_0	[%]
ε_{air}	Ratio of air content in oil	[%]
ϕ	Phase delay	[rad]
kappa	Adiabatic air constant	[-]
μ	Viscosity	[Ns/m^2]
ρ	Density	[kg/m^3]
θ_{arm}	Angular position of float arm	[rad]
ω_{arm}	Angular velocity of float arm	[rad]
ω_{w}	Wave frequency	[rad]
ω_{b}	Dampened float frequency	[rad]
τ_{PTO}	PTO torque	[kNm]
A	Area	[m^2]

A_{c}	piston area	[m^2]
A_{A}	Actuation area at port A	[m^2]
A_{B}	Actuation area at port B	[m^2]
A_{x}	pilot actuation area	[m^2]
A_i	Area of the i'th piston area	[m]
A_{w}	Wave amplitude	[m]
A_{d}	Orifice area	[mm^2]
$A_{\mathrm{d}}(\cdot)$	Orifice area function	[mm^2]
$A_{\mathrm{d,p}}$	Pilot valve orifice area	[mm^2]
a_{i}	Turn-on time for i'th box force	[s]
b_{i}	Turn-off time for i'th box force	[s]
b_{PTO}	Controller damping coefficient	[Ns/m]
b_{f}	Damping coefficient	[Ns/m]
C_{d}	Discharge coefficient	[-]
$C_{\mathrm{d,p}}$	Pilot valve discharge coefficient	[-]
d_{arm}	Moment arm	[m]
E_{har}	Harvested energy	[kJ]
E_{out}	Output energy	[kJ]
E_{sw}	Switching loss	[kJ]
F_{wave}	Wave force	[kN]
F_{ext}	Excitation force	[kN]
F_{rad}	Radiation force	[kN]
F_{Arch}	Archimedes force	[kN]
F_{Flow}	Flow force	[N]
F_{Friction}	Friction force	[N]
F_{PTO}	PTO force	[kN]
$F_{\mathrm{PTO.ref}}$	PTO force reference	[kN]
$F_{\mathrm{PTO.Cref}}$	Continuous PTO force reference	[kN]
$f_{\mathrm{PTO}}(t)$	Time function for PTO force	[kN]
$f_{\mathrm{PTO.T}}(t)$	Time function for PTO force i one wave period	[kN]
F_{g}	Gravitational force	[kN]
F_{i}	Force level for i'th box force	[kN]
$f_{\mathrm{i}}(t)$	Time function the i'th box force	[kN]
$\bar{F}_{\mathrm{vec}}$	Force combination vector	[kN]
F_{e}	Force error	[kN]
F_{b}	Force band	[kN]
F_{wave}	Wave force	[kN]
$H_{\mathrm{H,0}}$	Significant wave height	[m]
k	Integer for force choice	[-]
$k_{\mathrm{v},i}$	Valve coefficient	$[\frac{m^3}{s\sqrt{Pa}}]$
k_{f}	Spring coefficient	[N/m]
k_{spring}	Spring coefficient	[N/m]
k_{PTO}	Controller spring coefficient	[N/m]
L	Length	[m]
L_{d}	Damping length	[m]
m_{f}	Mass of float	[kg]

m_{pop}	Mass of poppet	[kg]
n	Number of poppets	[-]
n	Number of cylinder chambers	[-]
m	Number of common pressure line	[-]
P	Power	[kW]
P_{har}	Harvested power	[kW]
P_{out}	Output power	[kW]
$p_{\mathrm{c}.i}$	Pressure in i'th cylinder chamber	[bar]
$p_{\mathrm{l}.j}$	Pressure in j'th pressure line	[bar]
p_{S}	Supply pressure	[bar]
p_{T}	Tank pressure	[bar]
p_{A}	Pressure at Port A	[bar]
p_{B}	Pressure at Port B	[bar]
p_{x}	Pilot pressure	[bar]
p_{min}	Minimum system pressure	[bar]
p_{in}	Pressure at inlet	[Pa]
p_{out}	Pressure at outlet	[Pa]
p_{fric}	Pressure drop due to friction	[Pa]
S_+	Upper solution set	[]
S_-	Lower solution set	[]
S	Solution set	[]
T	Wave period	[s]
$\mathrm{T}_{0,2}$	Mean wave period	[s]
T_{sw}	Valve switching time	[s]
V_i	Volume of the i'th cylinder chamber	[m^2]
$V_{\mathrm{c}0}$	Dead volume of cylinder chamber	[m^2]
$V_{\mathrm{x}0}$	Dead volume of pilot chamber	[m^2]
$\bar{x}_{\mathrm{v},i,j}$	Nominal spool position	[-]
$\dot{x}_{\mathrm{v,ref}}$	Spool position reference	[m]
$\dot{x}_{\mathrm{v,max}}$	maximal spool velocity	[m/s]
x_{c}	Piston position	[m]
$x_{\mathrm{v,p}}$	Pilot valve spool position	[m]
x_{pop}	Poppet position	[m]
$x_{\mathrm{pop},0}$	Valve spring pre-compression	[m]
$Q_{i,j}$	Valve flow from j'th line to i'th chamber	[$\frac{m^3}{s}$]
$Q_{\mathrm{Nom}.i}$	Nominal valve flow	[m^3]
Q_{main}	Main stage flow	[m^3]
Q_{pilot}	Pilot stage flow	[m^3]
z_{f}	Float horizontal position	[m]
$\dot{z}_{\mathrm{f.w}}(t)$	Horizontal velocity float due to waves	[m/s]
$\dot{z}_{\mathrm{f.PTO}}(t)$	Horizontal velocity float due to PTO force	[m/s]
$\dot{z}_{\mathrm{f.PTO.T}}(t)$	Horizontal velocity float due to PTO force in one wave period	[m/s]
$u(t)$	Heaviside step function	[-]

Chapter 1

Introduction

The worlds increasing energy consumption, in parallel with an increasing awareness of humanity's environmental impact, have boosted research in the field of renewable energy. Especially with political tension on a global plan affecting oil and energy price, focus on renewable energy sources have been high. The wind energy industry has experienced a massive expansion in the last three decades and is the public forerunner in renewable energy in Denmark.

Conversion of surface ocean wave energy into a useful form is an old idea. Though the first patent by Girard and Son dates back to 1799, ocean wave energy still lacks a commercial breakthrough. More than 340 British patents in the years 1855 to 1973 indicates the diversity in proposed wave energy converter concepts [1]. Nowadays, still no wave energy converter technology has taken the lead, yet a couple of utility focusing concepts have bridged the proof-of-concept state and are developing in the pre-commercial phase e.g. Pelamis, Wavestar, Oyster. The most crucial research objective enabling a commercial breakthrough for wave energy converter companies is to lower the cost of energy (Euro/kWh).

For Wave Star A/S the research focus has in recent years been on improving the efficiency of the Power Take Off (PTO) system and thereby increasing the power production of each device. Wave Star A/s has with the Ph.D. project: *Design and Control of the Power Take-Off System for a Wave Energy Converter with Multiple Absorbers*, initiated a major technology enhancement in the PTO-system. The novel PTO-system is based on discrete fluid power technology utilising a secondary controlled fluid power system with common pressure lines throughout the machine.

The reader is through the remainder of the introduction familiarised with some of the leading wave energy concepts in terms of methods of energy extraction. Furthermore, an overview of some fluid power PTO-systems employed in wave energy converters are presented. A brief outline of digital fluid power systems and components are lastly established.

1.1 Wave Energy Converters

Wave Energy Converters (WECs) are devices designed to convert the energy in ocean waves into a useful form, nowadays typically electricity. As technology, wave energy still lacks a commercial breakthrough. Several WEC concepts have been, and are still being,

proposed, and lots have reached the proof-of-concept state showing the ability to extract energy from ocean waves. Yet only very few e.g. the Pelamis Wave Power is known to have a pre-commercial machine [2], which were deployed in a small Portuguese wave farm. The deployment though showed some issues to be bridged to succeed, e.g. storm survivability.

The important issue for WECs is to produce cheap energy while withstanding the extreme environment at sea. Hence, WECs must be robust against the harsh weather conditions and have a low total cost of energy.

Wave energy converter concepts are typically classified by the method used to extract energy of the waves. Throughout this section a brief presentation of some larger ongoing WEC projects is given. The presentation is organized by the classification: Over topping, Oscillation Water column, Attenuators and Point absorber.

1.1.1 Overtopping

Overtopping devices works by leading water into a reservoir as waves roll onto or into the device. From the reservoir water is led back to the ocean through a water turbine connected to a generator producing electricity. Hence, as the waves roll onto the machine potential energy is harvested and stored in a reservoir. Energy is then extracted as water flows back to the sea through the turbine. In Fig. 1.1 (a) a sketch of the overtopping technology is seen. The energy production may to some extent be controlled by controlling the turbine and the generator loading.

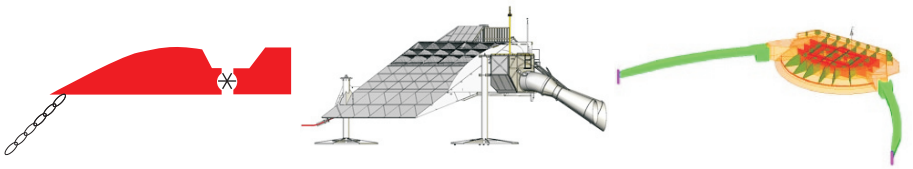

(a) (b) (c)

Figure 1.1: *(a) A sketch the overtopping technology. (b) sketch of wave plane[3] (c) drawing of wave dragon[4].*

The Wave Plane, by Wave Plane A/s and the Wave Dragon, by Wave Dragon Aps, in Fig. 1.1 (b) and (c) respectively, may be pointed out as two larger WEC projects base on the overtopping technology.

Wave Plane have since the project initiation in 1990 had several small scale test models, and a full scale prototype were deployed in 2008 at Roshage, Denmark. The mooring system, however, failed during a storm shortly after the deployment, before production results were gathered. A wave climate scaled model of the Wave dragon was deployed in Nissum Bredning in 2003. This featured six turbines and was tested continuously until 2005. In [5] some testing results for the Wave dragon test machine are given, a overall efficiency from wave to electrical power is seen up 20%, however mostly in the region

5-12%. Further the scaled sea tests indicates good coherence with basin tests.

1.1.2 Oscillating Water Column

Oscillating Water Column (OWC) devices works by using an entrapped water column to create a bidirectional air flow driving an air turbine powering an electrical generator. The air entrapment is realized either by natural rock formation or by a specially designed construction. The designed structure may be either bottom fixed or floating, see functional sketches in Fig. 1.2. These WECs excels in utilizing well known and tested technologies in the PTO-system, furthermore this type of machine is easily installed at the shoreline, and may be incorporated as a part of the coastal protection and breakwaters.

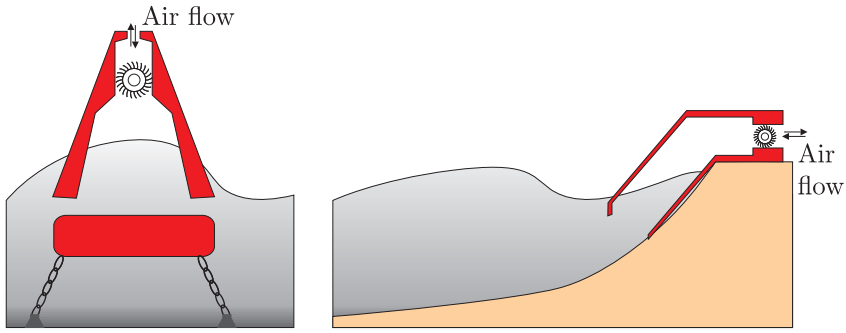

Figure 1.2: *Functional illustration of floating (a) and shore fixed (b) oscillating water column WECs.*

The Pico Power Plant project seen in Fig. 1.3 (a) and (b) is an OWC concept located at the shore of the Island Pico. Hence, the Pico device is a bottom fixed structure for which the OWC chamber is realised by the concrete structure along with the rocky coast line.

Figure 1.3: *Pictures of the OWC Pico power plant [6](a),(b) and the Mighty Whale (c)[1]*

Contrary to the Pico project the Mighty Whale, developed by the Japan Marine Science & Technology Center, seen in 1.3 (c), is a floating device utilising the OWC technology. The floating structure has three chambers in which water columns will raise and fall with the surrounding water. The floating structure is flexibly moored to the sea bed, hence, the buoyancy and frequency of this is crucial to the device. A 120 kW prototype has been operating at 40 m water dept 1.5 km off the coast at Nansei Town since 1998 [1]. [7] present some open sea test data from the Mighty Whale, the power output from the air chamber in various wave height are e.g. given. Furthermore the energy efficiency from wave to generated output is found to be in the range of 5-15% for significant wave heights of 0.6-1.6m.

1.1.3 Attenuators

Attenuator devices works with two or more floating bodies mechanically connected with a pivot joint. In addition actuators are mounted to allow damping of the movement around the pivot point. The concept is to extract energy in the damping actuators which apply an opposing force to the wave induced body movements, see Fig. 1.4. For the system to the left the actuator velocity times the actuator force gives the power extraction, hence, a linear actuator must be applied to extract energy of the change in x. Likewise for the system to the right, however this system occupies more actuators around each hinge. Here actuators are to extract energy around the first hinge from the linear change of y_1 and y_2.

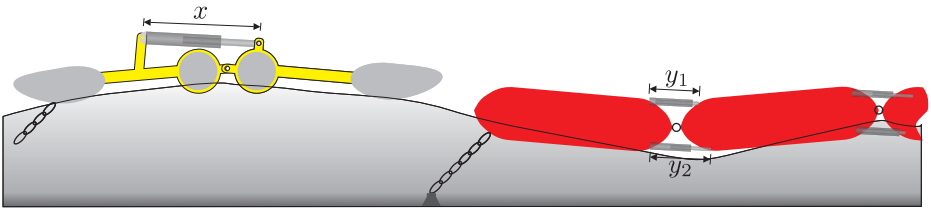

Figure 1.4: *Sketch of two attenuator type WECs, utilising linear force actuators in the PTO-system.*

The damping or PTO force applied by the actuators must be controlled to maximise the energy output. In small waves a low force is required since a force too large will yield very small movements resulting in low energy production in the damping actuators. The devices consist of at least two bodies as e.g. the Dexa WEC, in Fig. 1.5 (a). However, the device may also consist of multiple bodies composing a chain or snake-like form as the Pelamis WEC in Fig. 1.5 (b).

The Dexa project deployed a 1:5 scale model for sea testing at Roshage by the start of March 2011, however without PTO-system. In 2008 the Pelamis project deployed the first pre-commercial WECs in a small farm near the coast of Portugal. The Pelamis wave power is involved in several wave energy farms to come [9].

(a) (b)

Figure 1.5: *Dexa[8] and Pelamis[9] Wave Energy Coverters, left and right respectively.*

1.1.4 Point Absorber

Point absorber devices work by extracting energy from relative motion between two bodies, either two floating bodies or a floating body and a stationary body. The relative movement between the two bodies is what drives the PTO-system. The floating bodies are relative small compared to the wave length and the typical attenuator devices, thereby point absorber WECs excel in being unaffected by the direction of the incoming waves. In Fig. 1.6 three principal sketches are given for point absorber WECs. In Fig. 1.6 (a) a float (a1) moving relative to a bottom fixed structure (a3) is seen, energy extraction is realised with a linear actuator(a2). For this concept the PTO-system is place above sea level. A point absorber consisting of two floating bodies (b1) and (b3) is seen in Fig. 1.6 (b). The body (b1) is moored flexible to the sea bed via a line/chain. The PTO-system (b2) is feeding off the relative motion due to difference in buoyancy between the two bodies. In Fig. 1.6 (c) a buoy (c1) is connected flexible to a bottom fixed body (c3) through the PTO-system (c2). Hence, for this system the PTO-system is fully submerged.

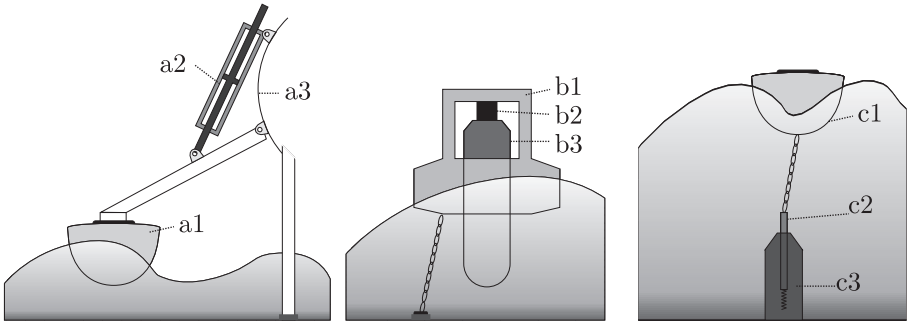

Figure 1.6: *Principal sketches of point absorber WECs.*

The Power Buoy, by Ocean Power Technologies(OPT) [10] and the Wavebob by Wavebob Ltd.[11] are both floating point absorbers, see Fig. 1.7 (a) and (b) respectively. Both are buoys consisting of two bodies, with one moored flexible to the seabed. The relative motion between the bodies is transformed to electricity by a fluid power PTO-system in

the Wavebob and a direct drive in the Power Buoy. The overall concept for Power Buoy and Wavebob is to place several buoys in an array/farm such the produced power can be joint and transported ashore in a single cable, similarly as for off shore wind farms. Several ocean tests have been conducted with the Power Buoy at the north Eastern coast of the US. The Wavebob has been sea tested since 2007 at the west coast of Ireland.

(a) (b) (c)

Figure 1.7: *Point Absorbers. Left to right: Power Buoy[10] , Wavebob[11] and Wave Star[12].*

The Wavestar, by Wave Star A/S[12] in Fig. 1.7 (c) is a multiple point absorber, hence, each device has several absorbers. The Wavestar differs from the former mentioned point absorbers by having a stationary platform, to which several floating bodies are mechanical attached. The Wavestar device utilises a fluid power PTO-system as well, to convert a linear movement to electricity. The Wavestar device carries a jacking system for storm protection, hence with a big storm coming in the device is taken out of production and jacks into safety riding out the storm. Wave Star A/S has been testing a 1:10 scale converter in Nissum Bredning since 2006 and a test section of the C5 device employing two floats have been operational at Roshage from September 2009 until August 2013, see Fig. 1.7 (c).

1.2 Fluid Power Power Take Off Systems

Fluid power PTO concepts have been proposed by several WEC concepts e.g. Dexa Wave, Wave Bob, Pelamis, Wavestar and many others [8, 9, 11, 12]. Two major advantages in utilising fluid power PTO-systems for WEC are the high force density and the controllability of fluid power systems. Hence, the ability to generate well controlled huge forces with relative small components. Fluid power PTO-systems are currently used in e.g. attenuators [8, 9], point absorber [10, 11, 12] and OCW WECs.

In [13] design, simulation and test of a discrete fluid power PTO-system for the Pelamis WEC are described. Here two differential cylinders are utilized to extract energy form a rotational movement around the pivot point between two floating bodies. An illustration of the fluid power system is given in Fig. 1.8.

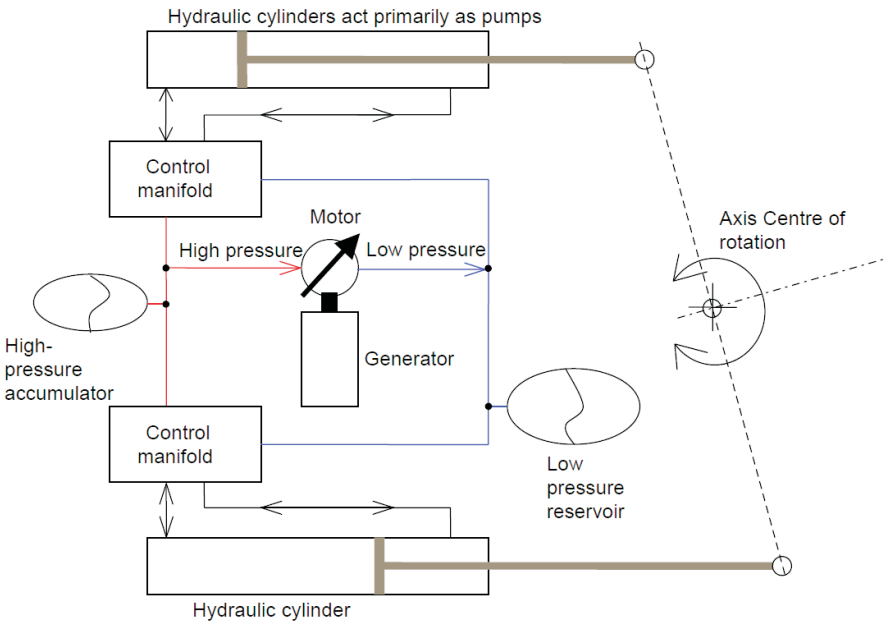

Figure 1.8: *Sketch of hydraulic Pelamis PTO-system[13]*

The two cylinders are connected to a low and high pressure line through a valve controlled manifold. Hence, each chamber can independently be connected to either low or high pressure, which with two identical cylinders with equal moment arms implies that eight different torques may be generated, to dampen the movement. The power harvested by each cylinder may be given as:

$$P = F\,v \tag{1.1}$$

Hence, the piston force times the piston velocity gives the harvested power, however, note that the velocity and force must be in opposite direction. The system works by connecting the various chambers to either the low or high pressure line to generate a damping torque as a torque is applied by the wave movement. With larger torques applied by the wave a larger damping torque is chosen. The cylinders and control manifolds this way extracts energy from the wave movement and convert it to potential energy stored in the high pressure line and accumulator. To extract energy from the high pressure line and converting it to electricity a hydrostatic motor driving an electrical generator is installed between the high and low pressure line. The pressure level in the high pressure line may somewhat be controlled by the motor.

In [14] a symmetric cylinder is directly connected to a floating body, with the stroke movement in the heaving direction of the floating body. Here the cylinder chambers are connected to either a high or low pressure accumulator through a rectifying valve system. For power extraction a hydrostatic motor is installed between the high and low

pressure accumulator, see Fig. 1.9 (a). Here the pressure levels in the accumulators are controlled by the motor. In [15] this type of fixed force controlled PTO-system is proposed for systems like the Wave Roller and the Oyster, see 1.9 (b). It is in [15] discussed how electricity may either be generated submerged locally at each device or generated centralised ashore by having common fluid low and high pressure lines for the system.

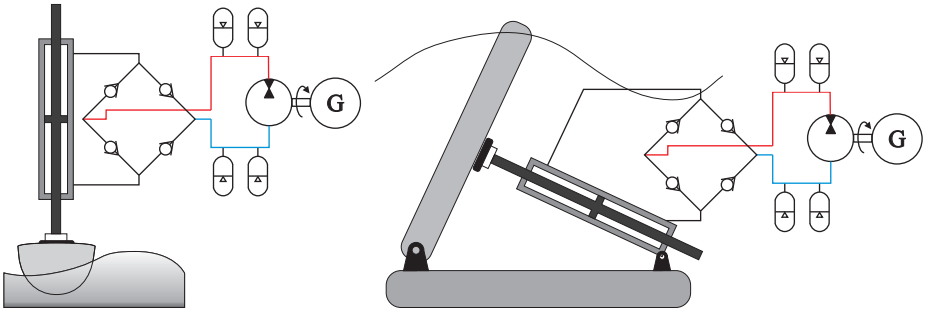

(a) (b)

Figure 1.9: *(a) Schematic of a fixed force level PTO-system for a heave buoy, (b) the Oyster/Wave Roller WEC concepts with fix force level PTO-system.*

The OWC system proposed in the patent [16], illustrated in Fig. 1.10, utilises common air lines for a multiple number of oscillating air columns. The oscillation chambers (1), (5) are connected through check valves to a low and high pressure line (4) and (3) respectively. The air lines are connected to the PTO (6) consisting of an air turbine.

This PTO-system works similar to the fluid power rectifier, where low pressure air is sucked into the air chamber when the water level is falling and air is pushed into the high pressure line as the water level is rising. This way a pressure difference is established between the high and low pressure lines. The pressure difference is propelling an air turbine driving an electrical generator.

In [17] the efficiency of a fluid power PTO-system consisting of a symmetric cylinder directly connected to a bidirectional variable axial piston motor/pump is investigated, a fluid power sketch is seen in Fig. 1.11 (a). The hydrostatic motor and the cylinder composes a closed circuit where the motor swash plate angle changes sign as the piston velocity changes sign. This implies the motor rotation is in same direction even when the flow direction varies. The direct connection between the cylinder and the hydrostatic pump/motor implies that the pressure in the cylinder is controlled with the load by the motor yielding great force controllability. In [17] the efficiency of this PTO-system is found to be low due to the huge variations in loading condition on the motor. This causes the motor to operate under non-optimal conditions with respect to efficiency. Hence, the system efficiency will never rise to a competitive level with the huge variations in the loading on the motor induced by the variation in power density in the waves.

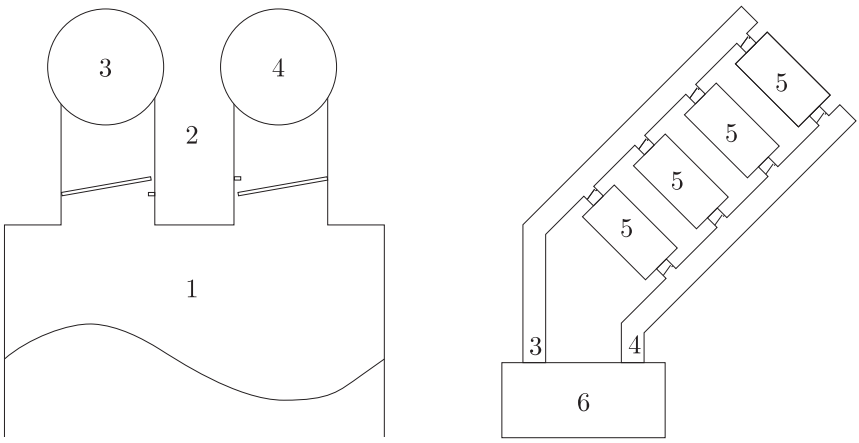

(a) (b)

Figure 1.10: *Illustration of the a common air pressure line oscillating water column WEC.*

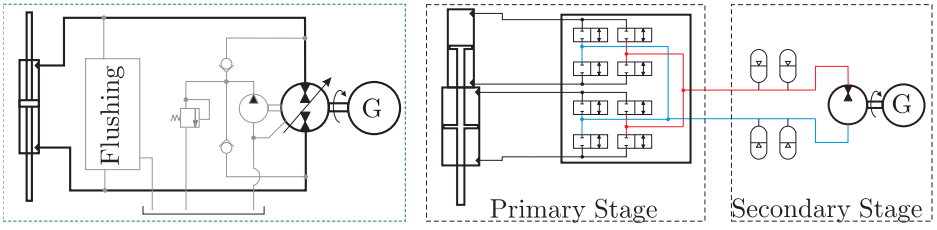

(a) (b)

Figure 1.11: *Sketch of a continuous (a) and a discrete (b) system design for the Wavestar PTO*

In [18] a novel PTO-system for point absorber WECs is presented. An illustration of this novel discrete PTO-system is given in 1.11 (b). The discrete fluid power PTO-system is a discrete force system where the force delivered is given by the valve states, hence, the pressure connected to each cylinder chamber entails the force delivered. So a force shift is experienced when the pressure in one cylinder chamber is shifted. This system is similar in nature as the PTO-system of the Pelamis WEC.

1.3 Discrete Fluid Power

Digital fluid power or discrete fluid power technology has been experiencing an increasing attention during the last period. Digital fluid power is characterised by performing

control by usage only of components with discrete states. A brief introduction is here given to some of the leading technologies so the reader may easily recognise the difference in e.g. cylinder drives controlled with Digital Flow Control Units (DFCUs), switch controlled cylinder drives and secondary control cylinder drives. Cylinder drives are utilised as illustration since this technology is employed later as a key element in the discrete PTO-system, however similar digital motor controlled systems may be realised.

The research focus within discrete fluid power systems has turned on utilising the technology of discrete fluid power to design energy efficient low cost robust systems. Discrete fluid power systems are mainly based on simple on/off poppet valves, which are inexpensive and durable, hence low cost and robust.

1.3.1 Digital Flow Control Units

One of the highly promoted utilisations of on/off valves in discrete system is the Digital Flow Control Unit (DFCU) where on/off valves are set in parallel to compose a discrete variable orifice area. The nature of the DFCU is illustrated in Fig. 1.12. Note that the lines on the DFCU symbol indicating proportionality is dashed pointing out that the opening area of the orifice is discrete in nature.

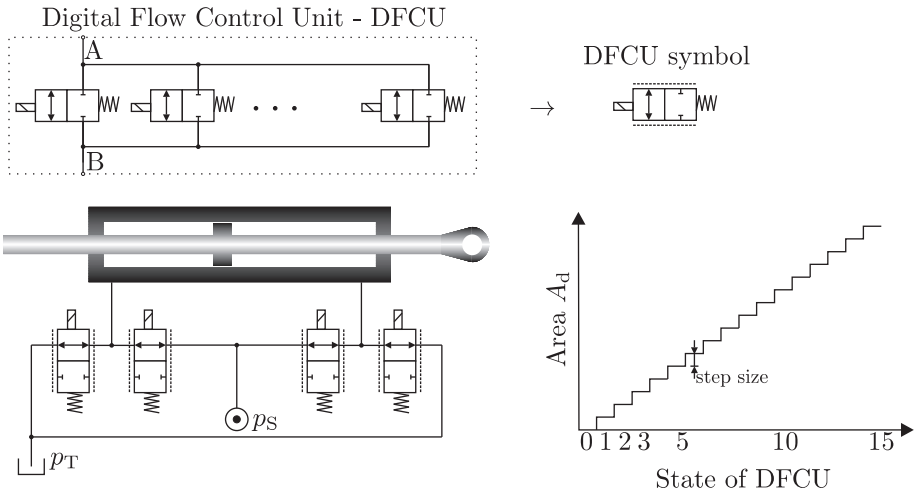

Figure 1.12: *Definitions and principal usage of DFCUs.*

The opening area is given in the lower right corner based on the valve state, here the discrete nature is profound. A schematic of how the DFCU may replace a servo or proportional valve is given in the lower left corner. In [19] a three-chamber fluid power cylinder is control by use of DFCUs. For that system the average reduction of energy losses was 33% compared with a traditional fluid power load sensing proportional valve. However, note that the energy saving is due to the introduction of separate metering edges imposing possibility of lowering the back pressure significantly. The possible savings will therefore be highly dependent on the operating situation. The DFCU is controlling flow by throttling as a traditional proportional control valves, yet the discrete

nature of the DFCU yield that the resolution of the flow controllability is depending on the number of on/off valves and the size of those employed in each DFCU.

In [20] a binary coding of the DFCUs is proposed, hence, the size of valve number 2 is twice the size of valve number 1 and the size of valve number 3 is twice the size of valve number 2 and so forth. This may imply a large valve with relative high resolution, whereas utilising equal sized valves yield a high number of valves if a large opening area and a high resolution are desired at same time. Yet recent research on utilising many small valves of same size have been carried out in [21] were a laminated valve manifold is proposed. This may support simple and standard valve production lines leading to low production costs. Further the laminated manifold may support a rather compact arrangement of the valves.

1.3.2 Secondary Controlled Cystems

In secondary controlled systems the on/off valves are utilised to connect one of multiple common pressure lines to each actuator port. Hence, secondary controlled systems are characterised by delivering a number of discrete forces based on the pressure line connection and the working area in each chamber. The numbers of applicable forces are determined by the number of common pressure lines and cylinder chambers. In Fig. 1.13 two multi-chamber cylinder layouts are illustrated in a two pressure line system, the low and high pressures are in this example 20 and 220 bar respectively.

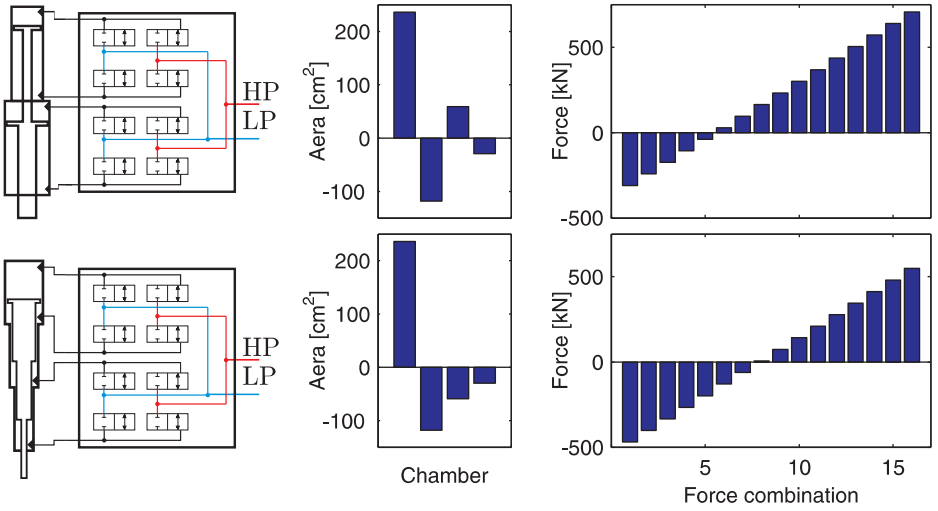

Figure 1.13: *Illustration of secondary controlled system: fluid power system schematic, area coding and applicable force levels. Top row: Asymmetric cylinder area coding. Bottom row: Symmetric cylinder area coding. Note, that the sign of the piston area are included to indicated force direction.*

Both cylinder codings are binary area layouts, however the adjacent area is added in

shifting direction for the upper coding here named asymmetric binary coding. For the symmetric binary coding the larger area is in positive direction whereas the following chambers all are generating force in negative direction. The force combinations for the asymmetric binary layout may be even more crooked if the pressure levels are close to each other.

Secondary controlled systems are most suited for use in systems with a relative high inertia load, since the step like force applied will impose infinite acceleration on zero inertia system. A secondary controlled multi-chamber cylinder drive is investigated in [22], where a position controller was designed. The usage of the secondary controlled system showed significant reduction in energy loss compared to a traditional load sensing valve, about 60%. A commercial attempt of utilising secondary controlled multi-chamber cylinder drives is realised by Norrhydro in what they call NorrDigiTM [23]. Figure 1.14 shows a schematic overview of the NorrDigiTM system employed on an off-road work machine.

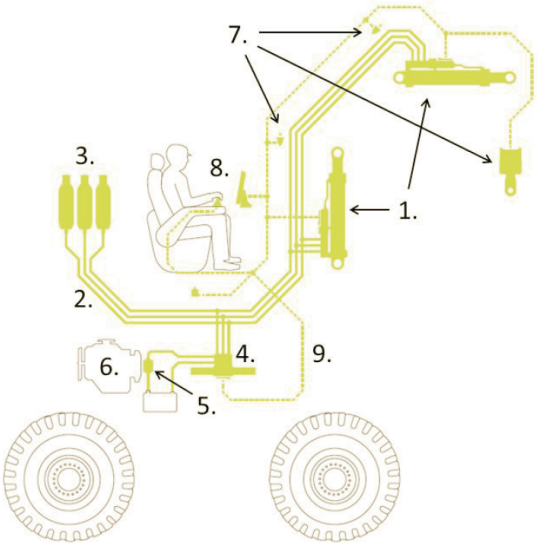

Figure 1.14: *Schematic of the NorrDigiTM technology applied to off road work machinery, [23]*

It is seen how the common pressure rails (2.) runs through the machine to all actuators (1.), the energy level management unit(4.) and how accumulators (3.) are connected to each line to stabilise the pressure and work as energy storage. The combustion engine (6.) drives a fixed displacement hydrostatic pump unit (5.) delivering the power to the fluid pressure rails. The user control (8.) and sensing (7.) interface runs with CAN BUS (9.). The focus of the NorrDigiTM system seems to be; lowering the power losses and enabling energy recovery and thereby lowering the power demand on the primary mover yielding fuel savings in off-road work machinery. As a side effect NorrDigiTm yield a

more fail safe system.

In secondary controlled systems the valves are single on/off valves for each line to chamber connection. The orifice area should be large without significantly compromising the valve dynamics. Contrary to the DFCU the valves in secondary controlled systems do not control by throttling but by connecting cylinder chamber to a common pressure line.

Hence, the DFCU is a throttling control, controlling the flow into the cylinder chamber and hereby the piston velocity. In the secondary controlled systems the valves connect a given pressure to each cylinder chamber leading to a discrete force control for the cylinder.

1.3.3 Switching Control

Fluid power switch mode control topologies, similar in principle to the well know electronic switch mode actuator control, have been proposed long time ago. However, switch mode control of fluid power system have experienced an increasing focus the last decades. Especially due to the possible decrease in energy loss, increased standardisation of system components, and increased robustness. Furthermore recent development of fast switching valves have enabled the technology. In Fig. 1.15 schematics for three switch mode control systems are given, two elementary valve switching systems and a buck converter valve-inductance set-up.

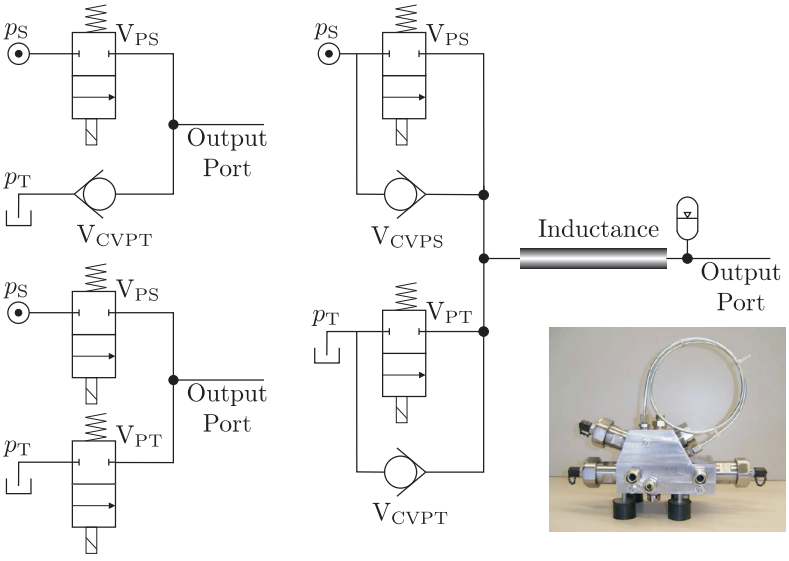

Figure 1.15: *Left top: Elementary one directional switching control schematic. Left bottom: Elementary two directional switching control schematic. Right: Sketch of hydraulic converter, and picture [24].*

In [25] a hydrostatic fixed displacement motor was controlled by PWM utilising an on/off valve and a check valve. Hence, the set-up utilised a valve configuration as the one given

in Fig. 1.15 upper left. The objective was to identify the parameters affecting the motor control. Jaakko et. al. [25] found that the switching frequency of the on/off valve has extensive influence on the rotary speed fluctuations of the motor, that is, the higher switching frequency the smaller speed fluctuations. Furthermore, the inertia of the load highly influenced the dynamic behaviour.

In [26] simulation and experimental results are given for a PWM control digital fluid power cylinder drive, see Fig. 1.16. Various valve types are compared and the influence of the valve speed on controllability and dynamic behaviour is investigated. It is seen that even though fast valves yield better controllability, extensive noise issues follows with the faster valves.

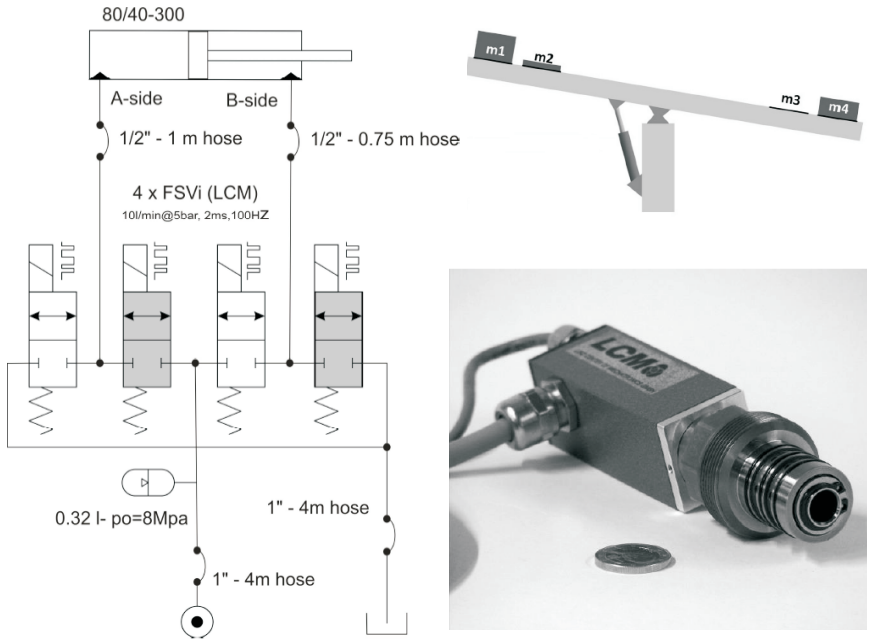

Figure 1.16: *Schematic of fluid power switch mode control system, mechanical test set-up and the utilised FVSi valve. [26]*

Digital fluid power valve switch mode control is in [27] investigated for use in a pneumatic force system and though showing a promising potential the controller developed showed room for improvements.

The hydraulic buck converter given in Fig. 1.15 right has been developed and extensively investigated at the Institute of Machine Design and Hydraulic Drives at Johannes Kepler University in e.g. [24, 28]. The investigations showed great energy efficiency improvements when compared to a traditional proportional valve controlled system. Furthermore energy recuperation is enabled with the buck converter set-up.

1.4 Switching Valves

For the technology of digital fluid power to be feasible, the valve opening and closing must be well known and fast typically in the ms-range. This leads to a survey of fast on/off valves. However, one must distinguish between two technologies. PWM control or other switch mode control schemes where the valve switching frequency is determined by the pulse carrier frequency for which valve switching occurs even at constant control input, and secondary or DFCU control where the valve switching occurs when control inputs or loading conditions are changed. Valves designed for switch mode systems, secondary controlled systems and DFCU controlled systems must enable valve switching with a pressure difference up to maximal system pressure.

1.4.1 Fast on/off Switching valves

The research area of fast on/off valves may roughly be divided into two areas, one where performance of existing valves are sought improved and one developing new valves.

Existing direct operated solenoid valves are tried improved in e.g. [20, 25, 29, 30, 31]. Here the movement, i.e. the opening and closing time of the valves are improved by the control input. The actuation force on the poppet/spool is for the solenoid valves related to the coil current. Hence, for a rapid valve opening a fast current rise time is needed. In the studies of [20, 25, 29, 30, 31] this is accomplished by applying a short time overvoltage to the coil. In [30] where the nominal coil voltage is 12[V], the coil is for example suppressed a higher voltage until the valve is open. The opening time was in [30] examined with an overvoltage of 24[V], 36[V] and 48[V], here it was found that both the delay and the opening time were decreased as the overvoltage was increased. This control strategy is known as boost and hold control. In [20] the boost and hold control strategy is used to improve the opening and closing time, furthermore it is stated that by replacing a big valve with several smaller valves a faster response is obtainable. Most of the direct actuated valves improved with boost and hold have a rated flow in the range of 10-30L/min.

In [32] commercially available 4/2 valves are connected as shown in Fig. 1.17 to work as an on/off valve. Three commercial valves are tested. The flow rated were in the range of 37 to 77 L/min, however the obtained dynamic performances are not competitive with the novel developed valves in the later paragraph. A switching time in the range of 10 to 15 ms was obtained.

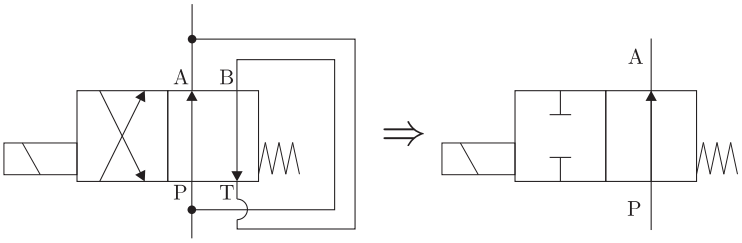

Figure 1.17: *Illustration of 4/2 valve utilised as on/off valve.*

When discussing novel developments with in switching valves, one may classify in direct operated and pilot operated valves. In [33] a direct operated switching valve is developed. It is developed as a 3/2 valve, however, it may also be purchased in a 2/2 version. The rated flow is 10 L/min@5bar and the switching time is approximately 1.5 ms. This valve was developed by LCM and IMH at Johannes Kepler University. The valve is pictured in the lower left of Fig. 1.16. Bucher Hydraulics have recently developed a compact direct actuated max 30 L/min on/off (WS22GD) valve with a switching time around 5-10 ms, which is designed mainly for usage in DFCU.

In [34, 35, 36] Winkler et. al presents the design of two novel fast on/off switching valves. Both designs are pilot operated and aims at realizing a fast opening and closing of the valve in the range of 1 ms and a rated flow in the range of 100 L/min. The novel design in [37] by Kudzma and Johnston is likewise pilot operated and aims at switching time in the range of 1 ms, however the rated flow target is 65 L/min. This valve is designed as a multi-edge spool valve, see Fig. 1.18 (a). In [34] the valve is realized as a seat valve with multiple metering edges as seen in Fig. 1.18 (b). The flow saturates as the poppet stroke exceeds half of the metering grooves. The maximum stroke will be 0.5 mm. Hence, a short poppet movement is demanded to open or close the valve. In [35] a multi-poppet solution is proposed. Hence, the valve is realised by 14 small poppets which are opened and closed by the same pilot stage. With the use of multiple poppets each poppet could be smaller to realize the same flow as one big poppet valve, hence as before the flow saturation occurs at a smaller stroke leading to faster valve opening and closing. This is due to the lighter poppet and the shorter poppet travelling distances.

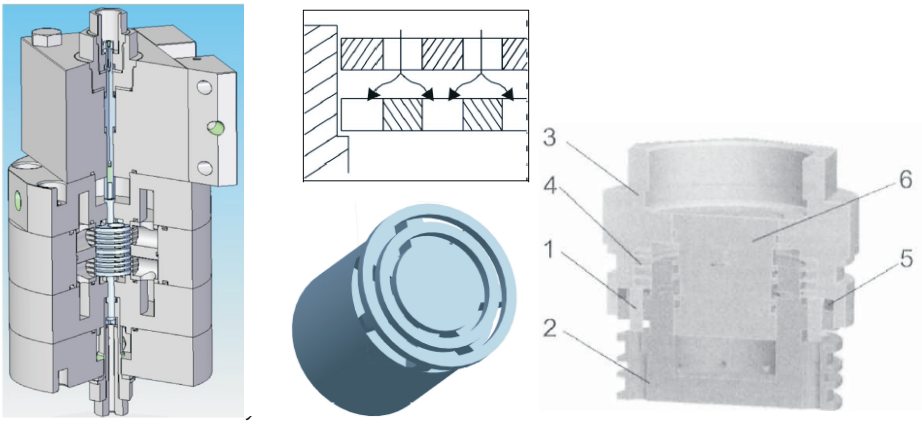

(a) (b) (c)

Figure 1.18: *Illustration of novel piloted switching valves. (a) Annular multi edge spool valve. (b) Annular multi edge poppet valve. (c) Multi-poppet valve*

1.5 Discrete Fluid Power - Technology and Industry

As indicated in the previous sections discrete/digital fluid power is a technology in growth and development. The novel fast switching valves enable energy efficient and robust system architectures, additionally systems which have comparable functional performance. Yet, the fluid power industry still has not introduced fast commercial switching valves. Hence, a great technology development mainly in valve design lacks, however, also effort in control and utilisation of the novel possibilities in discrete fluid power system are required.

1.6 Project Motivation

Wave Star A/S was established in 2003 and is one of the Danish forerunners within wave energy technology. The C5 Wavestar machine is a multi-point absorber device designed with 20 floats, each attached to a platform above the sea level, however with piles resting on the sea bed, see Fig. 1.19. The hemispheric-shaped floats are 5 meters in diameter and rigidly connected to a steel float arm hinged to the platform. Fluid power cylinders are hinged between each float arm and the platform so energy may be extracted from the relative motion between each float arm and the platform. Within the tube of the platform the fluid power transmissions are driving generators. As seen in the illustration below the machine incorporates a jacking system for storm protection and tide compensation. Hence, the PTO-system may be designed for production waves only, not compelled to withstand loads imposed in stormy conditions.

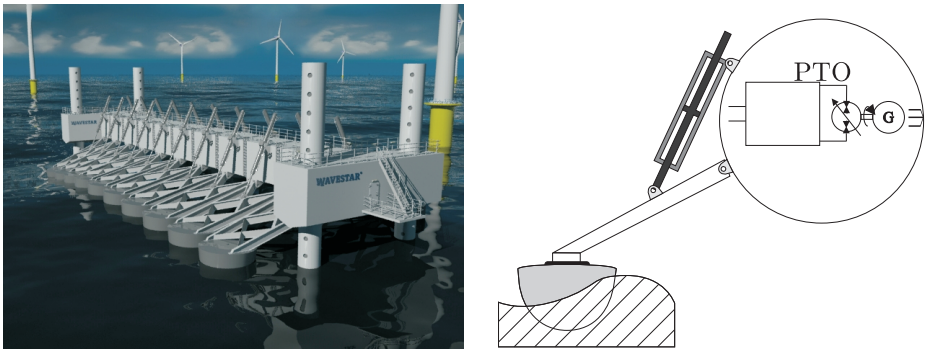

Figure 1.19: *Conceptual illustration of the Wavestar C5 machine.*

Wave Star A/S has performed several scaled model tests. In 2004 a 1:20 scaled model was tested in wave basins at Aalborg University. This model employed a common mechanical shaft with a mechanical break for energy dissipation. A 1:5 scaled model with 40 float was sea tested in 2006-2010 at Nissum Bredning. This model employed a simple fluid power PTO-system driving a common generator; however, energy extraction occured only on the float upward-strokes. A test section of the C5 machine was installed in 2009 at Hanstholm at the North West coast of Denmark, see Fig. 1.20 (a). This test machine employed two floats of 5 meters in diameter, driving a fluid power PTO-system.

The PTO-system in the C5 test machine is illustrated in Fig. 1.20 (c). The system is composed by a direct cylinder-motor fluid power system driving a generator. Hence, the C5 test machine carries one direct cylinder-motor system propelling one generator for each float.

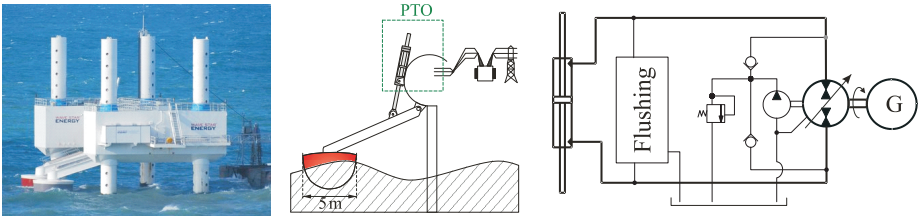

Figure 1.20: *Illustration of the Wavestar C5 test machine and the PTO system utilised.*

The basic principle of the Wavestar C5 test machine is that the buoyant float move along with the wave motion. This motion is controlled to be a circular movement by the float arm and the hinge at the platform. The fluid power cylinder is mounted so that it is extended as the float move down into a wave trough and compressed as the float moves up due to a wave crest. With the cylinder piston being driven in this motion by the float, it is utilised as a pumping unit rather that an actuator unit. The cylinder is in this way delivering an alternating flow where the pressure is controlled by the motor unit. A hydrostatic variable displacement motor is employed to extracted energy from the pressurised fluid flow. The motor runs unidirectional and copes with the bidirectional flow by swashing over centre. Fig. 1.21 gives a simple illustration of the function of the Wavestar fluid power PTO-system.

Assuming a standard linear damping control strategy for simplicity, where $F = Bv$, the working principle may be described as follows; (1) The float is moving up with a high velocity, a high pressure is generated in cylinder chamber A and the motor swash plate angle is large positive due to the high piston speed. (2) The float is moving up a with low velocity close to a stop, the pressure in cylinder chamber A is still high however the swash plate angle is approaching zero. (3) The float is moving downward at low velocity gaining speed, high pressure is here generated in cylinder chamber B and the swash plate angle is small and with negative sign due to the fluid flow being from B to A through the motor. (4) The float is moving downward at high velocity, the pressure in chamber B is still high however now the swash plate angle is largely negative. Like this high pressure fluid is generated and utilised to power the hydrostatic motor propelling an electrical generator. The power extracted from the waves is in the Wavestar project often measured as the fluid power at any instant:

$$P = A\,(p_{\mathrm{A}} - p_{\mathrm{B}})\,\omega_{\mathrm{arm}} d_{\mathrm{arm}} \tag{1.2}$$

The high pressure is controlled via the loading by the motor, for which the swash plate angle may then be controlled to fit a torque reference or a velocity reference.

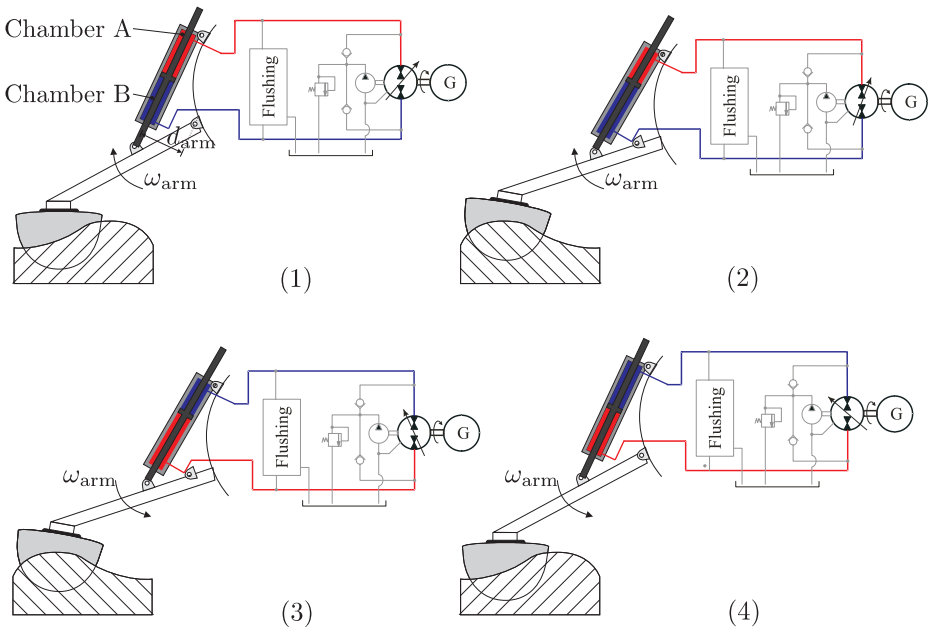

Figure 1.21: *Illustration of the Wavestar C5 test machine principle.*

In [38] a performance evaluation of the C5 test machine is presented. A good relation between expected (simulated) and measured power extraction is seen. This supports the utilised models for wave and float simulation. As briefly discussed the potential conversion efficiency of the direct cylinder-motor PTO-system in Fig. 1.20 utilised in the C5 test machine is deemed too low in [17]. The optimised system showed an expected over all efficiency (from extracted to grid) around 65% rapidly dropping to 45% in small waves. To reach a higher conversion efficiency Wave Star A/S have turned to discrete fluid power. The novel PTO-system proposed by Wave Star A/S in [18] employs a secondary controlled fluid power system as illustrated in Fig. 1.11. In [18] the technology of secondary controlled systems was deemed feasible for usage in the Wavestar WEC. Yet, the introduction of the discrete PTO-system raises several questions to be answered prior to a successful implementation:

- How many discrete force levels are feasible to realise to obtain reasonable energy extraction from the ocean waves for point absorber WECs? And at which force levels?
- How may a discrete fluid power force system be configured to enable the required force levels at a given installation site, while keeping energy losses low?
- How may the switching manifold be designed to enable adequate force tracking while minimising energy losses and system wear?

- How may low cost durable switching valves be designed for the switching manifold in a discrete PTO-system?
- Which discrete PTO force for a given sea state and operating condition must be applied to produce most energy?

1.6.1 Project Aims

The work documented through this dissertation aims at answering some of the above posted questions leading to implementation of the discrete fluid power force system in the Wavestar WEC. Hence, this project aims at;

- giving a method for choosing the system configuration of the Discrete Fluid Power Force system (DFPF-system) leading to the highest energy production in a given wave climate. This by; investigating wave energy extraction for a point absorber WEC in regular waves with a general discrete PTO force system and; by a model based investigation of the potential energy production with various system configurations.
- investigating feasible valve topologies for switching manifolds utilised in secondary controlled discrete fluid power systems. This is done by a model-based comparison of the potential energy production and system behaviour of switching manifolds occupying various valve topologies.
- giving a conceptual design of on/off- and bidirectional check valves for usage in the switching manifold of the DFPF-system employed in a wave energy converter PTO-system.

1.6.2 Project Activities

From the project aims above, the work throughout the project may be organised in the following three activities.

- An analysis of the system configuration of a discrete fluid power force system has been conducted. The shift from a continuous to a discrete PTO force system has been studied on a simplified float model operated in monochromatic waves. A model based investigation has been carried out on how both the sizing of the multi-chamber cylinder and the pressure line distribution affects the power output from the PTO-system of a WEC operating in irregular waves.
- Investigations on the switching manifold for a discrete fluid power force were conducted. A feasibility study on usage of bidirectional check valves serves as the basis for a conceptual valve design. A common main stage topology was developed for the on/off and the bidirectional check valves. The valve design was held on a conceptual level, for which proof of concept is provided with simulation models.
- Parallel to the theoretical work involvement in design and control of the full scale PTO test-bench has been under-taken. Within which preliminary tests have been conducted leading to significant findings for the valve requirements.

1.7 Main Contributions

The main contributions of this work is hence:

- A generic model of a discrete fluid power force system, usable for optimisation of the PTO-system in WECs.
- A system configuration study of the discrete fluid power force system, and system optimisation method for the discrete fluid power force system based on installation site wave climate.
- A conceptual design of both a on/off and a bidirectional check valve.
- Lab testing of the bidirectional check valve concept.
- Design, modelling and control of the full scale PTO test-bench.

A fundamental study on configuration of a fluid power force system for wave energy converters is given in chapter 2. The system configuration in term of choice of number of common pressure lines and the pressure level at which they should be operated is initially investigated and presented in paper [B]. Secondly the sizing of the multi-chamber cylinder is investigated in paper [C]. The combination of the studies on configuration of the common pressure lines and multi-chamber cylinder is presented in paper [D]. Here a framework for choosing the optimal system configuration for a given installation site is demonstrated.

The configuration of the switching manifold is investigated in terms of valve type and valve design. Hence, a topology investigation of a Bidirectional Check (BC) valve versus an on/off valve is initially conducted. A comparison of energy output, dynamic behaviour and structural loads when using BC- and on/off-valves are given in paper [E]. The studies show that systems using bidirectional check valves are highly competitive on energy output. However, this comes at the expense of an expected increase in structural loads. A conceptual valve design is given for the bidirectional check and the on/off valves in paper [F] and [G] respectively. A multi-poppet topology is utilised for the BC and on/off valve. Only minor difference in actuation area on the main stage and connection in the pilot system separates the two valve designs. A conceptual multi-poppet design is given for both the BC and the on/off valve allowing valve switching faster than 10 ms using a 3/2 way direct electronic actuated pilot valve.

The bidirectional check valve concept was tested in paper [F], where the concept was found applicable, however the utilised test set-up did not enable switching time measurement. Furthermore preliminary results from the full scale PTO test-bench are given in this dissertation, however no publication of the results have been submitted due to an ongoing commissioning phase.

1.8 Dissertation Outline

This dissertation servers as an extended summery of the appended papers, which are referenced to throughout the dissertation with paper [A], for paper A and so on. A list

of the appended papers are given in the start of appendix B and in the front of the dissertation. A brief overview of the contents of each chapter is given next:

Chapter 1 The chapter has presented a brief introduction to ocean wave energy converters to familiarise the reader with the topic. Some of the leading ocean wave energy converter technologies and concepts have been presented in term of mode of operation and development state. Furthermore an insight in some power take off systems utilising fluid power technology is given. The chapter likewise draws the reader into the re-emerging technology of digital or discrete fluid power. Here the diversity in cylinder drives controlled by means of switch mode valve control, digital flow control units or secondary control was in focus. Furthermore the current development on switching valves was outlined.

Chapter 2 An investigation of the optimal discrete PTO force profile for a simplified heave motion point absorber initiates this chapter, which treats the system configuration of a discrete fluid power force system. A generic model of the discrete fluid power force system is derived and utilised in a brute force optimisation of the system configuration when utilised as PTO element in the Wavestar. A method for choosing a proper system configuration based on maximal energy output, taking into account the time distribution of sea conditions, is illustrated.

Chapter 3 A model based feasibility study on utilisation of bidirectional check valves in the switching manifold in a secondary controlled PTO-system is conducted by comparison with an on/off valve switching manifold. Hereafter a conceptual design of large flow rate multi-poppet on/off and bidirectional check valves are performed, yielding valve concepts capable of active switching in less than 10 ms. The chapter is concluded with a proposal of utilising both on/off and one directional check valves with on/off valve possibilities in the switching manifold.

Chapter 4 Preliminary results from valve switching tests conducted on a prototype of the discrete fluid power force system are presented in chapter 4. It is shown how the valve switching time affects the cylinder chamber pressure and how pressure oscillations are experienced in the transmission lines from manifold to cylinder chambers.

Chapter 5 Summery of the main conclusion of the present work. The chapter furthermore contains an outlook on future challenges and issues to be handled.

Appendix A In the appendix a presentation of modelling and control of the full scale test-bench is given. The focus is on testing feedback linearisation as an opportunity to deal with the non-linearities in the system and the discrete loading conditions. With the test-bench still in commissioning publications on the feedback linearisation controller are yet to be realised, why this chapter is placed in the Appendix.

Appendix B The extended summery serves as an addition to the papers published and submitted in partial fulfilment of the requirements for the Ph.D. degree in Energy Technology. The papers are appended in the back of the thesis. The appended papers are given in the original layout, however resized to fit the present paper size.

Chapter 2

Configuration of DFP Force System for WECs

Configuration of the discrete fluid power force system is the focus point of this chapter. The configuration of the PTO-system for wave energy converters highly affects the system efficiency and the potential energy extraction. As shortly discussed previously the applicable forces affect the energy extraction by setting the bounds for the power levels obtainable in a given sea condition. Hence, the applicable forces may be optimised so a maximal energy extraction is reached. However, with the objective of the wave energy converter to produce energy to the power grid, large amounts of extracted energy is only a sub-objective. The conversion of the extracted energy into output energy is unaffected by the applicable force, however, highly affected by how the forces are generated, in particular the energy losses associated.

Hence the configuration of the discrete fluid power force system faces a trade-off between yielding good energy extraction ability and yielding high energy conversion efficiency. For commercial success of wave energy converters the energy output has to be high compared to the installation and maintenance cost, yielding a low cost of energy (Euro/kWh). With cost of energy as main focus high conversion efficiency and large energy extraction both becomes sub-objectives in the configuration of the PTO system. However, these two sub-objectives are both parameters which may aid the primary objective of having a high energy output of the PTO. Furthermore low system efficiency is often aligned with large wear in system components.

Throughout this chapter the system configuration of the discrete fluid power force system is investigated. Initiating with a discussion of how the number of discrete forces and the size of these affect the energy extraction capability of the wave energy converter. Secondly the construction of a generic simulation model of the discrete force system is given. The PTO model is combined with a model describing a single float of the Wavestar and the float wave interaction. The single float model utilising the generic discrete fluid power force system is used to conduct a system configuration optimisation of the discrete fluid power PTO-system. The parameters optimised are the multi-chamber cylinder and the common pressure lines, in terms of the chamber numbers and their size and the pressure levels and number of common pressure lines.

2.1 Energy Extraction with a Discrete PTO Force

Transferring from the well proven continuous direct cylinder-pump/motor fluid power PTO-system to the novel discrete fluid power PTO-system creates some design ques-

tions. One question is; how many force levels are needed and how should these be distributed to increase the potential extraction of energy? Some basic investigations are conducted to approach an answer. Another question discussed in a later section is the actual configuration of the multi-chamber cylinder and the common pressure lines. However, the initial investigation on the number of forces and the size of these are investigated without any practical system consideration. Hence losses in the PTO-system are unmodelled in this investigation, the investigation in section 2.2 includes the fluid power system and hence losses.

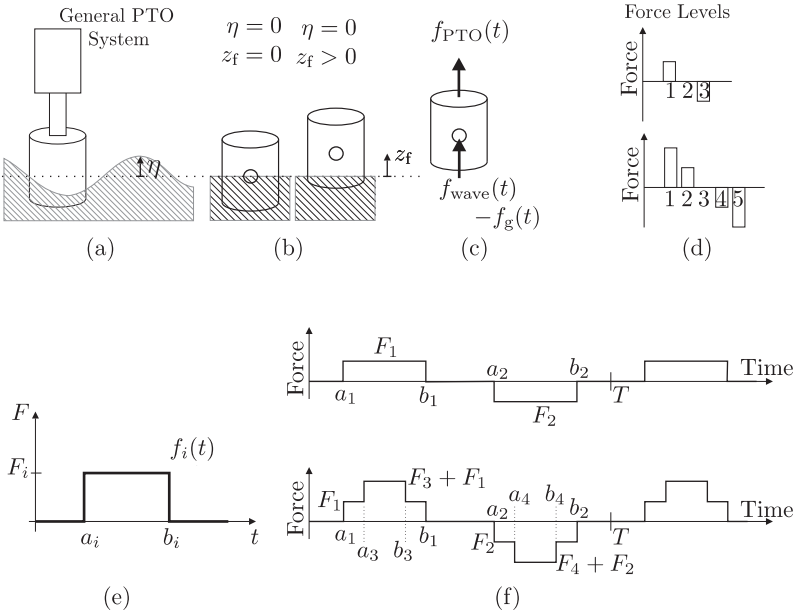

Figure 2.1: *Illustration of; the simple float model (a), (b), (c); applicable discrete force levels (d); single box force (e) and the discrete force profile(f).*

Through an analytical approach the problem of which discrete force levels and how many to apply is solved for a point absorber operating in monochromatic waves. This is done by developing a much simplified model for the float movement and the wave-float-interaction. By exploiting linearity of the simplified model an analytical solution of the float movement and the energy extraction is found, for the float working in monochromatic waves under influence of a discrete, however periodic PTO force. This via usage of superposition, Laplace transformation and the time shift-rule. An illustration of the simple float model and the periodic PTO-force profile is given in Fig. 2.1. Even with the much simplified model and a periodic and symmetric PTO force profile the analytical solution for a PTO-system with more than three discrete force levels gets large and cumbersome, this analysis is presented in paper [A]. To facilitate a solution of the energy extraction of PTO-systems with a large number of PTO force levels time series simulations of the simplified model are used.

2.1.1 Simplified Float Model

As well documented in e.g. [39], the motion of a point absorber operating in heave may be modelled by use of linear wave theory with Newton's second law of motion as:

$$\ddot{z}_\mathrm{f} = \frac{1}{m_\mathrm{f}} \left(F_\mathrm{wave} - F_\mathrm{g} - F_\mathrm{PTO} \right) \tag{2.1}$$

$$\ddot{z}_\mathrm{f} = \frac{1}{m_\mathrm{f}} \left(F_\mathrm{ext} - F_\mathrm{rad} + F_\mathrm{Arch} - F_\mathrm{g} - F_\mathrm{PTO} \right) \tag{2.2}$$

Where the force terms from the wave may be described as;

- F_g gravitational force on the float.
- F_ext is the force exerted by incoming waves on a float when held fixed.
- F_rad is the force needed to move a float in still water, hence, the force imposed by wave radiation.
- F_Arch is the Archimedes force (buoyancy) on a float due to displaced water.

In [40] a thorough description of a single float model is given. The float movement in the simple model is modelled with a second order differential equation:

$$\ddot{z}_\mathrm{f} m_\mathrm{f} = f_\mathrm{PTO}(t) + (\eta - z) k_\mathrm{f} + (\dot{\eta} - \dot{z}) b_\mathrm{f} \tag{2.3}$$

Hence, the force acting on the float is the PTO force, the resulting force of the buoyancy/gravity, and damping force. The wave height (free surface elevation) is η and the float position relative to the still water level is z_f. In this simplified model the damping term b_f and the float mass m_f are both held constant, which with a monochromatic wave input is reasonable (though changes appears for various monochromatic inputs).

The simplified model is rewritten in a standard form for solving the differential equation:

$$\ddot{z}_\mathrm{f} m_\mathrm{f} + \dot{z}_\mathrm{f} b_\mathrm{f} + z_\mathrm{f} k_\mathrm{f} = f_\mathrm{PTO}(t) + \eta k + \dot{\eta} b \tag{2.4}$$

$$\ddot{z}_\mathrm{f} m_\mathrm{f} + \dot{z}_\mathrm{f} b_\mathrm{f} + z_\mathrm{f} k_\mathrm{f} = f(t) \tag{2.5}$$

From (2.5) it is clear that the simplified float model is a non-homogeneous ordinary second order differential equation with constant coefficients. This is supported by the wave input being a well defined time function given as:

$$\eta = A_\mathrm{w} \cos(\omega_\mathrm{w} t - \phi) \tag{2.6}$$

With the wave amplitude and frequency given as A_w and ω_w respectively.

2.1.2 Float Movement in Monochromatic Waves and with Discrete PTO Force

The linearity of the simplified system model implies that the solution of the float movement may be given as the sum of the solutions to each input term. Hence, the input $f(t)$ may be split in an input regarding the wave and one regarding the PTO force. Further the PTO force may be split in smaller terms for which the solutions are easily found.

The discrete PTO force (2.7) is therefore given as a sum of box functions (2.8), cf. Fig. 2.1.

$$f_{\mathrm{PTO}}(t) = f_{\mathrm{PTO.T}}(t - mT) | m \in \mathbb{Z} \tag{2.7}$$

$$f_{\mathrm{PTO.T}}(t) = \Sigma_{i=1}^{n} F_i [u(t - a_i) - u(t - b_i)] \tag{2.8}$$

The float velocity if no PTO force is applied is given as:

$$\dot{z}_{\mathrm{f.w}}(t) = -\hat{A}_w \omega_{\mathrm{w}} \sin(\omega_{\mathrm{w}} t - \hat{\phi}) \tag{2.9}$$

Where $\hat{A}_{\mathrm{w}}$ and $\hat{\phi}$ are constants, however, depending on the system spring and damping constants along with the frequency and amplitude of the incoming wave. The float velocity with only the discrete PTO force applied is given by the sum of solutions for each of the force box functions:

$$\dot{z}_{\mathrm{f.PTO}}(t) = \dot{z}_{\mathrm{f.PTO.T}}(t - mT) | m \in \mathbb{Z} \tag{2.10}$$

$$\dot{z}_{\mathrm{f.PTO.T}}(t) = \Sigma_{i=1}^{n} \dot{z}_{\mathrm{f.i}}(t) \tag{2.11}$$

$$\begin{aligned} \dot{z}_{\mathrm{f.i}}(t) = F_i K_{\mathrm{c}} \; & [u(t - a_i) e^{-\alpha(t - a_i)} \sin(\omega_{\mathrm{b}}(t - a_i)) \\ & - u(t - b_i) e^{-\alpha(t - b_i)} \sin(\omega_{\mathrm{b}}(t - b_i))] \end{aligned} \tag{2.12}$$

Where K_{c}, ω_{b} and α are constant depending on the spring, damping and mass constants. A more explicit derivation of the solution and the constants K_{c}, ω_{b}, α, $\hat{A}_{\mathrm{w}}$ and $\hat{\phi}$ is given in paper [B].

However, the float velocity of the simplified model operating in a monochromatic wave while under influence of a discrete PTO force may be found by summation of (2.9) and (2.10).

$$\dot{z}_{\mathrm{f}}(t) = \dot{z}_{\mathrm{f.w}}(t) + \dot{z}_{\mathrm{f.PTO}}(t) \tag{2.13}$$

2.1.3 Extracted Energy

The extrated/harvested energy is defined as the time integral of the power in the PTO force system, hence, the extracted energy is for the simple model in this section given as;

$$E_{\mathrm{har}}(t) = \int -f_{\mathrm{PTO}}(t) \dot{z}_{\mathrm{f}}(t) dt \tag{2.14}$$

Note how the signs of the force and the float velocity must be opposite for energy to be harvested whereas equal signs indicated energy flow from the PTO-system to the waves through the float. Hence, energy is harvested when the PTO force is opposing the float movement.

With the incoming wave and the PTO force being periodic the energy extraction may be found as the energy extraction during one period multiplied by the number of periods. The energy extraction for a wave period is, hence, calculated by imposing the start and end of a time period as limits for the integral in Eq. (2.14). In Fig. 2.2 the float velocity is illustrated when a discrete PTO force is applied to a float in still water, where no incoming wave is imposed. The PTO force is seen in the upper window whereas the

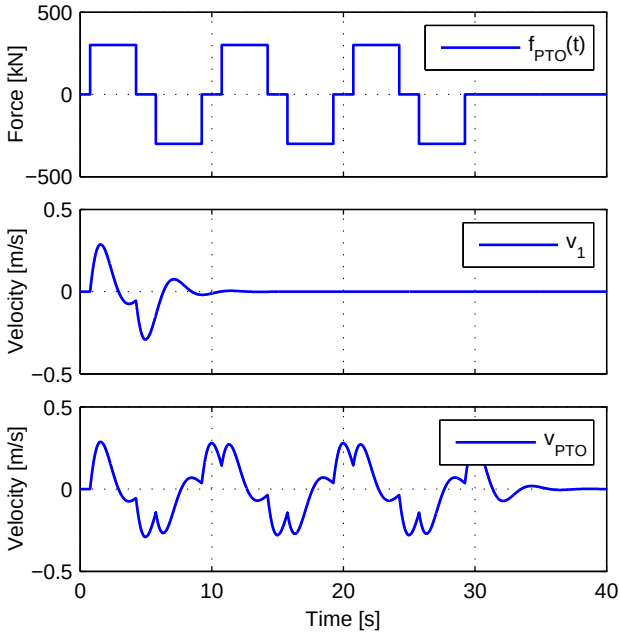

Figure 2.2: *Illustration of float velocity when imposing a discrete PTO force.*

float velocity due to the PTO force is seen in the lower window. The middle window shows the float velocity due to the first PTO box force applied in the first time period as if the PTO force in the following periods is set to zero.

One may notice that the float velocity at a given point is depending on the previous applied PTO force, therefore the velocity utilised to calculate the energy output is based on the PTO force applied in the current and the two previous time periods. Hence, to solve the velocity in one time period one needs the PTO force applied in the previously and the assumption of the incoming wave to be monochromatic. Here it is chosen to utilise the velocity induced by the PTO force in the previous two time periods since Fig. 2.2 indicates that velocity contribution form each box force is zero half way through the next time period. For the PTO system having three force levels as in Fig. 2.2 an analytical solution for the harvested energy may be found and graphically illustrated as a function of the force level and force width, see Fig. 2.3 (a). Hence, the energy harvested in one time period is plotted for varying box force level (F_1) and varying box force width (L_1). In Fig. 2.3 (b) and (c) the partial derivative of the harvested energy with respect to force level and force width is given respectively. The black lines indicates the nullclines, hence, the crossing of the black lines indicates the extreme points for the extracted energy.

The optimal configuration for a force profile with three force levels, working in monochromatic waves may hence be found analytically. The solution for maximal energy extrac-

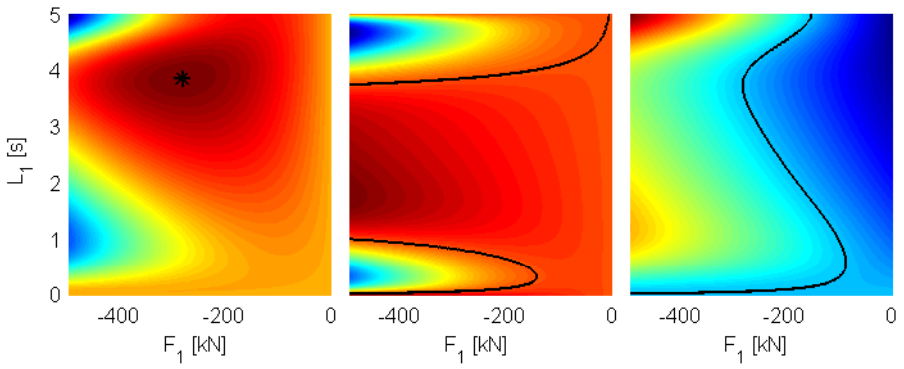

Figure 2.3: *The graphical solution to the optimisation of the PTO force profile with three force levels. (a) Extracted energy. (b) Partial derivative of extracted energy with respect to force level. (c) Partial derivative of extracted energy with respect to force width.*

tion is given graphically in Fig. 2.3 for a system with mass, damping and spring constants $m_\mathrm{f} = 1e5$ kg, $b_\mathrm{f} = 5e5$ Ns/m and $k_\mathrm{f} = 1e6$ N/m working in a monochromatic waves with amplitude and wave frequency $A_\mathrm{w} = 0.3$ m and $\omega_\mathrm{w} = \frac{1}{10}$ Hz.

The introduction of more force levels enforces more parameters (a_i b_i F_i) for the optimisation and increases the analytical solution by orders of magnitude for the energy extracted. Therefore analytical optimisation of force profiles with more force levels is practically impossible and the optimisation is therefore carried out by employing time simulations and numerical optimisation routines.

2.1.4 Optimal Force Profile

The optimisation of the force profile is carried out with two different objective functions. With energy production as the overall objective for the WEC, the natural objective is to maximise the energy extraction from the ocean waves, hence the optimal force profile may be found from:

$$f_{\mathrm{PTO.T}}(t) = \arg\min(-E_\mathrm{har}(t)) \tag{2.15}$$

Hence, the problem is to identify the PTO force profile that yields the highest energy extraction. Note that the energy output is unmodelled in this simple model since a generic PTO force is applied.

The second objective utilised in the force profile optimisation is to minimise the force error, whereby the optimal force profile may be found from:

$$f_{\mathrm{PTO.T}}(t) = \arg\min(F_\mathrm{e}(t)) \tag{2.16}$$

Where F_e is the force tracking error defined in (2.17). Hence, the discrete PTO force profile is optimised such that it tracks a continuous force reference with minimal error.

$$F_e(t) = |f_{PTO.Cref}(t) - f_{PTO}(t)| \tag{2.17}$$

The continuous force reference is generated with a reactive control algorithm utilising the float position and velocity as feedback.

$$f_{PTO.Cref}(t) = b_{PTO}\dot{z}_f(t) + k_{PTO}z_f(t) \tag{2.18}$$

With the coefficients b_{PTO} and k_{PTO} optimised for maximal energy extraction they are given as:

$$b_{PTO} = b_f \tag{2.19}$$

$$k_{PTO} = m_f\omega_w^2 - k_f \tag{2.20}$$

When the PTO-system efficiency is assumed equal to 1. m_f, b_f and k_f are system parameters from Eq. (2.3). Notice that the coefficients are constant for a constant wave frequency.

Throughout the optimisation general constrains for the discrete PTO force profile, seen in Fig. 2.1 (f), are given as:

$$\begin{aligned} &a_i < b_i,\ |i \in \mathbb{N} \\ &a_j < a_{j+1},\ b_j > b_{j+1},\ |j \in \mathbb{N}\,\text{odd} \\ &a_l < a_{l+1},\ b_l > b_{l+1},\ |l \in \mathbb{N}\,\text{even} \\ &a_2 > b_1,\ b_2 - a_1 < T \end{aligned} \tag{2.21}$$

The optimised discrete force profile when utilising five force levels in a monochromatic wave is seen in the bottom of Fig. 2.4. The discrete PTO force are here compared with the optimal continuous force reference Eq. (2.18). The upper and middle plot gives the float position and velocity compared to the wave height and wave height velocity respectively.

Note that the PTO force enforces the float movement to be larger than the wave height, hence resonance is obtained as with the optimal continuous control. Note however, that the PTO force is optimised so the maximum energy is extracted from the waves. Hence, the operation point imposed by this control may dramatically degrade the conversion efficiency when implemented in a practical PTO-system where imperfect conversion is employed. The optimal discrete PTO force profile is seen to be close to equal to the continuous force reference.

In Fig. 2.5 (a) the optimal PTO force profiles are given for a system utilising five force levels working in three different wave heights but with the same wave frequency. In Fig. 2.5 (b) the optimal force profile for a system utilising 3, 5 or 7 force levels are given when working in the same monochromatic wave. As one would expect larger waves calls for larger PTO forces. Further it is seen that the timing of the force shifts are unchanged with the increasing wave heights when utilising a fixed number of force levels

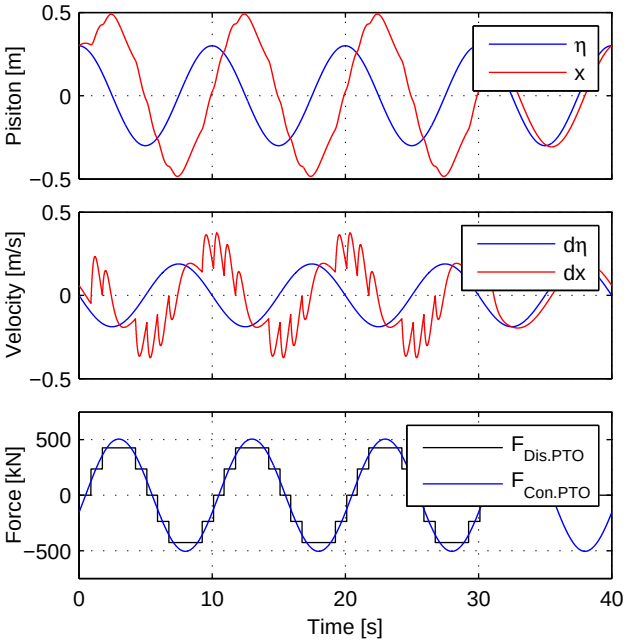

Figure 2.4: *Illustration of float position and velocity with optimal discrete force profile and a monochromatic incoming wave.*

(a). However, both the timing and size for the forces differ for systems with various numbers of force levels (b).

The force error and energy optimised force profiles are compared in Fig. 2.5 (c). It is seen that with an increasing number of force levels, the two objective functions result in more equal optimal force profiles.

In a physical discrete force system the number and size of forces may not easily be changed, why a fixed number of forces must be chosen. However, the on and off timing, i.e. when switched from one value to the next, of these forces may still be optimised. In Fig. 2.6 the optimal force profiles are given for a system with seven force levels when operating in waves with varying amplitude. Note how the need for a smaller force is met by imposing a shorter on time for the large force and even refraining from using the maximum force level in some situations. This way the force profile is fitted to the need by fitting the on time for each force level.

In table 2.7 the energy extraction is compared for a system working with a fixed number and size of force levels where the timing is optimised.

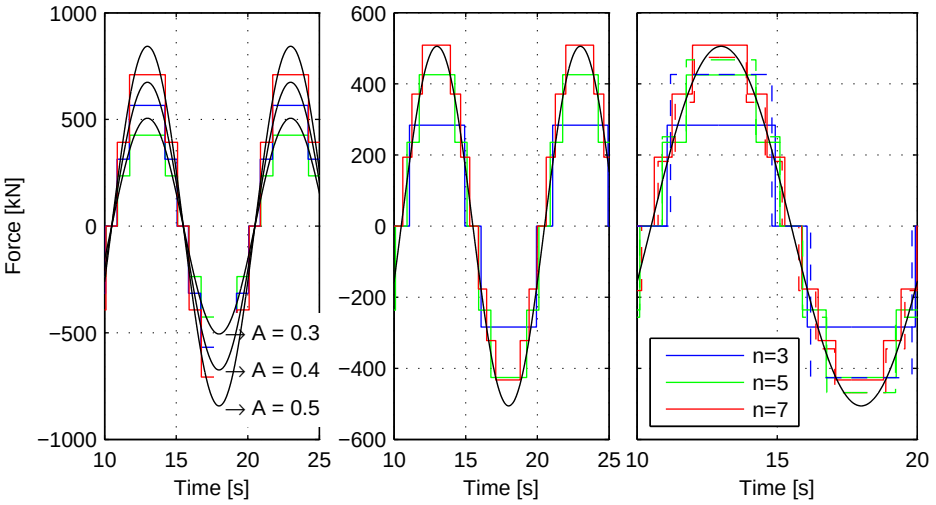

Figure 2.5: *Optimal discrete force profiles. (a) For varying wave input and five force levels. (b) 3,5 or 7 force levels for fixed input wave. (c) Energy(solid) and force error(dashed) optimised force profiles. Note; the force axis for (b) and (d) are equal.*

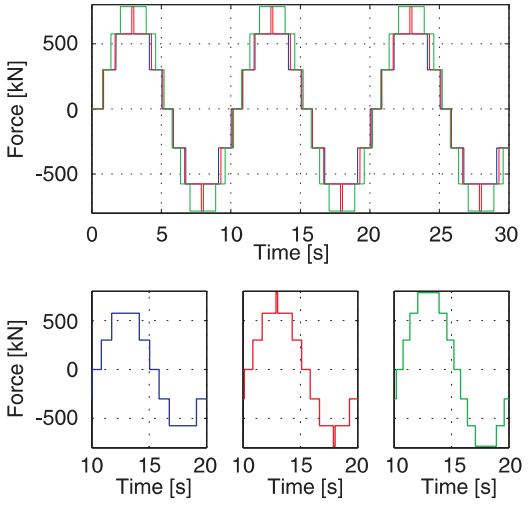

Figure 2.6: *Optimised force profiles with fixed number of available force levels*

Wave		Number of Forces		
A_w	ω_w	3	5	7
0.3	$\frac{2\pi}{10}$	66.8	60.7	81.1
0.4	$\frac{2\pi}{10}$	64.2	89.5	92.2
0.5	$\frac{2\pi}{10}$	58.2	90.6	97.4
0.5	$\frac{2\pi}{5}$	87.5	95.2	98.3
0.5	$\frac{2\pi}{3}$	96.6	99	98.7

Figure 2.7: *Normalised extracted energy in % during one wave period, utilising fixed force levels and optimised force shapes. The energy extraction is normalised with the energy extraction by a optimal continuous force system.*

2.1.5 Discrete Force Profile

The investigation of the discrete force profile for a generic PTO force system utilised for a simple heave motion point absorber shows that; the size of the optimal force is highly influenced by the size of the incoming wave whereas the timing is depending on both the wave frequency and the wave height. Furthermore, it is seen that a reasonable energy extraction may be obtained with 7 fixed force levels even for varying sea conditions when the on and off switching of the force is optimised. However, the analytical approach imposing the symmetric and periodic nature of the PTO force profile is inadequate when irregular waves are examined. Furthermore, one should recall that no losses in the PTO-system are included. Yet the results for the monochromatic waves indicate that tracking the optimal continuous force reference is reasonable and that relative few force levels are needed.

The investigation is extended to irregular waves by constructing a simulation model including a generic model of the discrete fluid power force system. Hence, the energy losses in the switching manifold may be included.

2.2 Modelling of Generic DFP Force System

A model of the discrete fluid power force system is presented in the following. The model is constructed so the number of working areas and pressure lines may easily be changed. Hence this model will represent various system designs. The number of working areas are in the model indicated with the integer n whereas the integer m indicates the number of pressure lines. The counter values i and j will be used for summation over working chambers and pressure lines respectively. The discrete fluid power force system is evaluated by implementation in a single float point absorber WEC simulation model of the Wavestar. Hence, the discrete PTO-system model is combined with a float and wave model, so the PTO-system may be evaluated when implemented in a WEC operating in irregular waves. In Fig. 2.8 an illustration of the combined system is given. The model includes irregular wave modelling, wave-float interaction and the primary stage of the discrete fluid power force system.

The wave-float interaction model is based on linear wave theory and the point absorber being small compared to the wave length. The wave-float interaction model utilised is described by Hansen and Kramer in [40]. Here it is seen that the float dynamics is modelled with Newton's second law and that the forces induced on the float are dependent on the float design and the wave height and frequency. Times series modelling of ocean waves may be conducted in several ways, however, white noise filtering is utilised according to [40]. However, when comparing various system configurations three fixed wave times series are utilised whereby equal inputs are experienced by the systems under comparison. The three wave series resemble three sea conditions, small, medium and large waves relative to the wave climate at Hanstholm, a previous Wavestar test site. The wave climate at Hanstholm, Denmark is given by the scatter diagram in Tab. 2.1. The wave climate is given by the wave significant height ($H_{\mathrm{m},0}$) and the mean wave time period ($T_{0,2}$). The significant wave height is often defined as the mean wave height (trough to crest) of the highest third of the waves. The three sea states utilised in the modelling are marked in boldface blue in Tab. 2.1 and their density spectrums are

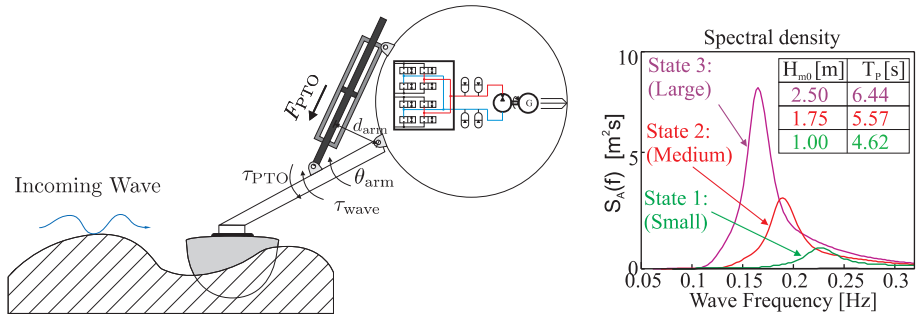

(a) (b)

Figure 2.8: *Illustration of single float point absorber model with discrete fluid power PTO system and the wave density spectrums utilised for the three sea states.*

given in Fig. 2.8 (b). One may note that the C5 machine installed at Hanstholm is in production for wave in the range of $H_{\mathrm{m.0}} = [0.5 - 3.0]$.

$H_{\mathrm{m},0}$ [m]	Mean wave period $T_{0,2}$[s]							Sum [%]
	2-3	3-4	4-5	5-6	6-7	7-8	8-10	
0.0 - 0.5	2.65	8.18	1.84	0.38	0.14	0.03	0.01	13.2
0.5 - 1.0	1.22	**19.2**	11.4	2.21	0.18	0.06	0.02	34.4
1.0 - 1.5	0.00	**6.84**	13.0	2.96	0.30	0.04	0.00	23.2
1.5 - 2.0	0.00	0.33	**9.58**	3.05	0.29	0.04	0.00	13.3
2.0 - 2.5	0.00	0.02	3.34	**4.60**	0.20	0.04	0.00	8.20
2.5 - 3.0	0.00	0.01	0.22	**3.89**	0.21	0.01	0.01	4.40
3.0 - 3.5	0.00	0.00	0.00	1.38	0.51	0.01	0.01	1.90
3.5 - 4.0	0.00	0.00	0.00	0.17	0.57	0.02	0.01	0.80
4.0 - 4.5	0.00	0.00	0.00	0.00	0.24	0.07	0.00	0.30
4.0 -	0.00	0.00	0.00	0.00	0.07	0.21	0.06	0.30
Sum[%]	3.87	34.6	39.5	18.6	2.72	0.52	0.16	100

Table 2.1: *Scatter diagram for Hanstholm pear. The sea state utilised ($H_{m,0}$,$T_{0,2}$), SSI: (1m, 3.95s). SSII: (1.75m, 4.76s). SSIII: (2.5m, 5.50s) [40]*

2.2.1 PTO Cylinder Force

The force generated by the multi-chamber PTO cylinder is defined as the combined force generated by the fluid pressure in the cylinder chambers.

$$F_{\mathrm{PTO}}(t) = \sum_{i=1}^{n} A_i p_{\mathrm{c},i}(t) \tag{2.22}$$

Here the working areas, A_i, are either positive or negative values to indicate the force direction. This is done to be able to easily change the number of chambers and forces in the system. $p_{\mathrm{c},i}(t)$ is the pressure in the i'th cylinder chamber.

2.2.2 Fluid Flow Through Switching Valves

The fluid volume flow through the switching valves in the manifold are modelled with the orifice equation [41], all flows through the valves are modelled positive into the cylinder chambers;

$$Q_{i,j}(t) = k_{\mathrm{v},i}\overline{x}_{\mathrm{v},i,j}\sqrt{|p_{\mathrm{l},j}(t) - p_{\mathrm{c},i}(t)|}\mathrm{sign}(p_{\mathrm{l},j} - p_{\mathrm{c},i}(t)) \tag{2.23}$$

Where $k_{\mathrm{v},i}$ is the valve coefficient given as $\frac{Q_{\mathrm{Nom},i}}{\sqrt{\Delta p_{\mathrm{Nom}}}}$, with $Q_{\mathrm{Nom},i} = A_i\dot{x}_{\mathrm{c,Nom}}$. $\overline{x}_{\mathrm{v},i,j}$ is the normalised spool position for the valve connecting the i'th cylinder chamber and the j'th pressure line. $p_{\mathrm{l},j}$ and $p_{\mathrm{c},i}$ are the pressure in the j'th pressure line and the i'th cylinder chamber respectively. The flow into the i'th chamber is hence defined as:

$$Q_{\mathrm{c},i}(t) = \sum_{j=1}^{m} Q_{i,j}(t) \tag{2.24}$$

Whereas the flow into the j'th pressure line is defined as:

$$Q_{\mathrm{l},j}(t) = -\sum_{i=1}^{n} Q_{i,j}(t) \tag{2.25}$$

Recall that $Q_{i,j}(t)$ is the flow into the i'th cylinder chamber through the i,j'th valve in the switching manifold, why minus is applied in (2.25).

2.2.3 Pressure Dynamics of Fluid in Cylinder Chambers

The pressure dynamics for each cylinder chamber is modelled with the flow continuity equation [41]. Hence the pressures dynamic for the i'th cylinder chamber is given as:

$$\dot{p}_{\mathrm{c},i}(t) = \frac{\beta_{\mathrm{eff}}(p_{\mathrm{c},i}(t))}{V_i(t)}(Q_{\mathrm{c},i}(t) - A_i\dot{x}_{\mathrm{c}}(t)) \tag{2.26}$$

Where $\beta_{\mathrm{eff}}(p)$ is the effective bulk modulus of the fluid under the pressure p, as given in eq. (2.27). The current volume of the i'th chamber is $V_i(t)$ and $\dot{x}_{\mathrm{c}}$ is the cylinder piston velocity. The bulk modulus model utilised incorporates pressure dependency and air content in the oil. An adiabatic air constant of $\kappa = 1.4$ is used.

$$\beta_{\mathrm{eff}}(p) = \frac{1}{\frac{1}{\beta_{\mathrm{oil}}} + \frac{\varepsilon_{\mathrm{air}}(p)}{\beta_{\mathrm{air}}}} \tag{2.27}$$

The dissolved air in the oil is pressure dependent and modelled as:

$$\varepsilon_{\mathrm{air}}(p) = \left(\frac{p_0 \cdot \varepsilon_{\mathrm{air},0}}{p}\right)^{\frac{1}{\kappa}} \tag{2.28}$$

Where $\varepsilon_{\mathrm{air},0}$ is the air contents at atmospheric pressure p_0. The volumetric air content is set to 1% at atmospheric pressure. β_{oil} is set to 16000 bar and β_{eff} is furthermore upper limited to 10000 bar.

The pressures in the common pressure lines are assumed constant in the investigation of the system configuration. In the real system this is approached by fitting accumulators to all pressure lines.

2.2.4 Dynamics of Switching Valves

The on/off switching valves of the manifold are each modelled with a rate limit such that:

$$\dot{x}_{\mathrm{v}} = \begin{cases} \dot{x}_{\mathrm{v,max}} & \text{for } x_{\mathrm{v}} < x_{\mathrm{v,ref}} \\ 0 & \text{for } x_{\mathrm{v}} = x_{\mathrm{v,ref}} \\ -\dot{x}_{\mathrm{v,max}} & \text{for } x_{\mathrm{v}} > x_{\mathrm{v,ref}} \end{cases} \tag{2.29}$$

This model is utilised to reduce the number of state in the simulation model, and is furthermore found to be a good approximation of the valve movement.

2.2.5 Extracted Energy

The extracted energy from the ocean waves is defined as the mechanical energy which is absorbed by the cylinder from the waves. The extracted energy by a one float system is hence given as:

$$E_{\mathrm{har}}(t) = \int F_{\mathrm{PTO}}(t)\dot{x}_{\mathrm{c}}(t)dt \tag{2.30}$$

Here energy is extracted when the PTO force and the piston velocity are of the same sign, hence opposite in direction. Note the definition $\dot{x}_{\mathrm{c}} = d_{\mathrm{arm}}\omega_{\mathrm{arm}}$, see Fig. 2.8. The extracted energy is naturally dependent on the incoming wave, but also the PTO force influence the energy extraction.

The average power extraction is given as:

$$\bar{P}_{\mathrm{har}} = \frac{E_{\mathrm{har}}(T)}{T} \tag{2.31}$$

Where T is the time duration of the time series wave input to the simulation model.

2.2.6 Energy Output to the Common Pressure Lines

The output energy to the common pressure lines from one float is given as:

$$E_{\mathrm{out}}(t) = \int \sum_{j=1}^{m} \left(Q_{\mathrm{l}.j}(t)\ p_{\mathrm{l},j}(t)\right) dt \tag{2.32}$$

Where $Q_{\mathrm{l}.j}(t)$ is the fluid flow into the j'th pressure line. The sign of the flow indicates if the pressure line is receiving or supplying power/energy to the PTO cylinder. The average power output is given as the energy output divided by the time duration of the simulation.

$$\bar{P}_{\mathrm{out}} = \frac{E_{\mathrm{out}}(T)}{T} \tag{2.33}$$

The length of the time series for the simulation vary from one sea state to another, therefore average power output is utilised for comparison.

2.3 Force Shift Algorithms

The choice of which force to apply is performed with a Force Shift Algorithm (FSA). The force control algorithms utilised are divided into a general FSA and a valve control algorithm for the bidirectional check valves (discussed in chapter 3) deciding whether the valve is to perform active or passive switching for a given force shift. The on/off valves are controlled solely based on the FSA.

Based on the system configuration, (selection of working areas and pressure lines) a force vector, $\bar{F}_{\text{vec}}$, containing the applicable forces is constructed. A force error for the discrete force may then be defined as:

$$F_{\text{e}}(k) = F_{\text{PTO.ref}}(t) - \bar{F}_{\text{vec}}(k) \tag{2.34}$$

Hence, with $F_{\text{PTO.ref}}$ being the PTO force reference the force error when applying force number k is given by $F_{\text{e}}(k)$.

FSA-I is given by;

$$k = \arg\min\{|F_{\text{e}}(k)|\} \tag{2.35}$$

Hence, the force combination leading to the smallest force error, $F_{\text{e}}(k)$, is chosen.

FSA-II is given by;

$$k = \arg\min\{|F_{\text{e}}(k_-)|, |F_{\text{e}}(k_0)|, |F_{\text{e}}(k_+)|\} \tag{2.36}$$

$$k_- = \arg\min_{k\in S_-}\{E_{\text{sw}}(k)\} \quad , S_- = \{k \,|\, F_{\text{PTO.ref}} - F_{\text{b}} < \bar{F}_{\text{vec}}(k) < F_{\text{PTO.ref}}\} \tag{2.37}$$

$$k_+ = \arg\min_{k\in S_+}\{E_{\text{sw}}(k)\} \quad , S_+ = \{k \,|\, F_{\text{PTO.ref}} < \bar{F}_{\text{vec}}(k) < F_{\text{PTO.ref}} + F_{\text{b}}\} \tag{2.38}$$

However, if

$$S = S_- \cup S_+ = \emptyset \tag{2.39}$$

$$k = \arg\min\{|F_{\text{e}}(k)|\} \tag{2.40}$$

$E_{\text{sw}}(k)$ is a function describing the switching loss associated with a force shift from the current force to the force k, see Eq. (2.41).

The control furthermore includes a minimum on-time for each force to reduce chattering. During the investigation of energy production this minimum on-time, T_{minOn} is set to 350 ms. The force band is set to, $F_{\text{b}} = 150$kN. The settings of the minimum on-time and the force band are chosen based on time series simulations in paper [B] and [C]. Setting F_{b} too high will impose poor force tracking while a low value of F_{b} will impose a large number of switchings. An illustration of FSA-II is given in Fig. 2.9. Note that at the time instant of a force shift the algorithm may only choose a force level within the grey force band $\pm F_{\text{b}}$. Furthermore the algorithm choose the force within the grey force band leading to the smallest energy loss $E_{\text{sw}}(k)$. Hence, the force error is not minimised, see e.g. the red line. Here the force error could be significant lower, however the lower force level is chosen since it leads to the smallest switching loss $E_{\text{sw}}(k)$.

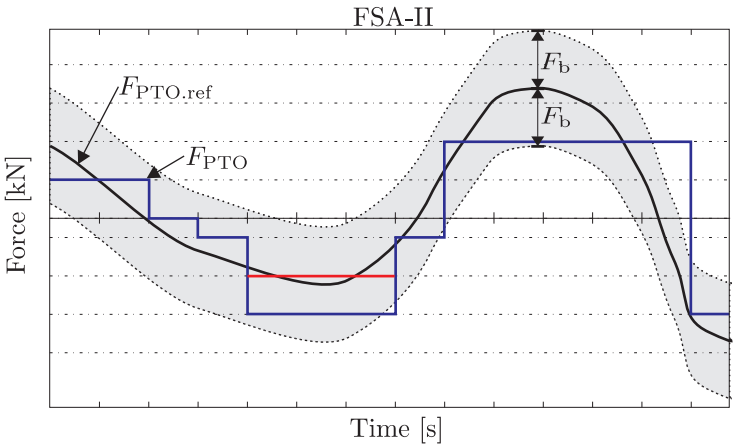

Figure 2.9: *Illustration of FSA-II. The horizontal lines indicates the applicable force levels.*

The pressure line which a given cylinder chamber should be connected to is hence based on eq. (2.35) or (2.36). The inevitable energy loss associated with a force shift is the sum of losses due to the pressure shifts performed in each cylinder chamber. The switching loss in a non-moving cylinder chamber is given as:

$$E_{\mathrm{sw}}(k) = \sum_{i=1}^{i=n} \frac{V_i}{2\beta} \left(p_{\mathrm{c},i}(k_0) - p_{\mathrm{c},i}(k)\right)^2 \tag{2.41}$$

Recall that k_0 indicates the current force applied and k indicates the force to switch to. As clearly seen from (2.41) the energy loss associated with a force shift depends on the size of the pressure change and on the size of the volume. Consequently a given force shift may lead to various energy losses accordingly to the piston position, why the switching loss must be calculated online in the controller.

2.4 System Configurations

For the generic simulation model two parameter sets, U_{PL} and U_{A} holding various system configurations are constructed and used as inputs to the simulation model. Based on the results in paper [B] and [C] it is chosen to utilise systems with two or three pressure lines in combinations with multi-chamber cylinders with two or three cylinder chambers for the brute force optimisation. The set, U_{PL}, of pressure line combinations are constructed such that the low pressure line always is 20 bar, no pressure lines have equal value, and the maximum pressure setting is 260 bar. The pressure line set is given as:

$$U_{\mathrm{PL}} = U_{\mathrm{P2}} \cup U_{\mathrm{P3}} \tag{2.42}$$

Where the subset for two and three pressure lines are given as:

$$U_{\mathrm{P2}} = \left\{ \begin{array}{c} P_{\mathrm{L}} \\ P_{\mathrm{H}} \end{array} \middle| \left\{ \begin{array}{c} 20 \\ 20 + 30l_1 \end{array} \right\} \text{ for } l_1 = \{1..8\} \right\} \tag{2.43}$$

$$U_{\mathrm{P3}} = \left\{ \begin{array}{c|c|cc} P_{\mathrm{L}} & \left\{ \begin{array}{c} 20 \\ 20+30l_1 \\ 20+30l_2 \end{array} \right\} & \text{for} & \begin{array}{c} l_1 = \{1..7\} \\ l_2 = \{2..8\} \\ l_1 < l_2 \end{array} \\ P_{\mathrm{M}} & & & \\ P_{\mathrm{H}} & & & \end{array} \right\} \tag{2.44}$$

As seen the minimum pressure difference between adjacent lines is set to 30 bar.

For the working areas the set, U_{A}, is constructed such that, the cylinder is symmetric, the maximum and minimum size of a working area is 420 cm^2 and 21 cm^2 respectively, which corresponds to a full circle with diameter of approximately 23 cm and 5 cm. The area set is given as:

$$U_{\mathrm{A}} = U_{\mathrm{A2}} \cup U_{\mathrm{A3}} \tag{2.45}$$

Where the subset for two and three working areas are given as:

$$U_{\mathrm{A2}} = \left\{ \begin{array}{c|c} A_1 & \left\{ \begin{array}{c} a_1\hat{A}_{\max} \\ -a_1\hat{A}_{\max} \end{array} \right\} \text{ for } a_1 = \{1, 2..20\} \\ A_2 & \end{array} \right\} \tag{2.46}$$

$$U_{\mathrm{A3}} = \left\{ \begin{array}{lr|c} A_1 = & a_1\hat{A}_{\max} & a_1 = \{2..20\} \\ A_2 = & -a_2\hat{A}_{\max} & a_2 = \{1, 2..19\} \\ A_3 = & (a_2 - a_1)\hat{A}_{\max} & a_1 > a_2 \end{array} \right\} \tag{2.47}$$

Where the factor $\hat{A}_{\max}$ is a measure for the resolution used in the analysis and given as:

$$\hat{A}_{\max} = \frac{A_{\max}}{20} = 21 \text{ cm}^2 \tag{2.48}$$

With these pressure line and cylinder area sets given, a number of systems defined by PL and AP which are pressure line and area vectors belonging to each of the to sets. Hence;

$$PL(6) = [20\ 200] \text{ bar} \tag{2.49}$$

$$PL(10) = [20\ 50\ 110] \text{ bar} \tag{2.50}$$

Likewise for the cylinder areas;

$$AP(1) = [-210\ 210] \text{ cm}^2 \tag{2.51}$$

$$AP(10) = [-231\ 105\ 126] \text{ cm}^2 \tag{2.52}$$

2.5 Optimal System Configuration

The discrete nature of the discrete PTO system configuration leads to several local optimums why a brute force optimisation approach is employed. Hence, the energy extraction from with each system combination defined above (PL(n1) and AP(n2)) is found through simulations. The performance for each system is calculated for the WEC when exposed to each of the three sea states, see Fig. 2.10 for average power output in sea state II and III (Extracted power, output power and conversion efficiency in the three sea states may be found in paper [D]). The axes AP and PL indicate the various multi-chamber and pressure line configurations respectively.

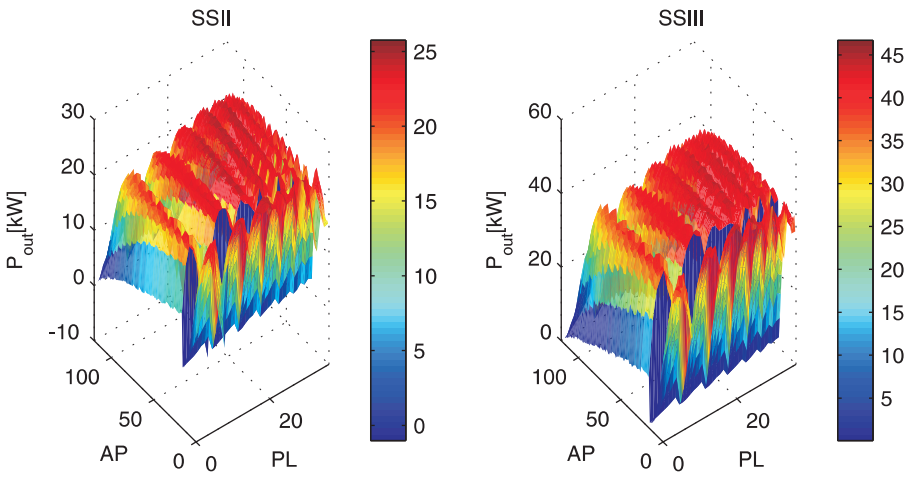

Figure 2.10: *Average power output to the common pressure lines in sea state II and III. The pressure lines and area vectors (PL and AP) are given in section 2.4.*

With these solution sets of average extracted and output power for each system configuration in the three sea states one may chose the system configuration yielding the best performance. Best performance is here depending on the objective; highest energy extraction, highest energy output or highest conversion efficiency.

A WEC installation site may be represented by a scatter diagram holding the time distribution of wave conditions for the given site, as seen in Tab. 2.1. One may see T_{sea} in (2.53) as a very simple representation of the scatter diagram, where T_{sea} indicates time distribution between sea state I, II and III.

$$T_{\text{sea}} = [T_{\text{SS1}}\ T_{\text{SS2}}\ T_{\text{SS3}}] \tag{2.53}$$

Naturally one could include more sea states in T_{sea}, however, with a corresponding significant increase in computation time of the optimisation. T_{sea1} and T_{sea2} are utilised as examples where the optimal system configuration is desired for these two site conditions.

$$T_{\text{sea1}} = [0.8\ 0.1\ 0.1] \tag{2.54}$$
$$T_{\text{sea2}} = [0.1\ 0.7\ 0.2] \tag{2.55}$$

The objective function maximising the energy output to the common pressure lines is chosen, so the system configuration vectors may be given as:

$$(\underline{A}_{\text{p}},\ \underline{P}_{\text{L}}) = \arg\max\left(\Sigma_{SS=1}^{3}\left[\bar{P}_{\text{out}}(\underline{A}_{\text{p}},\ \underline{P}_{\text{L}}, SS)T_{\text{sea}}(SS)\right]\right) \tag{2.56}$$

The optimisation hence gives the piston areas for the multi-chamber cylinder and the common pressure lines leading to the maximal average power output to the common pressure lines in the sea conditions given by the time distribution T_{sea}. In Fig. 2.12 the average power extraction and average power output to the common pressure lines are given for the two site conditions T_{sea1} and T_{sea2} respectively. Furthermore the conversion efficiency is given. The results are plotted as "functions" of the system configuration, hence, the configuration of the multi-chamber cylinder and the common pressure lines.

As expected the discrete nature of the system imposes several local optima. It is seen that the surfaces are arranged in mountain chains and valleys. Due to the difference in sea condition applied by T_{sea} a significant difference is seen in energy results for the two columns. The optimal configuration for the two sea conditions T_{sea1} and T_{sea2} in term of maximal average power output to the common pressure lines are given in table 2.2. Note, that both configurations consists of a three chamber cylinder and three common pressure lines.

	A_{p} [cm^2]	p_{L} [bar]
T_{sea1}	[−273 105 168]	[20 140 230]
T_{sea2}	[−357 147 210]	[20 110 170]

Table 2.2: *Optimal system configuration for T_{sea1} and T_{sea2} when optimised for maximal average power output in each wave condition.*

2.6 Discussion of System Configuration

The configuration of the discrete fluid power force system highly affects the performance of the WEC. It is clear that the number of cylinder chambers and pressure lines entails the number of applicable forces, and that the size of the piston area and the pressure level dictates the size of the forces. As evident, from the energy losses in a switching chamber being proportional to the square of pressure change and proportional to the volume, the choice of introduce more or larger force by extra pressure lines or cylinder chamber impose different results in conversion efficiency. Practical issues are however not address in the earlier study. Yet introduction of an extra pressure line requires larger effort throughout the entire machine, and requires an extra set of valves in the switching manifold. Employing a cylinder with one more chamber on the other hand only requires a set of extract valves in the switching manifold.

In Fig. 2.11 the normalised average power output to the common pressure lines are given for all the system configurations in each sea state. The normalisation is performed with respect to the maximal average power output,

$$\bar{P}_{\text{out.Nom}}(AP(i), PL(j)) = \frac{\bar{P}_{\text{out}}(AP(i), PL(j))}{\max\left(\bar{P}_{\text{out}}(\underline{AP}, \underline{PL})\right)} \tag{2.57}$$

Hence, this indicates the performance of a system configuration within a given sea state. It is clearly seen how the optimal configuration differ from sea state to sea state. From

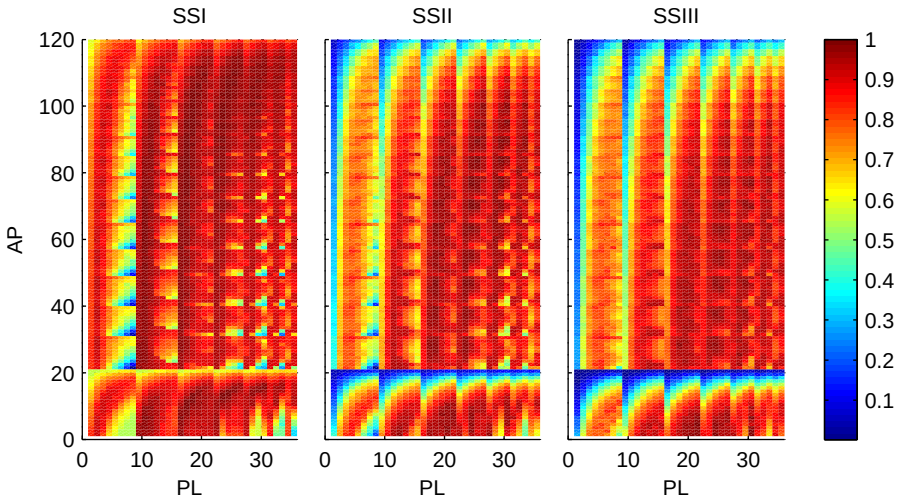

Figure 2.11: *Energy Output for in the three sea states, normalised with the maximum energy output for the given sea state.*

Fig. 2.11 it may been seen how one may choose a symmetric cylinder ($AP = [1\ 19]$) and still reach a good power output. However, if one needs to choose one symmetric cylinder usable in all sea state the pressure levels have to be adjustable to reach high power output in all sea states. Adjustable pressure lines may though not be suitable since the accumulator capacity requirements will increase significantly.

The studies in this chapter shows that numerous system configurations lead to a high energy production, however, it was also shown that numerous system configurations lead to a low energy production. Through the investigations it is seen that an analytical optimisation of the system configuration is infeasible when optimising for energy production in irregular waves. The method utilising time series simulations incorporates the sea state time distribution given by the wave climate at a given installation site. It was shown that the time distribution of the sea state highly influences which system configuration leads to the highest energy production. Hence, one must carefully chose the system configuration based on the wave climate at the installation.

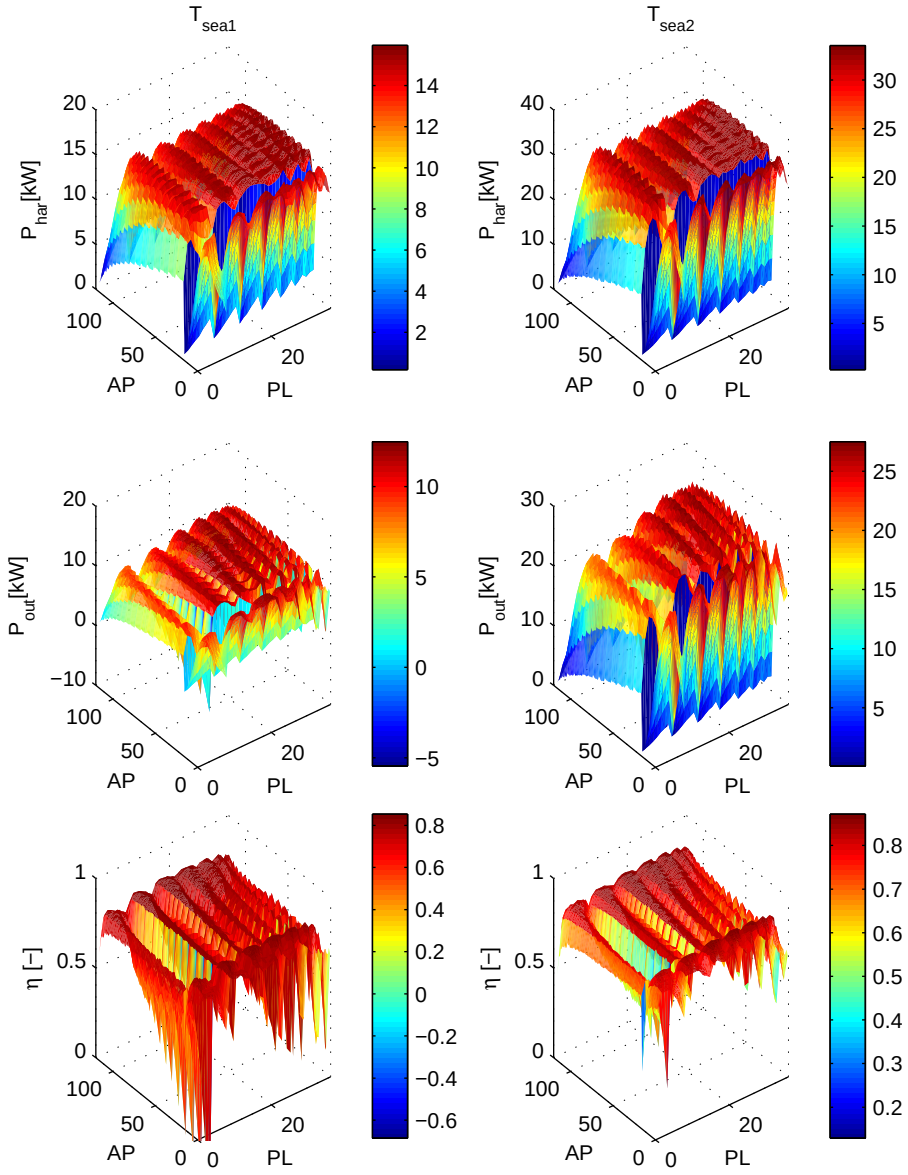

Figure 2.12: *Average extracted and output power along with the conversion efficiency for the site conditions T_{sea1} and T_{sea2} in left and right column respectively. The pressure lines and area vectors (PL and AP) are given in section 2.4.*

Chapter 3

Switching Manifold for DFP Force System

The primary stage of the discrete fluid power force system consists of a multi-chamber cylinder, multiple common pressure lines and a switching manifold. The switching manifold is the controlling element in the force system, which controls the force by controlling which of the common pressure lines are applied to each cylinder chamber. Hence, the valves in the switching manifold control the system not by throttling but by controlling flow directions. As discussed in the previous chapter a valve opening inevitable introduces an energy loss when switching the pressure in a fixed fluid volume. However, if the volume is changing in size the valve opening area influences the energy loss since a throttling loss due to displacement flow occurs in addition to the compressibility loss.

The timing of the disconnection and connection of pressure lines and cylinder chambers affect the pressure in the cylinder chamber, especially if the cylinder chamber volume is changing. If a chamber is cut off from all pressure lines too long the pressure may increase or decrease inappropriately. Connecting two or more pressure lines at the same time on the other hand leads to significant short circuit flow and substantial energy losses.

Hence, both timing of disconnection and connection of the pressure lines and the valve switching time have influence on the energy loss in the switching manifold. The timing between disconnection and connection of the pressure lines is a control issue which is dependent on the valve switching time, the volume gradient, chamber pressure and the fluid compressibility. The valve switching time is on the other hand a design issue, for the valve designer.

In the current chapter two valve topologies are compared and evaluated considering feasibility to support a good PTO force control with low energy losses. Furthermore a conceptual design of piloted on/off and bidirectional check valves are given. Initiating from a theoretical investigation simulation models are utilised to demonstrate an expected dynamic behaviour of the valve concepts. The chapter concludes with a discussion of the valve configuration in the switching manifold.

3.1 Analysis of Valve Topology

On/off valves are proposed whereby the PTO force may be directly controlled by which pressure line is connected to each of the cylinder chambers. This will impose a PTO force continuously controlled by the valve settings. However, the inevitable energy loss due to the pressure shifts and the timing issues in valve actuation may be addressed

by utilising bidirectional check valves. A bidirectional check valve (BCV) is a valve configuration working as a spring loaded check valve for which the checking direction may be changed.

In the following the feasibility of using BCVs and on/off valves in a discrete fluid power force system is discussed. It is discussed for a general discrete force system and for a discrete force system designed for WECs. During the analysis the valves are designed with equal nominal pressure drop at nominal piston velocity, hence, the flow rate for each valve fits the cylinder chamber to which it is connected. The on/off valves are in the topology analysis modelled as simple 2/2 valves. The bidirectional check valves are on the other hand modelled as ideal spring loaded check valves, for which the flow direction may be changed. The opening area is for both valves types modelled linearly proportionally to the valve poppet position and the valve flow is modelled utilising the orifice equation [41]. The dynamics of both the on/off and BC valves are modelled ideally, hence the on/off valve switches states infinitely fast and force balance is always present for the BCV poppet.

The pressures in the cylinder chambers are in the proposed discrete fluid power force system controlled by the pressure line to which each chamber is connected. However, during connection shifts varying pressure dynamics may be experienced in the cylinder chamber, e.i. the pressure gradient is determined based on whether the cylinder is extending or retracting.

The application of the discrete force system entails the loading on the force system. Hence, if the force system is utilised to actuate a system with a low inertia and driving force the force from the cylinder chamber pressures may easily overcome the load and inertia and entail the system movement. On the other hand, a system with large inertia and large driving force (As for the Wavestar float arm) may be able to overcome the force from the cylinder pressures. This way the fluid force is only opposing the movement enforced by the load. Hence, the kinetic energy of the float and the force applied on the float are sufficient to induce a pressure build-up in the cylinder chamber. In the weak loaded system where the load do not carry energy enough to induce a pressure build-up a pressure change from one pressure line to another may only be accomplished by switching the valves and this way changing the amount of oil in the chamber. However, for a system with a load force exceeding the fluid force from the discrete system a pressure change may be accomplished by closing all valves and using the driving load force to enforce the compression or decompression required to yield a pressure change.

Hence, the bidirectional check valves are not feasible in systems where the discrete force system is the driving system. In wave energy converters the PTO-system is obviously utilised to extract energy from the movements imposed by ocean waves, why, the PTO-system is mainly applying a force smaller than the load, only damping the movement enforced by the waves. The WEC is in other words driving the motion of the PTO-system and bidirectional check valves may be feasible.

The feasibility of bidirectional check valves is analysed by comparing BCVs to on/off valves, in paper [E]. The two valve types are compared by time simulations of a single float Wavestar WEC model utilising the on/off and bidirectional check valves respec-

tively. The comparison is carried out with two system configurations (given in a later section) in terms of the multi-chamber cylinder and the common pressure lines. The valves are evaluated on the energy output to the common pressure lines, the system behaviour and the structural loading imposed.

3.1.1 Pressure dynamics

The pressure dynamics in the multi-chamber cylinder are affected by using bidirectional check valves compared to using on/off valves. Furthermore the pressures in the cylinder chambers are highly affected by the switching time of the valves and the timing between disconnecting from one pressure line until connecting to another pressure line. The pressure dynamics is both depending on the displacement of the piston and the valve flow into or out of the cylinder chamber, further the hydraulic capacitance given by chamber volume and oil stiffness entails the pressure gradient at a given difference in volume change and oil inflow.

In Fig. 3.1 a force shift is illustrated, while the piston has a negative velocity. In chamber 1 a pressure shift from line 3 to 1 is made by disconnecting from line 3 and letting the piston moment impose a pressure decrease by increasing the chamber volume, while connecting to line 1 when the chamber pressure gets just below line pressure 1. On the other hand the pressure decrease in chamber 2 from line pressure 3 to 2 is accomplished by actively disconnecting from line 3 and in same instant connecting to line 2, hence the pressure decrease is accomplished by the flow out of the chamber across the valve.

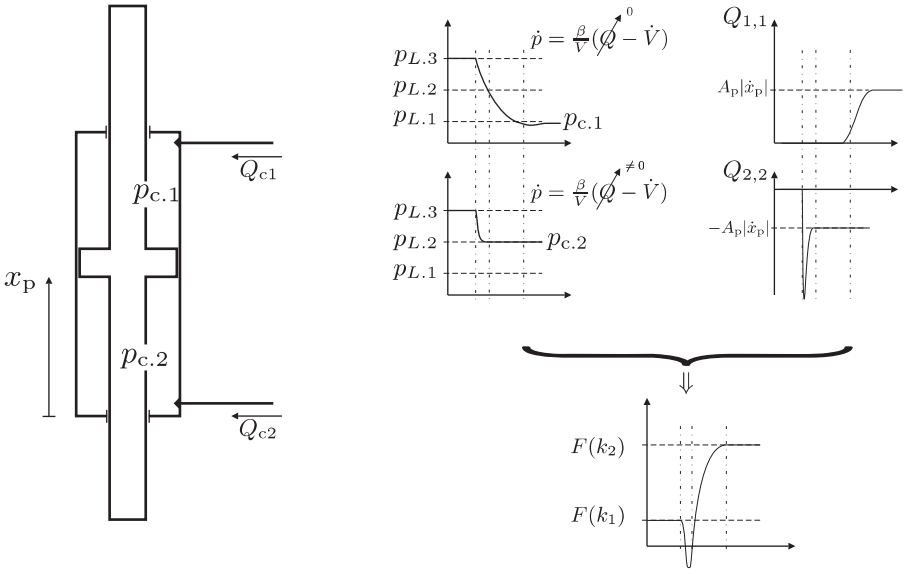

Figure 3.1: *Illustration of chamber pressure dynamics and resulting cylinder force.*

It is seen in Fig. 3.1 how the two type of pressure shifts impose significant different

pressure dynamics in the cylinder chambers. Further it is seen how the valve flow differs with the active valve leading to a significant flow peak yielding a high energy loss. Lastly the resulting force is illustrated, from which one should note that the large difference in pressure gradients impose an unwanted force peak.

The large flow peaks due to the connection of a cylinder chamber at a given pressure to a pressure line with significantly different pressure will enforce energy losses due to throttling. The force peaks may result in poor PTO force tracking hereby degrading the energy extraction from the ocean waves. While this may decrease the energy production, the force peaks may also impose and increase structural loads on the float arm.

3.1.2 Comparison of Valve Topology

The extracted energy, the energy output to the common pressure lines and the dynamic performance of the system utilising on/off or BC valves are investigated in paper [E]. The investigations in paper [E] are conducted for the two system configurations seen in Fig. 3.2. System 1 consist of a symmetric two chamber cylinder in connection with four common pressure lines, whereas System 2 consist of a three chamber cylinder and three common pressure lines. The valve connection is here illustrated as two check valves, indicating the function of the BC-valve working as check valve in either direction based on the pilot settings.

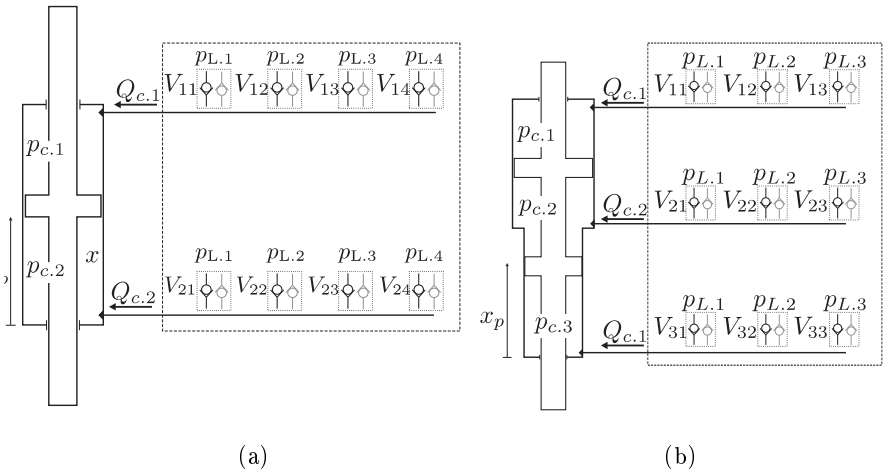

Figure 3.2: *Illustration of the system configuration utilised in the feasibility study of BC valves. System 1 (a) and System 2(b).*

The extracted energy and the energy output to the common pressure lines showed in paper [E] are close to equal for the system utilising on/off and BC valves, however the conversion efficiency is seen to be slightly higher for the BCV system. Hence, a smaller energy loss is obtained in the system which may result in less wear. On the other hand the amount of extracted energy is higher for the on/off valve system due to a better force tracking. An example of the energy results are given in Fig. 3.3, note the very

small difference in the average power obtained.

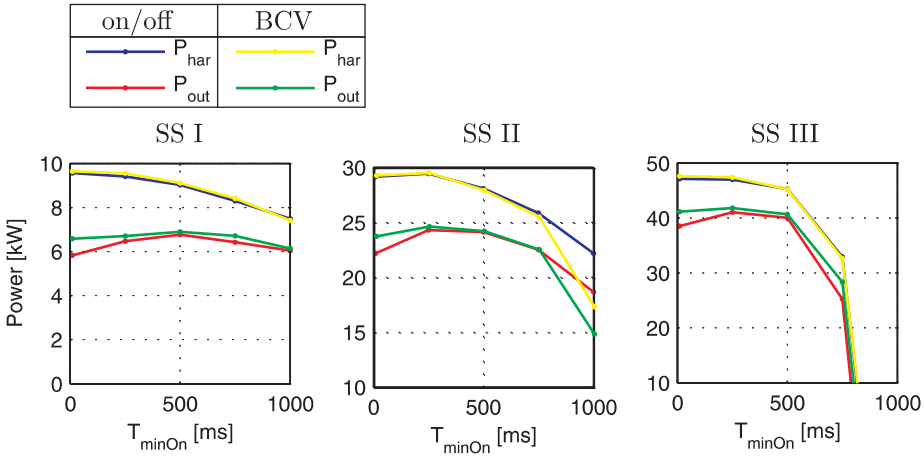

Figure 3.3: *Average harvested power and power output for systems utilising on/off and bidirectional check valves respectively. The results are given for the three sea states.*

The bidirectional check valves impose some pressure shifts with huge difference in pressure gradients yielding a large number of unwanted force peaks. These extra force peaks may lead to fatigue problems due to the added number of loads and the increased loads. The force shift steps imposed are counted and arranged in intervals. In Fig. 3.4 the count of force shift steps in each interval is given in blue bars for the discrete force reference and in black bars as the actual applied force steps in the simulation for one of the test systems (system 2) utilising on/off and BC valves respectively.

The actual force applied is clearly seen to be shifted to the right for the BCV system, hence larger force shift steps are imposed than entailed by the reference. For the on/off valve system on the other hand the actual force shift steps are rather close to those of the force reference. Similar results are obtained when employing system configuration 1, though the force shifts imposed are larger.

The topology analysis demonstrates that bidirectional check valves and on/off valves imposes approximately equal energy output, however the use of bidirectional check valves yield some minor increase in the structural loads applied to the float arm from the multi-chamber cylinder. The final conclusion given in paper [E] states bidirectional check valves to be feasible for use in the wave energy converters, however not necessarily better than on/off valves. The choice of valve topology is discussed further in the end of this chapter.

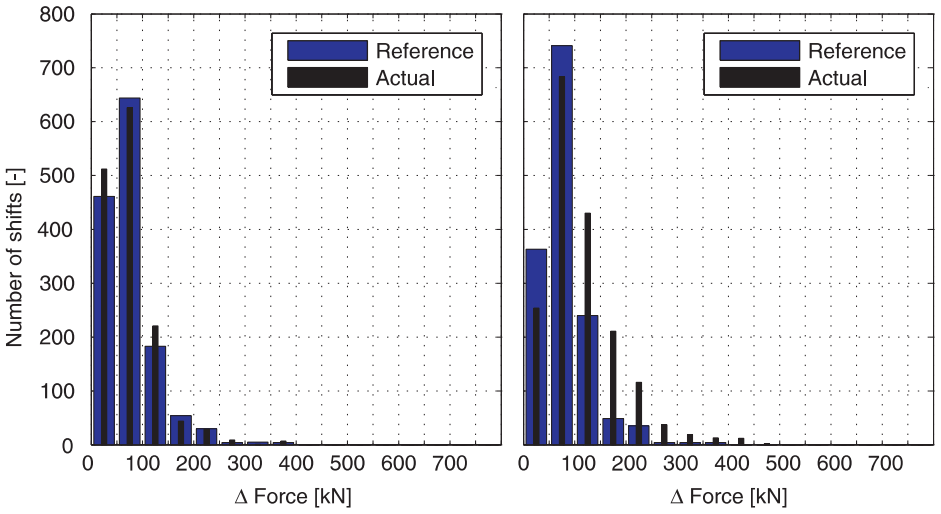

Figure 3.4: *Force shifts counts for system 2 utilising on/off and bidirectional check valves left and right respectively.*

3.2 Conceptual Design of Valve for Switching Manifold

The valves for the switching manifold will be designed as a two stage piloted valve independently of whether it is of the on/off or bidirectional check type. In this section the conceptual design of the valves will be discussed. Both the main stage, the pilot stage and the combination of the two stages are discussed. A major issue is the configuration of the pilot system since this entails the functionalities obtainable and some practical requirements for the manifold design. In Fig. 3.5 various set-ups of the pilot system are illustrated.

Some concepts; (b) and (c) are fully electronic controlled, whereas concepts (a), (d), (e) and (f) are partly hydro-mechanically controlled. The shuttle valve included in (a), (d), (e) and (f) induces a stay closed stage, and hence, the requirements for the pilot valve may be lowered. The functionality of the six valve concepts in Fig. 3.5 are briefly described in the following:

(a) This valve concept is an on/off valve. The pilot pressure p_x may either be set to tank pressure or the highest valve port pressure, leading to a valve having two states. Closed or opened, for the pilot pressure equal to highest port pressure and tank pressure respectively. This concept requires an external tank connection and a shuttle valve.

(b) This valve concept is an on/off valve. The pilot pressure p_x may either be set to tank pressure or pilot supply pressure, leading to a valve having two states. Closed or opened, for the pilot pressure equal to pilot supply port pressure and

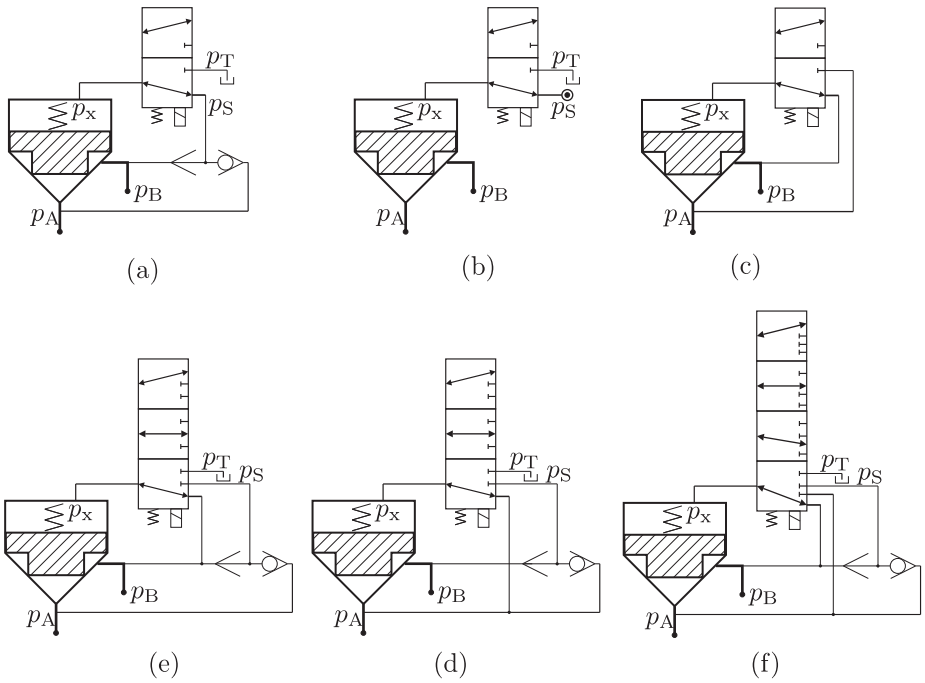

Figure 3.5: *Illustrations of conceptual pilot system configurations.*

tank pressure respectively. This concept requires an external tank and supply line. Furthermore, the pilot supply pressure must be higher than the highest pressure at the valve ports at any time.

(c) This valve concept may be utilised both as an on/off valve and a bidirectional check valve. The pilot pressure p_x may be set to either of the port pressures p_A or p_B, leading to a valve having two states. However, which of the pilot settings that leads to an open or closed main stage is dependent on the sign of the port pressure difference defined as $\Delta p = p_A - p_B$. This valve concept do hence not require any external connection, but pressure measurements are required when choosing pilot valve position based on opened or closed signal. This valve concept works as a check valve with flow from A to B by letting $p_x = p_B$ and vice versa for opposite flow direction.

(d, e) These concepts are one directional check valves with forced on/off valve possibility. The pilot pressure p_x may either be set to tank pressure, the highest valve port pressure or the port pressure at A or B for (d) or (e) respectively, leading to three states for the valve control. The first two gives opened and closed states and the third gives checking possibility in one direction. (d) checking from port B to A and (e) checking from A to B, this third stage make little sense when the

area configuration is made as on/off valve. This concept requires an external tank connection and a shuttle valve.

(f) This valve concept is primarily a bidirectional check valve with forced on/off possibility. The pilot pressure p_x may either be set to tank pressure, the highest valve port pressure or either of the two port pressures p_A or p_B, leading to opened or closed stage for pilot pressure equal to highest port pressure and tank pressure respectively and checking in each direction depending on the connected port pressure. This valve requires an external tank connection and a shuttle valve.

3.2.1 Main stage topology

The main stage of the switching valve is designed with a rated flow of 1000 L/min@5bar. Further the main stage is designed to allow fast valve switching. In [42] a switching time of less than 15 ms was found feasible for the proposed discrete PTO-system. Two poppet topologies are described, investigated and evaluated in a theoretical analysis. The two poppet topologies are illustrated in Fig. 3.6 (a) and (b). Both valves have main flow path between p_1 and p_2. The pilot pressure, p_x may be set to either tank pressure, p_T and the pressure at port 1, p_1. Hence, the valves given in Fig. 3.6 are similar to the valve concept in Fig. 3.5 (a), though, the shuttle valve is omitted and only port A/1 may be utilised. However, with some minor adjustments the illustrated valve may be equal to that in Fig. 3.5. In the valves given here the pilot valve is build into the valve housing enabling a compact valve design.

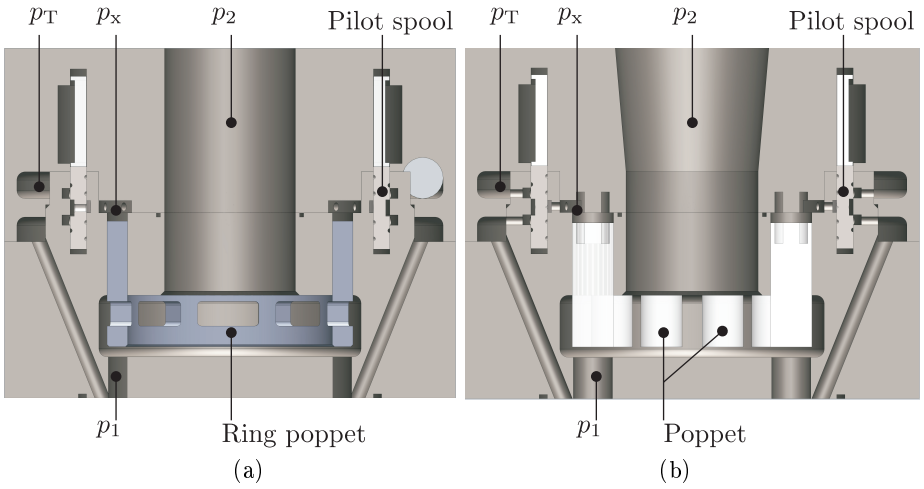

Figure 3.6: *Illustration of the two poppet topologies proposed for the main stage. (a) Ring-poppet. (b) Multi-poppet.*

The ring-poppet topology (a) utilises a single poppet shaped as a ring. The ring shape is proposed to decrease the poppet mass and the pilot volume compared to a traditional solid poppet. The multi-poppet topology (b) utilises a multiple number of solid poppets.

The multiple numbers of poppets requires smaller poppets leading to shorter stroke length and thereby smaller pilot volume. For both poppet topologies a rated flow of 1000 L/min@5bar is utilised as main design criteria. The two poppet topologies are further illustrated in the Fig. 3.7.

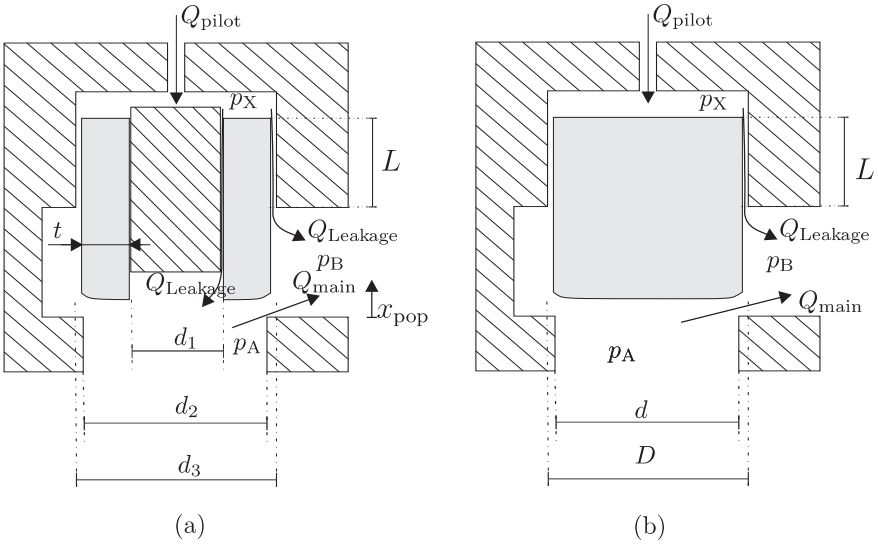

Figure 3.7: *Illustration of main stage topologies, (a) ring-poppet (b) multi-poppet.*

Design functions describing the poppet diameter, the average needed pilot flow for a full valve stroke and expected leakage flow are derived in paper [F] and [G] for the bidirectional check and on/off valve respectively, and reprinted here for the BC-valve for both the ring- and multi-poppet topology. The functions are based on the nomenclature given in Fig. 3.7.

Multi-poppet	Ring-poppet
$d = \sqrt{\frac{1}{n}} \left(\frac{Q_{\text{nom}}}{C_{\text{d}} \frac{\pi}{4} \sqrt{\frac{2}{\rho} \Delta p_{\text{nom}}}} \right)^{\frac{1}{2}}$ $D = \sqrt{2} d$	$d_1 = -t + \sqrt{d_2^2 - t^2}$ $d_2 = \left(\frac{Q_{\text{nom}}}{C_d \frac{\pi}{4} \sqrt{\frac{2}{\rho} \Delta p_{\text{nom}}}} \right)^{\frac{1}{2}}$ $d_3 = t + \sqrt{d_2^2 - t^2}$
$\Delta V_{\text{X}} = n \frac{d^3 \pi}{8}$	$\Delta V_{ring} = t d_2 \frac{\pi}{4} \sqrt{d_2^2 - t^2}$
$Q_{\text{pilot}} = n \frac{d^3 \pi}{8 T_{\text{sw}}}$	$Q_{\text{pilot.ring}} = t d_2 \frac{\pi}{T_{\text{sw}} 4} \sqrt{d_2^2 - t^2}$
$Q_{\text{leakage}} = n d \sqrt{2} \frac{\pi \varepsilon^3}{12 \mu L} \Delta p_{\text{x-B}}$	$Q_{\text{leakage.ringA}} = d_1 \frac{\pi \varepsilon^3}{12 \mu L} \Delta p_{\text{x-A}}$ $Q_{\text{leakage.ringB}} = d_3 \frac{\pi \varepsilon^3}{12 \mu L} \Delta p_{\text{x-B}}$

Table 3.1: *Design function for the bidirectional check valve.*

The results of the design functions for the bidirectional check and the on/off valve are seen to be similar for the two main stage topologies. In Fig. 3.8 the needed pilot flow, expected leakage and the poppet diameters are given for the ring- and multi-poppet topology in (a) and (b) respectively, for the bidirectional check valve design.

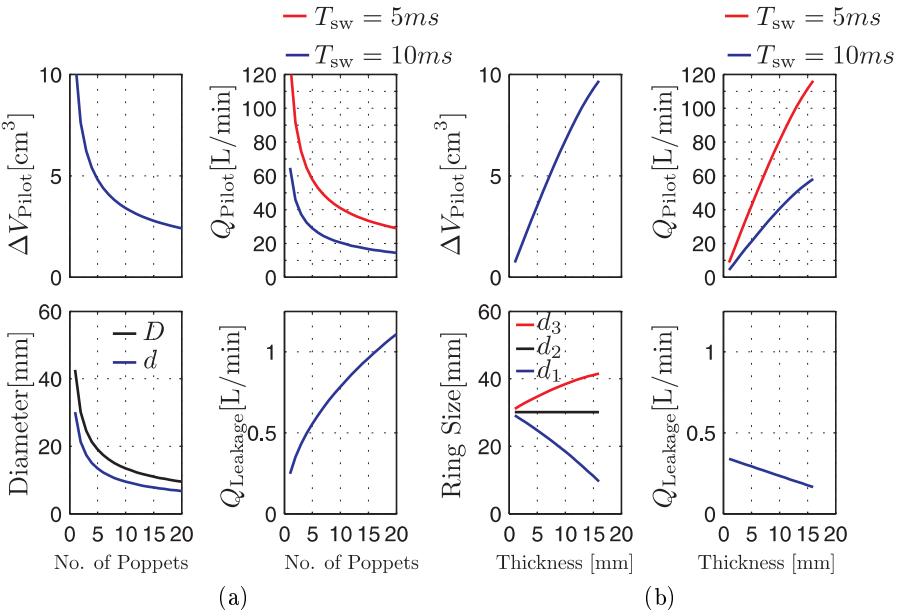

Figure 3.8: *Average pilot flow requirements, expected leakage flow and poppet diameter as a function of ring thickness and number of poppets respectively (a) and (b).*

From the design functions in Fig. 3.8 it is seen that the multi-poppet topology requires less pilot flow when the ring thickness exceeds a reasonable 5 mm and the multi-poppet number exceeds 8. This is seen true for the on/off valve at ring thickness of 5 mm and only 3 multiple poppets in paper [G]. Due to this, the multi-poppet topology is chosen for further studies. However the increase in poppet numbers is followed by an increasing leakage and increasing complexity in the geometric placement of poppets and pilot system.

3.2.2 Pilot Valve

Design of the pilot valve has not been included in the current work, however some various issues concerning the pilot valve have been discussed. In the simulation studies of valve configurations three pilot valves are utilised. The pilot valves included in the simulation models are all state of the art valves. The pilot valves are all 3/2 way valves, the possibility of employing two 2/2 way valves are not included in the simulation model, however shortly mentioned in paper [F] and [G]. Furthermore, special dynamic requirements on the pilot valves for the stay closed state of the bidirectional check valve,

3.5 (c), are discussed in paper [F]. The investigations showed that for on/off valves the rated flow is of great importance. This is also the cased for the BC-valve, however, the BC-valve further requires a fast pilot valve switching if the BC-valve is to be used at intermediate pressure line. In the following chapter test results from a BC-valve concept test are given. For the BC-valve the pilot valve switching time must be in the range of 2 ms, to avoid unintended opening of the check valve. The required rated flow is found to be highly dependent on the main stage design, however the expected required rated flow is in the range of 20 - 40 L/min@5bar.

3.2.3 Test of Bidirectional Check Valve Concept

The simplest concept proposed for the BC-valve is the one in Fig. 3.5 (b) where a logic main stage with area configuration A:B:X = 1:1:2 is utilised combined with a direct actuated 3/2 valve. The test set-up in Fig. 3.9 was constructed to test the proposed BC-valve concept. A commercial WL22SD.. (size 10 - 125L/min@5bar) Bucher valve was employed as main stage while a FSVi 2.0 (10L/min@5bar) valve from LCM was utilised as pilot valve.

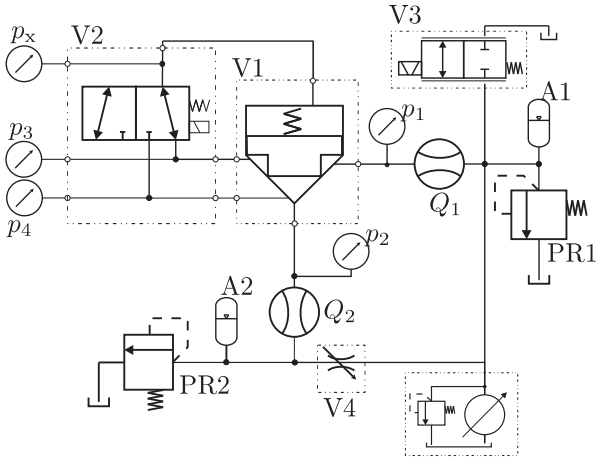

Figure 3.9: *Functionality test set-up for the bidirectional check valve concept. V1 is the main stage and V2 is the pilot stage.*

With the test set-up the proposed BC-valve concept was shown achievable. In Fig. 3.10 pressure and flow measurements are given for passive and active valve switching as well as for the stay closed mode. All plots in the figure follow the same color code and show the same data in the same plot position. Color code: p_1-red, p_2-blue, p_x-black, Q_1-green, Q_2-magenta, u_{v3}-dash dot blue, u_{v2}-dash dot black.

From Fig. 3.10 the BC-valve concept proposed is seen to work as intended. However, the used test set-up did not allow for a measurements of the valve switching time, which have to be proven in a later design phase.

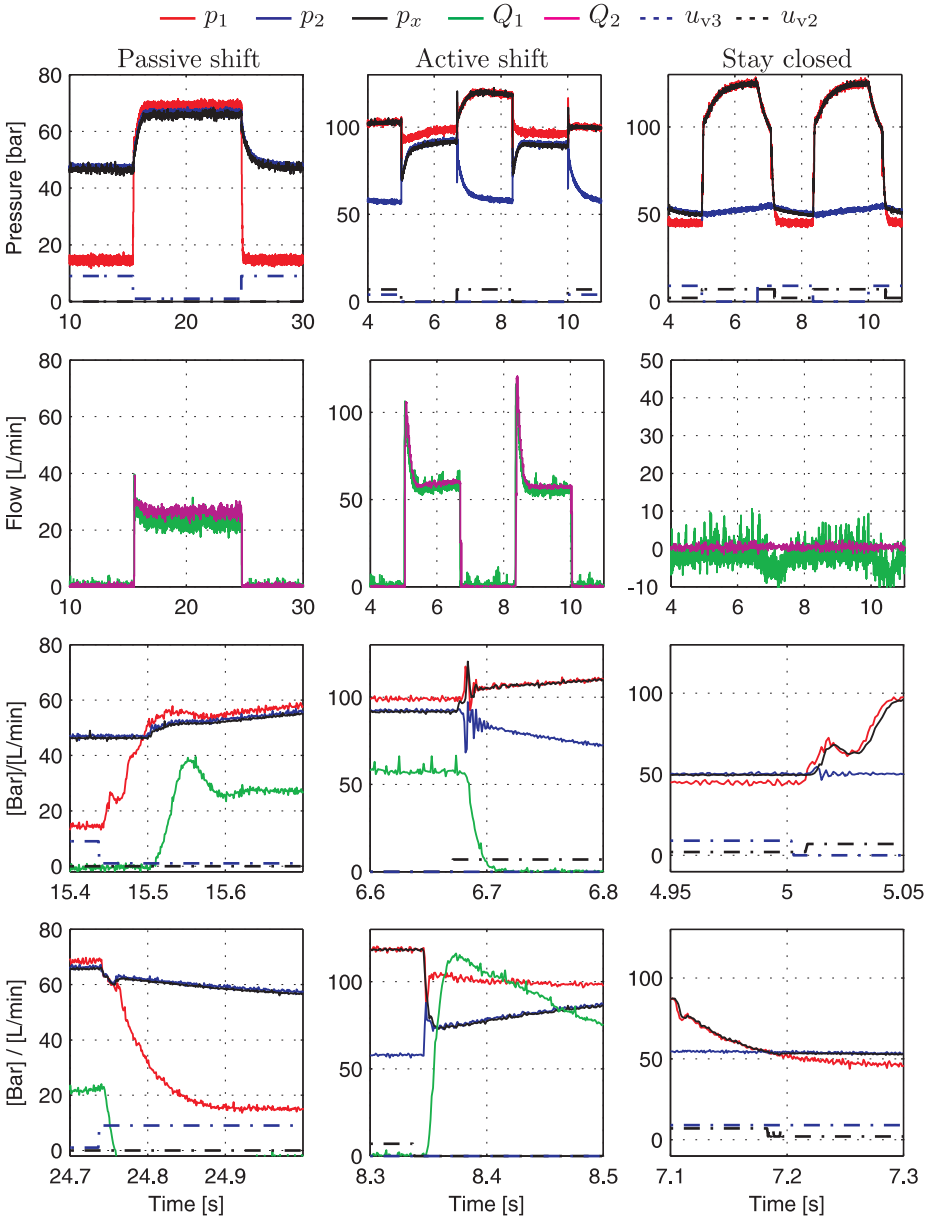

Figure 3.10: *Measurements from the functionality test of the BC-valve concept. Results for Passive and active valve shifts are given along with results from the stay closed mode.*

3.2.4 Simulation of on/off Valve

To facilitate an evaluation of various valve configurations, in terms of number of poppets, choice of pilot valve and pilot pressure configuration, a simulation model is constructed. The system modelled is illustrated in Fig. 3.11. The valve configuration is directly connected to a cylinder chamber, which is utilised to emulate the volume chamber experienced in the multi-chamber cylinder. The other valve port is connected to a fixed volume with a constant pressure through a fixed orifice. As seen the pilot valve may be connected to either tank pressure, p_{T} or to the pilot supply pressure, p_{S}. The pilot supply pressure is either the highest internal pressure, hence, $p_{\mathrm{X}} = \max(p_{\mathrm{A}}, p_{\mathrm{B}})$ or the pilot supply given as an external supply pressure $p_{\mathrm{X}} = p_{\mathrm{ex}}$.

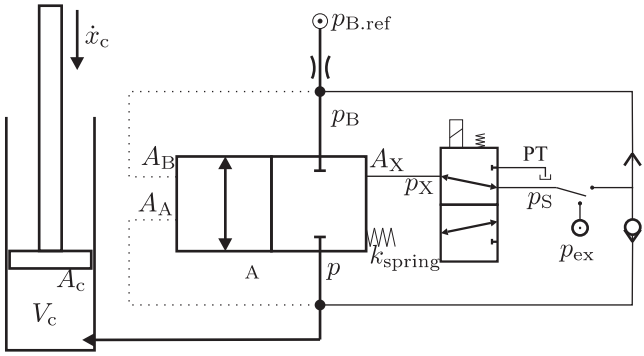

Figure 3.11: *Valve test set-up, where the main stage from A to B is given as a multiple number of poppets. The pilot pressure is either taken from external p_{ex} or the internal shuttle valve.*

The valve model is constructed in a generic way to facilitate comparison of various valve configurations. Hence, numbers of main stage poppets, size and dynamics of pilot valve, spring setting and operating conditions are changeable. The model utilises the orifice equation to model the flow through the main and pilot stage.

$$Q_{\mathrm{main}} = C_{\mathrm{d}} n d x_{\mathrm{pop}} \sqrt{\frac{2}{\rho}|p_{\mathrm{A}} - p_{\mathrm{B}}|}\,\mathrm{sign}(p_{\mathrm{A}} - p_{\mathrm{B}}) \tag{3.1}$$

$$Q_{\mathrm{pilot}} = C_{\mathrm{d,p}} A_{\mathrm{d,p}}(x_{\mathrm{v,p}}) \begin{cases} \sqrt{\frac{2}{\rho}|p_{\mathrm{s}} - p_{\mathrm{X}}|}\,\mathrm{sign}(p_{\mathrm{s}} - p_{\mathrm{X}})\,, \hat{x}_{\mathrm{v,p}} = -1 \\ \sqrt{\frac{2}{\rho}|p_{\mathrm{T}} - p_{\mathrm{X}}|}\,\mathrm{sign}(p_{\mathrm{T}} - p_{\mathrm{X}})\,, \hat{x}_{\mathrm{v,p}} = 1 \end{cases} \tag{3.2}$$

Where n is the number of poppets, x_{pop} is the poppet position and $x_{\mathrm{v,p}}$ is the pilot valve spool position. The dynamics of the main poppets are modelled as a single poppet with the use of Newton's second law:

$$\begin{aligned} \ddot{x}_{\mathrm{pop}} m_{\mathrm{pop}} = \; & p_{\mathrm{A}} A_{\mathrm{A}} + p_{\mathrm{B}} A_{\mathrm{B}} - p_{\mathrm{X}} A_{\mathrm{X}} - F_{\mathrm{Friction}} \\ & -k_{\mathrm{spring}}(x_{\mathrm{pop}} + x_{\mathrm{pop,0}}) + F_{\mathrm{Flow}} \end{aligned} \tag{3.3}$$

Where k_{spring}, F_{Flow} and F_{Friction} are the stiffness of the main stage spring, the flow force and the friction force working on the poppet respectively. The friction force is modelled

as the shear forces applied by the oil when the poppets are moving in the housing:

$$F_{\text{Friction}} = \frac{n\mu D\pi L}{\varepsilon}\dot{x}_{\text{pop}} \tag{3.4}$$

The dynamics of the pilot valve is modelled using a critically dampened linear second order system. The flow force on the poppets is found by employing Newtons second law applied to a control volume [41]:

$$F_{\text{Flow}} = \frac{d}{dt}\int_{\text{cv}} u\rho dV + \int_{\text{cs}} u\rho u dA \tag{3.5}$$

Splitting the flow force in a transient and steady state part implies two parts given as:

$$F_{\text{flow.ss}} = Q^2\rho\left(\frac{\cos\phi_{\text{flow}}}{A_2} - \frac{1}{A_1}\right) \tag{3.6}$$

$$F_{\text{flow.tr}} = c_d d\pi\rho L_{\text{d}}\left(\sqrt{\frac{2}{\rho}\Delta p}\dot{x}_{\text{pop}} + \frac{x_{\text{pop}}}{\sqrt{2\rho\Delta p}}\Delta\dot{p}\right) \tag{3.7}$$

Where ϕ_{flow} is the angle at which the flow leaves the control volume and L_{d} is the so called damping length, see Fig. 3.12.

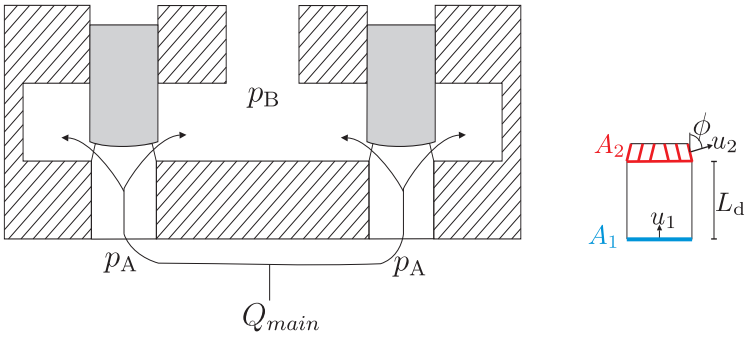

Figure 3.12: *Illustration of the flow path assumed when deriving the flow force.*

The pressure in the pilot chamber and the two volumes at port A and B are modelled using the continuity equation [41]. The volume at port A is given as a cylinder volume connected directly to the valve port A, whereas the volume at port B is a fixed volume connected to the valve and an external pressure source, $p_{\text{B.ref}}$, through a fixed orifice.

$$\dot{p}_{\text{X}} = \frac{\beta}{V_{\text{X0}} - A_{\text{X}}x_{\text{v.pop}}}\left(Q_{\text{pilot}} + A_{\text{X}}\dot{x}_{pop} - Q_{\text{leak}}\right) \tag{3.8}$$

$$\dot{p}_{\text{A}} = \frac{\beta}{V_{\text{c0}} - A_{\text{c}}x_{\text{c}}}\left(-Q_{\text{main}} + A_{\text{c}}\dot{x}_{\text{c}}\right) \tag{3.9}$$

$$\dot{p}_{\text{B}} = \frac{\beta}{V_{\text{B}}}\left(Q_{\text{main}} + \sqrt{|p_{\text{B.ref}} - p_{\text{B}}|}K\text{sign}(p_{\text{B.ref}} - p_{\text{B}})\right) \tag{3.10}$$

Where V_{x0} and V_{c0} are the initial dead volume of the pilot and the cylinder chamber respectively.

The simulation model is utilised to investigate which pilot valve, main stage spring stiffness and initial spring compression that yield the required performance. The pilot supply pressure is the higher of p_A/p_B or $p_{ex} = 250$ bar as seen in Fig. 3.11.

The initial spring force on the main stage is set equal to half of the actuation force applied by the minimum system pressure when opening the valve. By doing so the minimum closing force and minimum opening force are equal. This way a reasonable closing and opening is secured. Hence the initial spring compression and the spring constant must fulfil:

$$x_{\text{pop.0}} = \frac{A_X p_{\min}}{2k_{\text{spring}}} \tag{3.11}$$

Several simulation results are given in [F, G, H] for various combinations of pilot valve data, number of poppets and system pressure. From the simulations the valve parameters in Tab. 3.2 are found for the on/off multi-poppet valve design, as the best possible compromise.

n	Number of poppets	10
d	Inlet diameter	9.5mm
D	Poppet outer diameter	10mm
k_{spring}	Spring constant	1560N/m
$x_{\text{pop.0}}$	Initial spring compression	38mm
Δx_{pop}	Poppet stroke	2.5mm
	Pilot valve	FSVi 2.0*
	Pilot supply	Internal

Table 3.2: *Valve parameter for on/off multi-poppet valve.*

Simulated poppet position and velocity for the multi-poppet valve with the parameters given in Tab. 3.2 are shown in Fig. 3.13 for the opening and closing of the valve. The results are for three system pressure levels where $p_{\text{B.ref}} = [20\ 120\ 220]$ and the open and close signals are given at 0.15 s and 0.20 s respectively, see Fig. 3.11.

From the figure one must note that the closing of the valve is not depending on the system pressure level, contrary the opening of the valve is seen highly dependent on the system pressure. Both the opening and closing time is seen to be well under 10 ms especially if excluding the delay from signal to valve movement. The designer may adjust the spring constant to fit the system pressure if this is relative constant as is the case in the common pressure lines of a secondary controlled system. Hence, the opening and closing may be matched more equal as for a system pressure of 20 bar. The delay is partly due to delay of the pilot valve movement, and with the valve delay being consistent and well known a compensation strategy may be included in the force control.

3.3 Configuration of Switching Manifold

Based on the above findings for possible valve designs, a conceptual design for on/off and bidirectional switching valves capable of active valve switching in under 10 ms are

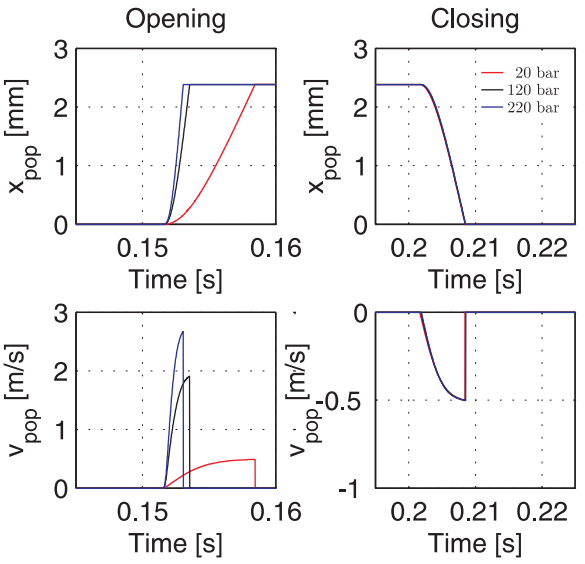

Figure 3.13: *Poppet movement, with values from table 3.2 and system pressure of [20 120 220] bar.*

given in the previous sections. Further the utilisation of either on/off or bidirectional check valve were deemed feasible in paper [E], however feasibility of a combination of the two valve type have yet to be proven.

However, there is a potential in a switching manifold utilising the one directional check valves with stay opened and closed possibilities seen in Fig. 3.5 (d) and (e) in combination with the on/off valve in Fig. 3.5 (a).

The novel proposed manifold layout is seen in Fig. 3.14. The one directional check valve with on/off possibilities is utilised for chamber connections to the low and high pressure line. Like this the cylinder chambers will hydro-mechanically be connected to low pressure if the chamber pressure drops below the low pressure line, this without any control effort. Likewise the cylinder chambers will hydro-mechanically be connected to high pressure if the chamber pressure exceeds the high pressure line. The mid pressure line are fitted with on/off valve connections to the cylinder chambers.

This configuration of the manifold requires two types of pilot valves or pilot valve set-ups. The on/off valve for the mid pressure line requires a 3/2 pilot valve and a shuttle valve, the one directional check valve with on/off possibilities on the other hand requires a 3/3 pilot valve and a shuttle valve.

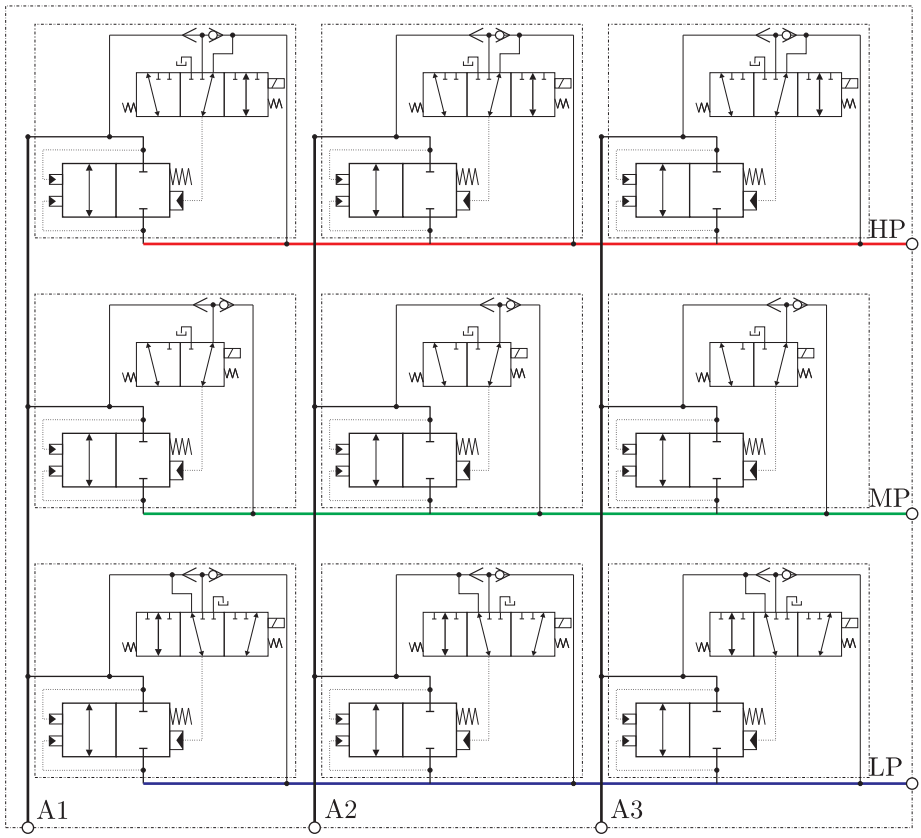

Figure 3.14: *Schematic of a switching manifold utilising one directional check valve with on/off possibilities and on/off valves.*

Chapter 4

Preliminary Test Results

A full scale PTO testbench was designed in paper [I], and installed at Aalborg University, see Fig. 4.1. A prototype of the novel proposed discrete fluid power PTO-system has been installed for testing. However, the testbench and prototype is in the writing moment still in commissioning. Yet a few preliminary test results are included in this dissertation.

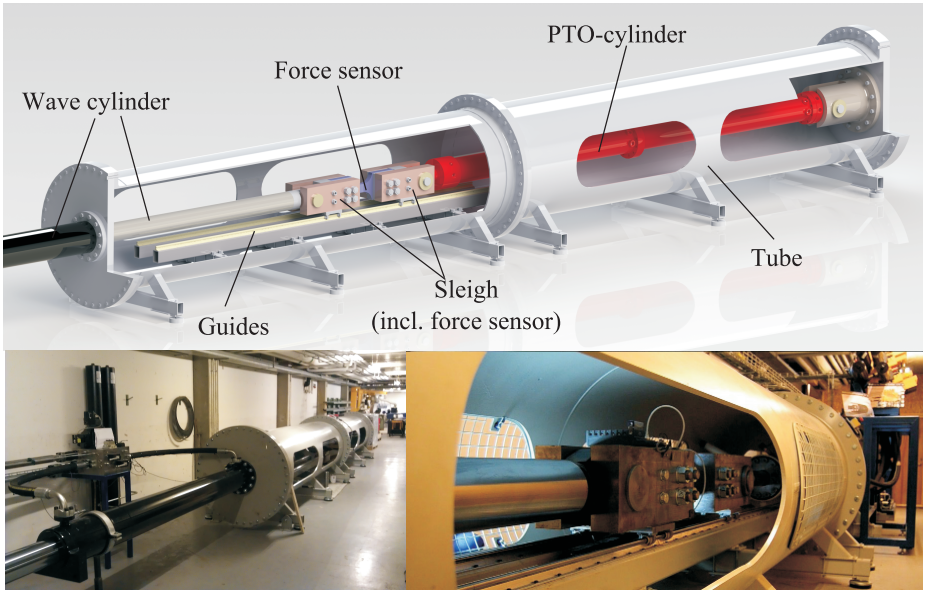

Figure 4.1: *Illustration of the test-bench. [I]*

The discrete fluid power PTO-system prototype tested consists of a five chamber multi-chamber cylinder and three common pressure lines, however the cylinder is operated as a three chamber cylinder by connecting some of the chambers in parallel. The valves employed in the switching manifold are fast 2/2 proportional valves. The proportionality and controllability of the switching valves enables a wide range of possibilities in testing the influence of the valve opening characteristics on the system behaviour. Hence, the proportional valves are utilised for development purpose.

In the following valve shifts are tested while the PTO cylinder piston is moved at a constant velocity, 0.3 m/s and -0.3 m/s respectively. The pressure characteristics in cylinder chamber 3 are given in Fig. 4.2 and 4.3 during pressure shifts with various valve switching times. The chamber pressure is shifted from high to low pressure and from low to high pressure in Fig. 4.2 and 4.3 respectively. Here focus is on how the chamber pressure is changed prior to the new line connection is established. Hence, how much the pressure changes before the valve shift is accomplished.

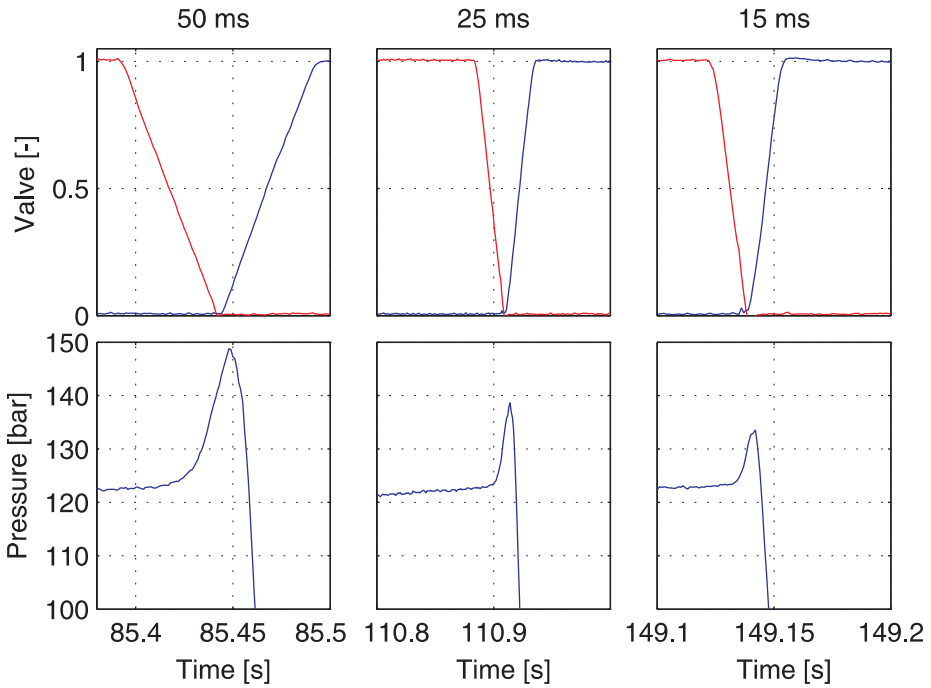

Figure 4.2: *Pressure characteristics during high to low pressure shifts in PTO cylinder chamber 3 with constant piston velocity. Co-published in [43]*

It is seen that a relative large switching time yield a large pressure increase or decrease respectively prior to the end of the valve shift. Hence, this supports the initial requirement on having valves with a switch time in the range of 15 ms seconds.

In Fig. 4.4 the chamber pressure characteristics just after a valve shift is seen, once again for varying valve switching time and piston velocities of 0.3 m/s and -0.3 m/s.

It is clearly seen in Fig. 4.4 that a faster valve switching yield large pressure oscillations in the cylinder chambers. Hence, with a low switching time only a small pressure peak is experienced before finishing the switching whereas large pressure oscillations are seen due to the fast valve switching.

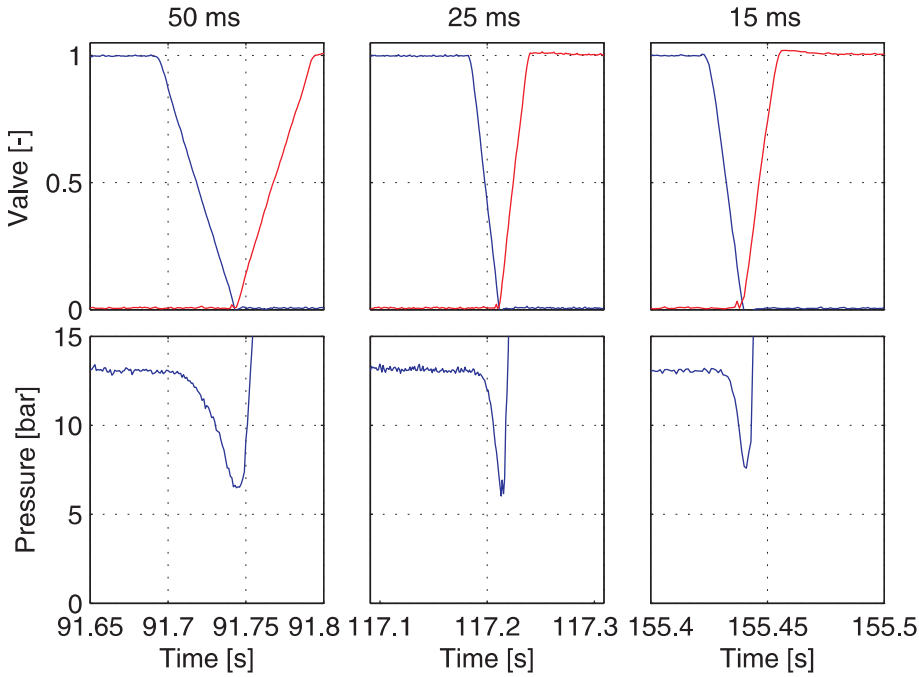

Figure 4.3: *Pressure characteristics during low to high pressure shifts in PTO cylinder chamber 3 with constant piston velocity. Co-published in [43]*

R.H. Hansen has in [43] proposed an improvement of the valve opening characteristic which may lower the pressure oscillations in the cylinder chamber due to a valve switching. This improved valve switching characteristics and according pressure measurements are seen in Fig. 4.5. Here it is compared with the nominal valve switching. For the improved valve switching valve closing is performed as in the normal valve switching, hence, a fast linear closing of the valves is performed. The valve opening is on the other hand performed in a small steep step and a long soft curve. As clearly seen in Fig. 4.5 this improved valve shift significantly decreases the pressure oscillations, hence, this type of opening characteristic may therefore be sought after in the final valve design.

Note how the improved opening characteristic results in a very smooth pressure characteristic in the cylinder chamber. In addition the pressure at the switching manifold is seen to be very smooth, however the pressure change in the cylinder chamber is much slower for the improved valve opening. Hence, the avoidance of the pressure oscillations may be with a significant energy loss resulting.

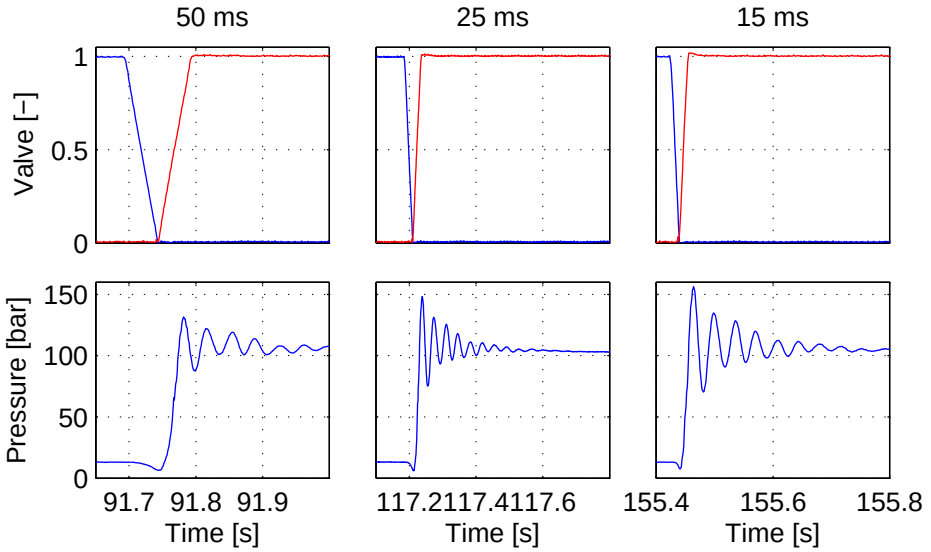

Figure 4.4: *Pressure oscillation in PTO cylinder chamber 3 during pressure shifts for constant PTO cylinder speed. Co-published in [43]*

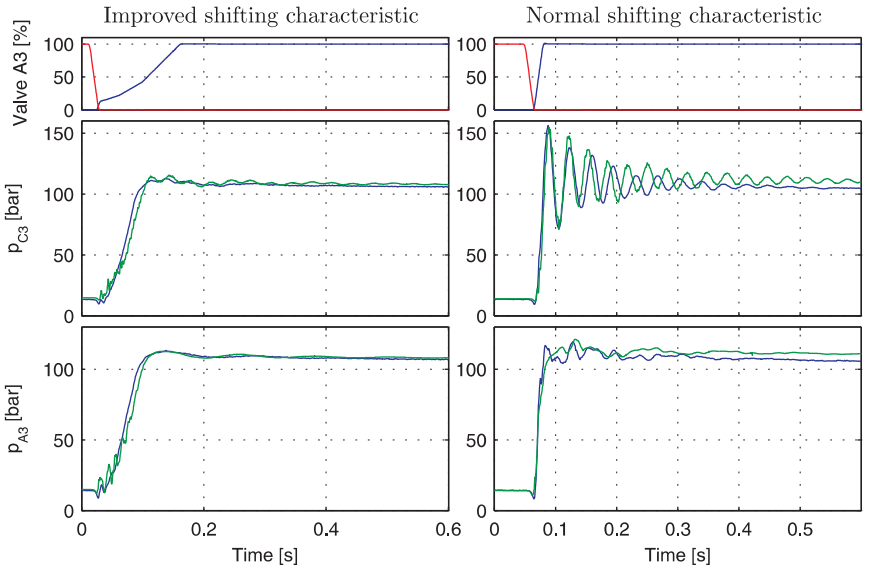

Figure 4.5: *Test results with improved and normal shifts. [43]*

Chapter 5

Conclusion and Future Work

In the appending papers [B] and [C] the energy output of the novel proposed discrete fluid power PTO-system showed to be highly depending on the system configuration in terms of either the multi-chamber cylinder design or number of common pressure lines. Especially addition of extra pressure lines resulted in an improvement in conversion efficiency.

The optimal configuration of the discrete fluid force system showed to be highly influenced by the working condition in [D], i.e. in terms of sea states. Hence, the sea condition at the installation site for the WEC dictates the optimal system configuration. A method for locating the optimal system configuration for a given installation site wave climate was therefore demonstrated in paper [D].

From the results given in section 2.5 a good energy production may be reached by utilising a two chamber symmetric cylinder and three pressure lines for which the pressure levels however should be controllable. Such a system configuration allows for utilisation of well proven cylinder technology with a simple construction. On the other hand the pressure line accumulators need to span a broader pressure range, resulting in an increasing accumulator capacity requirement.

Feasibility studies in paper [E] deemed utilisation of the bidirectional check valves in the manifold feasible, however with minor increase in experienced force steps. From the conceptual design of the bidirectional check valve it is clear that the pilot valve and pressure measurement need to be fast to ensure no unexpected valve opening during a cylinder chamber pressure crossing a pressure line [F]. On the other hand the pilot valve flow capability show much greater influence than the pilot switching time for the on/off valve designed in paper [G]. A conceptual multi-poppet valve design yielding an active valve switching time under 10 ms is given in paper [F] and [G] for a bidirectional check and on/off valve respectively.

The results of the above has lead to the suggested switching manifold presented in section 3.3 utilising the on/off valve for mid pressure connection and one directional check valve with on/off capabilities for low and high pressure connection. However detailed studies of the benefits and implications are still to come.

5.1 Future Work

As the system configuration analysis were held at a relative confined number of cylinder chambers and pressure line combinations due to extensive simulation time, an enhancement of the generic simulation model of the discrete fluid power force system is relevant. This to generate a power matrix for a broader spectrum of system configuration and larger number of sea states. With a power matrix covering more sea states scatter data from various installation sites may be represented yielding an approximation of the potential power production while utilising various system configuration. This permits an optimal choice of system configuration for each installation site from a power production point of view.

With the test-bench still in commissioning, verification of the system configuration optimisation have not yet been possible, however, it is desirable to test the average power output for various system configurations. With the current test set-up fully operational it is possible to test a system with a three chamber cylinder and two or three pressure lines for which the pressure level may be varied. Furthermore a two chamber cylinder may be emulated by operating two cylinder chamber in parallel. These tests are applicable in validating the investigation of the system configuration.

Based on the conceptual valve design and the preliminary switching tests final valve designs may be initiated. The geometrical placement of the multiple poppets, the pilot valve and the fluid connections are still open. Furthermore the geometry around the poppet seat is to be designed with low flow loss and wear while seeking to minimise the stiction forces in the seat area. The preliminary shifting tests however showed significant pressure oscillations with normal on/off valve opening and how these may be avoided with an improved valve opening characteristic. Consequently an analysis of the coherence between valve opening characteristics and pressure oscillations in fluid transmission lines may be conducted to clarify an advantageous valve opening characteristics. Depending on the results of this analysis, a novel on/off valve may be designed with an opening characteristics reducing provocation of pressure oscillations in the transmission lines. Further such a study may include an investigation on the added energy losses due to the improved valve switch.

Bibliography

[1] Alain Clement, Pat McCullen, António Falcão, Antonio Fiorentino, Fred Gardner, Karin Hammarlund, George Lemonis, Tony Lewis, Kim Nielsen, Simona Petroncini, M.-Teresa Pontes, Phillippe Schild, Bengt-Olov Sjoĺstroĺm, Hans Christian Sørensen, and Tom Thorpe. Wave energy in europe: current status and perspectives. *Renewable and Sustainable Energy Reviews*, 6:405–431, 2002.

[2] Pelamis Wave Power. *Pelamis P-750 Wave Energy Converter*. Pelamis Wave Power.

[3] WavePlane. www.waveplane.com/en. web. Viewed 03/2011.

[4] Wavedragon. www.wavedragon.net. web. Viewed 3/2011.

[5] J. Tedd, J.P. Kofoed, W. Knapp, E. Friis-Madsen, and H.C. Sørensen. Wave dragon, prototype wave power production. In *Proceedings of the 9th World Renewable Energy Congress: WREC IX, Florence, Italy, August 2006*, 2006.

[6] A. Sarmento, A. Brito-Melob, and F. Neumann. Results from sea trials in the owc european wave energy plant at pico, azores. In *Proceedings WREC IX*, 2006.

[7] Yukihisa Washio, Hiroyuki Osawa, and Teruhisa Ogata. The open sea tests of the offshore floating type wave power device "mighty whale" -characteristics of wave energy absorption and power generation. In *OCEANS, 2001. MTS/IEEE Conference and Exhibition (Volume:1)*, 2001.

[8] DEXAWAVE. www.dexawave.com.

[9] Pelamis Wave Power. www.pelamiswave.com/.

[10] Inc Ocean Power Technologies. www.oceanpowertechnologies.com. Viewed 03/2011.

[11] Wavebob Ltd. http://www.wavebob.com/. Viewed 03/2011.

[12] WaveStarA/S. www.wavestarenergy.com.

[13] Ross Henderson. Design, simulation, and testing of a novel hydraulic power take-off system for the pelamis wave energy converter. *Renewable Energy*, 31(2):271 – 283, 2006. PTO Concepts, PTO System, Hydraulics, Digital Hydraulics; Pelamis.

[14] António F. de O. Falcão. Modelling and control of oscillating-body wave energy converters with hydraulic power take-off and gas accumulator. *Ocean Engineering*, 34:2021–2032, 2007. WPEA, PTO System, PTO Concepts, Hydraulics; SEAREV.

[15] Yukio Kamizuru and Hubertus Murrenhoff. Improved control strategy for hydrostatic transmissions in wave power plants. In *The Twelfth Scandinavian International Conference on Fluid Power*, 2011.

[16] 2009.

[17] Rico H. Hansen, Torben O. Andersen, and Henrik C. Pedersen. Model based design of efficient power take-off systems for wave energy converters. In *Proc. The Twelfth Scandinavian International Conference on Fluid Power, SICFP'11*, Tampere, Finland, May 18-20 2011.

[18] Rico H. Hansen, Torben O. Andersen, and Henrik C. Pedersen. Analysis of discrete pressure level systems for wave energy converters. In *International Conference On Fluid Power And Mechatronics*, 2011.

[19] Huova Mikko, Laamanen Arto, and Linjama Matti. Energy efficiency of three-chamber cylinder with digital valve system. *International Journal of Fluid Power 11*, 3:15–22, 2010.

[20] Linjama Matti and Vilenius Matti. Digital hydraulics towards perfect valve technology. In *The Tenth Scandinavian International Conference on Fluid Power SICFP07*, 2007.

[21] Miika Paloniitty, Matti Karvonen, Matti Linjama, and Tuomo Tiainen. Laminated manifold for digital hhydraulic - principles, challenges and benifits. In *The Fifth Workshop on Digital Fluid Power*, 2012.

[22] M. Linjama, H-P. Vihtanen, A. Sipola, and M. Vilenius. Secondary controlled multi-chamber hydraulic cylinder. In *The 11th Scandinavian International Conference on Fluid Power, SICFP09, June 2-4, 2009, Linköping, Sweden*, 2009. WE3.1.3.1, ME1.1.1.

[23] Ari Sipola, Jussi Mäkitalo, and Jouni Hautamäki. The product callad norrdigi(tm). In *The Fifth Workshop on Digital Fluid Power*, 2012.

[24] Kogler Helmut, Scheidl Rudolf, Ehrentraut Michael, Guglielmino Emanuele, Semini Claudio, and Galdwell Darwin G. A compact hydraulic switching converter for robotic applications. In Johnston Dr. D. N. and Plummer Professor A. R., editors, *Fluid Power and Motion Control*, 2010.

[25] Mikkola Jaakko, Ahola Ville, Lauttamus Timo, Luomaranta Markku, Linjama Matti, and Vilenius Matti. Improving characteristics of on/off solenoid valves. In *The Tenth Scandinavian International Conference on Fluid Power SICFP07*, 2007.

[26] Andreas Plöckinger, Mikke Huova, and Rudolf Scheidl. Simulation and experimental results of pwm control for digitalhydraulics. In *The Fifth Workshop on Digital Fluid Power*, 2012.

[27] Bernhard Manhartsgruber. Digital fluid power applied to a pneumatic force control system. In *The 13th Mechatronics Forum International Conference, Vol 3*, 2012.

[28] R. Scheidl, B. Manhartsgruber, H. Kogler, B. Winkler, and M. Mairhofer. The hydraulic buck converter - concept and experimental results. In *6th International Fluid Power Conference, Dreden*, 2008.

[29] Reuter Johannes, Maerkl Sebastian, and Matthias Jaekle. Optimized control strategies for fast switching solenoid valves. *International Journal of Fluid Power*, 11, 2010.

[30] Lähteenmäki Teemu, Ijas Mika, and Mäkinen Esa. Characteristics of digital hydraulic pressure reducing valve. In Dr. D N Johnston, editor, *Fluid Power and Motion Control (FPMC 2010)*, 2010.

[31] Lee Yeong. Switching response improvement of a high speed onoff solenoid valve by using a 3 power source type valve driving circuit. In *IEEE*, 2006.

[32] Ilari Hyöty. Commercial high flow on/off-valves for digital hydraulics. In *The Fifth Workshop on Digital Fluid Power*, 2012.

[33] Andreas Ploeckinger, Bernd Winkler, and Rudolf Scheidl. Development and prototyping of a compact, fast 3/2 way switching valve with integrated onboard electronics. In *Proceedings of the 11th Scandinavian International Conference on Fluid Power*, 2009. ISBN 978-91-02-7393-588-3.

[34] Winkler Bernd and Scheidl Rudolf. Development of a fast seat type switching valve for big flow rates. In *The Tenth Scandinavian International Conference on Fluid Power SICFP07*, 2007.

[35] Winkler Bernd, Andreas Ploeckinger, and Scheidl Rudolf. A novel piloted fest switching multi poppet valve. *International Journal of Fluid Power*, 3:7–14, 2010.

[36] Rudolf Scheidl and Bernd Winkler. Optimization of a fast switching valve for big flow rates. In *Power Transmission and Motion Control - PTMC*, 2006.

[37] Sylwester Kudzma and Nigel Johnston. A high flow fast switching valve for digital hydraulic systems. In *The Fifth Workshop on Digital Fluid Power*, 2012.

[38] Morten Kramer, Laurent Marquis, and Peter. Frigaard. Performance evaluation of the wavestar prototype. In *Proceedings of the 9th European Wave and Tidal Conference, 9th ewtec 2011*, 2011.

[39] J. Falnes. *Ocean Waves and Oscillating Systems.* Cambridge University Press, 2002.

[40] Rico H. Hansen and Morten M. Kramer. Modelling and control of the wavestar prototype. In *EWTEC 2011*, 2011.

[41] Herbert E. Merritt. *Hydraulic Control System.* John Wiley & Sons, Inc., 1967.

[42] Rico Hjerm Hansen, Torben Ole Andersen, and Henrik C. Pedersen. Determining required valve performance for discrete control of pto cylinders for wave energy. In Nigel Johnston and Andrew R. Plummer, editors, *Proceedings of ASME Symposium on Fluid Power and Motion Control, FPMC 2012.* American Society of Mechanical Engineers, 2012.

[43] Rico Hjern Hansen. *Design and Control of the Power Take-Off System for a Wave Energy Converter with Multiple Absorbers.* PhD thesis, Faculty of Engineering and Science at Aalborg University, 2013.

Appendix A

Control of Full Scale PTO testbench

The fluid power system of the full scale PTO test-bench is modelled with traditional lumped parameter modelling. Components are modelled base on data sheet information. The model is coded in Matlab Simulink and tuned based on tests carried out on the physical system.

A.1 Modelling of the Testbench

The modelling of the wave simulator is divided in three parts. First the mechanical motion, which is computed based on the pressure force delivered from the wave and the PTO cylinder respectively on the combined mechanical structure consisting of the wave piston, the PTO piston and the sleigh connecting the two pistons. Secondly, the fluid power system of the wave simulator cylinder is modelled and lastly the modelling of the PTO-system is described. For later use the model is constructed such the PTO-system may easily be substituted with an other load system.

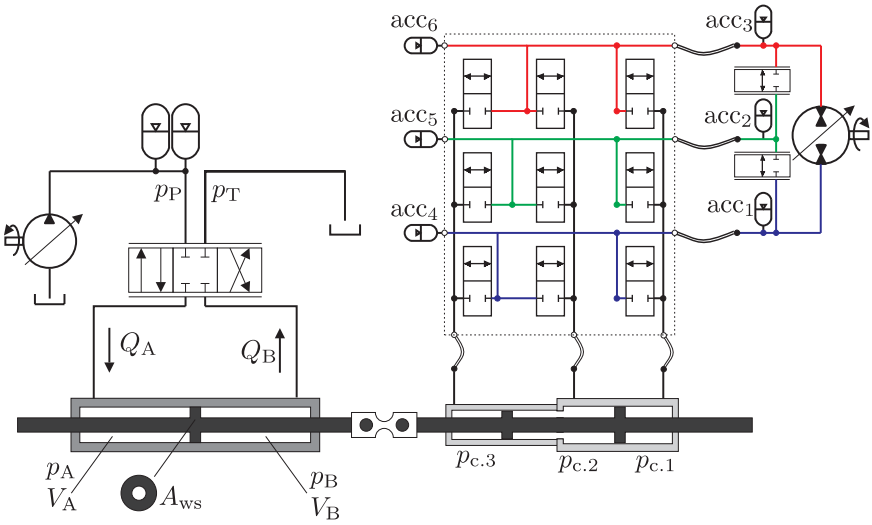

Figure A.1: *Sketch of the fluid power diagram, including the components included in the simulation model.*

A.1.1 Modelling of mechanical motion

The sleigh and the two cylinder pistons are modelled as a rigid body for which the motion is modelled using Newton's second law of motion.

$$\begin{aligned}\ddot{x}_{\mathrm{ws}}(m_{\mathrm{ws}}+m_{\mathrm{c}}+m_{\mathrm{s}}) = \; & A_{\mathrm{ws}}\,(p_{\mathrm{A}}-p_{\mathrm{B}}) \\ & +(A_1p_1-A_2P_2-Ap_3-A_4p_4) \\ & -F_{\mathrm{fric}}(\dot{x}_{\mathrm{ws}})\end{aligned} \tag{A.1}$$

The friction model includes coulomb and viscous friction. A hyperbolic tangent function is utilised to overcome numerical problems due to the discontinuity.

$$F_{\mathrm{fric}}(\dot{x}_{\mathrm{ws}}) = -\tanh\left(\frac{\dot{x}_{\mathrm{ws}}}{\gamma_{\mathrm{c}}}\right)\left(F_{\mathrm{c}1}+F_{\mathrm{c}2}e^{-|\dot{x}_{\mathrm{ws}}|}\right)-B_{\mathrm{v}}\dot{x}_{\mathrm{ws}} \tag{A.2}$$

Here γ_{c} is used to control the slope of the friction curve when crossing zero velocity.

A.1.2 Wave Simulator

The wave simulator consists of a symmetric cylinder connected to supply through two servo valves in parallel, a Parker D111FPE01 and a Moog D633 100L/min@70bar. The cylinder dimensions are 250 x 180 x 3000 mm. The power supply consists of two variable displacement pumps a 125cc and a 250cc respectively, running at 1500 RPM nominal. The supply pressure line is fitted with two 28L accumulators close to the servo valves, this to enable emulation of peak wave conditions.

The pressure build up in the two cylinder chambers are model with use of the flow continuity equation [41]:

$$\Sigma Q_{\mathrm{in}}-\Sigma Q_{\mathrm{out}} = \frac{dV}{dt}+\frac{V}{\beta}\frac{dp}{dt} \tag{A.3}$$

Hence, for the wave cylinder the chamber pressures are modelled as:

$$\dot{p}_{\mathrm{A}} = \frac{\beta_{\mathrm{eff}}(p_{\mathrm{A}})}{V_{\mathrm{A}}(x_{\mathrm{ws}})}\left(Q_{\mathrm{A}}-\dot{x}_{\mathrm{ws}}A_{\mathrm{ws}}\right) \tag{A.4}$$

$$\dot{p}_{\mathrm{B}} = \frac{\beta_{\mathrm{eff}}(p_{\mathrm{B}})}{V_{\mathrm{B}}(x_{\mathrm{ws}})}\left(Q_{\mathrm{B}}+\dot{x}_{\mathrm{ws}}A_{\mathrm{ws}}\right) \tag{A.5}$$

Where the volume of the connecting hoses are included in the dead volume of each chamber and the effective bulk modulus is modelled as:

$$\beta_{\mathrm{eff}}(p) = \frac{1}{\frac{1}{\beta_{\mathrm{oil}}}+\frac{\varepsilon_{\mathrm{air}}(p)}{\beta_{\mathrm{air}}}} \tag{A.6}$$

Where the dissolved air in the oil is pressure dependent and modelled as:

$$\varepsilon_{\mathrm{air}}(p) = \left(\frac{p_0\varepsilon_{\mathrm{air},0}(p)}{p}\right)^{\frac{1}{\kappa}} \tag{A.7}$$

Where $\varepsilon_{\mathrm{air},0}$ is the air content at atmospheric pressure p_0. In this model the volumetric air content is set to 1% at atmospheric pressure and β_{eff} is limited to 10000 bar.

The volume flow through the servo valves are modelled utilising the orifice equation [41]:

$$Q = C_{\mathrm{d}} A_0(x_{\mathrm{v}}) \sqrt{\frac{2}{\rho}(p_1 - p_2)} \tag{A.8}$$

With $A_0(x_{\mathrm{v}})$ describing the opening area of the valve as a function of the valve spool position. The Moog D633 has a full circle zero lap spool which imply the area function to be linear. Hence, the flows into the two cylinder chambers through the Moog valve are modelled as:

$$Q_{\mathrm{A,M}} = \begin{cases} k_{\mathrm{v}} \bar{x}_{\mathrm{v,M}} \sqrt{|p_{\mathrm{P}} - p_{\mathrm{A}}|}\mathrm{sign}(p_{\mathrm{P}} - p_{\mathrm{A}}) \ , \bar{x}_{\mathrm{v,M}} \geq 0 \\ k_{\mathrm{v}} \bar{x}_{\mathrm{v,M}} \sqrt{|p_{\mathrm{A}} - P_{\mathrm{T}}|}\mathrm{sign}(p_{\mathrm{A}} - P_{\mathrm{T}}) \ , \bar{x}_{\mathrm{v,M}} < 0 \end{cases} \tag{A.9}$$

$$Q_{\mathrm{B,M}} = \begin{cases} -k_{\mathrm{v}} \bar{x}_{\mathrm{v,M}} \sqrt{|p_{\mathrm{B}} - P_{\mathrm{T}}|}\mathrm{sign}(p_{\mathrm{B}} - P_{\mathrm{T}}) \ , \bar{x}_{\mathrm{v,M}} \geq 0 \\ -k_{\mathrm{v}} \bar{x}_{\mathrm{v,M}} \sqrt{|p_{\mathrm{P}} - p_{\mathrm{B}}|}\mathrm{sign}(p_{\mathrm{P}} - p_{\mathrm{B}}) \ , \bar{x}_{\mathrm{v,M}} < 0 \end{cases} \tag{A.10}$$

With the valve coefficient $k_{\mathrm{v}} = \frac{Q_{\mathrm{nom}}}{\sqrt{\Delta p_{\mathrm{nom}}}}$ describing the flow characteristic for the valve.

The opening area of the Parker valve is given in Fig. A.2. It is seen that the Parker valve has an overlap spool with non-linear characteristic outside the lap area.

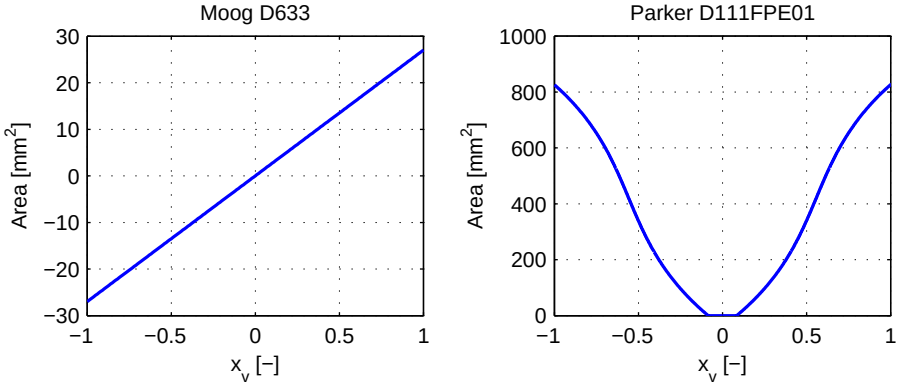

Figure A.2: *(a) Opening area for Moog valve as a function of nominal spool position. (b) Opening area for Parker valve as a function of nominal spool position.*

Implementation of this area characteristic is conducted by constructing a Lookup table in Simulink. However, the volume flows through the Parker valve are modelled as;

$$Q_{\mathrm{A,P}} = \begin{cases} C_{\mathrm{d}} A_{\mathrm{d}}(\bar{x}_{\mathrm{v,P}}) \sqrt{\frac{2}{\rho}|p_{\mathrm{P}} - p_{\mathrm{A}}|}\mathrm{sign}(p_{\mathrm{P}} - p_{\mathrm{A}}) \ , \bar{x}_{\mathrm{v,P}} \geq 0 \\ -C_{\mathrm{d}} A_{\mathrm{d}}(\bar{x}_{\mathrm{v,P}}) \sqrt{\frac{2}{\rho}|p_{\mathrm{A}} - P_{\mathrm{T}}|}\mathrm{sign}(p_{\mathrm{A}} - P_{\mathrm{T}}) \ , \bar{x}_{\mathrm{v,P}} < 0 \end{cases} \tag{A.11}$$

$$Q_{\mathrm{B,M}} = \begin{cases} -C_{\mathrm{d}} A_{\mathrm{d}}(\bar{x}_{\mathrm{v,P}}) \sqrt{\frac{2}{\rho}|p_{\mathrm{B}} - P_{\mathrm{T}}|}\mathrm{sign}(p_{\mathrm{B}} - P_{\mathrm{T}}) \ , \bar{x}_{\mathrm{v,P}} \geq 0 \\ C_{\mathrm{d}} A_{\mathrm{d}}(\bar{x}_{\mathrm{v,P}}) \sqrt{\frac{2}{\rho}|p_{\mathrm{P}} - p_{\mathrm{B}}|}\mathrm{sign}(p_{\mathrm{P}} - p_{\mathrm{B}}) \ , \bar{x}_{\mathrm{v,P}} < 0 \end{cases} \tag{A.12}$$

Here the discharge coefficient and fluid density are given as C_d and ρ respectively.

The dynamics of the servo valves are modelled based on data sheet information. Leading to a second order linear model for the Moog valve given as:

$$\frac{\bar{x}_{\mathrm{v,M}}(s)}{\bar{x}_{\mathrm{v,ref}}(s)} = \frac{\omega_{\mathrm{n.M}}^2}{s^2 + 2\zeta_\mathrm{M}\omega_{\mathrm{n.M}}s + \omega_{\mathrm{n.M}}^2} \tag{A.13}$$

Where the undampend eigenfrequency and the damping are set to $\omega_{\mathrm{n.M}} = 2\pi\, 40\ \mathrm{s}^{-1}$ and $\zeta_\mathrm{M} = 0.8$ respectively. The dynamic of the Parker valve is modelled with a linear third order system in combination with a non-linear term to account for velocity saturation. The data sheet bode and the simulation model bode plot is seen in Fig. A.3.

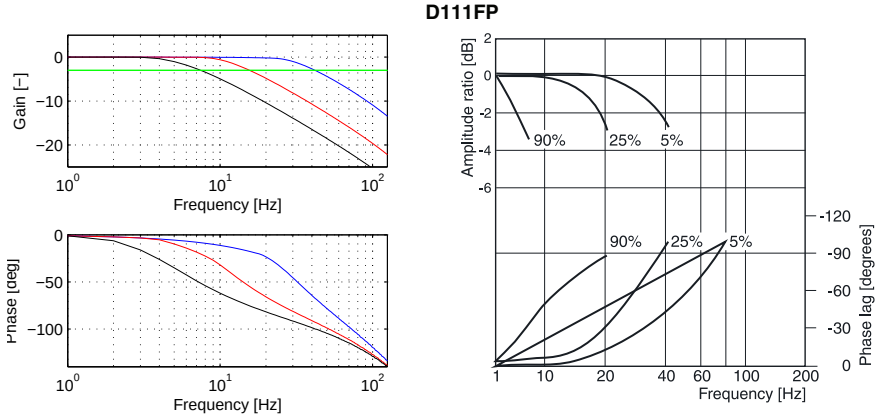

(a) (b)

Figure A.3: *Data sheet bode plot compared with simulation model bode.*

A.1.3 PTO-System Model

The discrete fluid power force system consists of a multi-chamber cylinder with 5 chamber (operated as 3 chamber) connected to three common pressure lines through a switching manifold composed of nine on/off valves and additional safety valves. The on/off valves deployed in the switching manifold are of the Parker TDP32 valve type. Which is a 2/2 proportional valve.

The pressure build up in the cylinder chambers are modelled with the flow continuity equation leading to:

$$\dot{p}_i = \frac{\beta_\mathrm{eff}(p_i)}{V_i(x_\mathrm{c})}\left(Q_i - \dot{V}_i\right) \tag{A.14}$$

Where $\dot{V}_i = \dot{x}_\mathrm{c}A_i$, with the piston area including the sign of the force direction for the current area. The effective bulk modulus model utilised was given in eq. (A.6).

The flow through the on/off valves are modelled with the orifice equation, hence the flow into the i'th chamber from the j'th pressure line is given as:

$$Q_{i,j} = k_{\mathrm{vTDP}}(\bar{x}_{\mathrm{v}.i,j})\sqrt{|p_j - p_i|}\mathrm{sign}(p_j - p_i) \tag{A.15}$$

This implies that the flow into the i'th cylinder chamber is:

$$Q_i = \sum_{j=1}^{m} Q_{i,j} \tag{A.16}$$

Furtheremore the flow into the j'th pressure line is given as:

$$Q_j = \sum_{i=1}^{n} -Q_{i,j} \tag{A.17}$$

The dynamics of the TDP valves are modelled as a linear second order system, with an undampend eignen frequency and damping of $\omega_{\mathrm{n}} = 95\mathrm{Hz}$ and $\zeta = 0.7$ respectively. This is implemented with a transfer function:

$$\frac{x_{\mathrm{v}}(s)}{x_{\mathrm{v,ref}}(s)} = \frac{\omega_{\mathrm{n}}^2}{s^2 + 2\zeta\omega_{\mathrm{n}}s + \omega_{\mathrm{n}}^2} \tag{A.18}$$

In the PTO-system transmission line models are imposed due to expected pressure oscillations in the hoses due to the fast opening and closing of the on/off valves connecting the cylinder chambers to the common pressure lines. The transmission line model utilised is a lumped parameter model where the transmission line is split into a fixed number of elements for which a pressure, a flow and a friction pressure is calculated, see Fig. A.4.

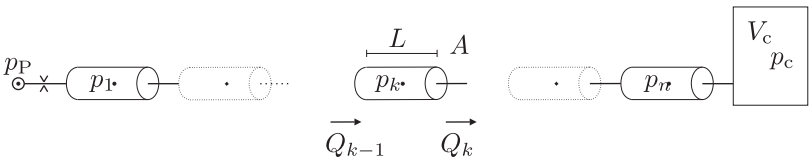

Figure A.4: *Illustration for the transmission line model.*

The acceleration of the fluid is calculated based on Newton's second law:

$$\ddot{x} = \frac{A\left(p_{\mathrm{in}} - p_{\mathrm{out}} - p_{\mathrm{fric}}\right)}{m} \tag{A.19}$$

Exploiting that the mass may be written as volume times density and that acceleration times flow area is the volume flow acceleration gives:

$$\dot{Q} = \frac{A\left(p_{\mathrm{in}} - p_{\mathrm{out}} - p_{\mathrm{fric}}\right)}{L\rho} \tag{A.20}$$

With L as the length of each line segment and A as the flow area. The pressure in each line segment is modelled with the flow continuity equation:

$$\dot{p} = \frac{\beta_{\mathrm{eff}}(p)}{AL}\left(Q_{\mathrm{in}} - Q_{\mathrm{out}}\right) \tag{A.21}$$

The bulk modulus follows the model in (A.6), however the limit is set to 7000 bar for hoses and 15000 bar for pipes. The friction pressure is modelled as the pressure loss due to a given flow through fluid power hose [41]:

$$\begin{array}{ll} \frac{\Delta p}{L} = \frac{128\mu}{\pi d^4} Q & \text{for laminar flow} \\ \frac{\Delta p}{L} = 0.242 \frac{\mu^{0.25} \rho^{0.75}}{d^{4.75}} Q^{1.75} & \text{for turbulent flow} \end{array} \tag{A.22}$$

The transition between the laminar and turbulent regime is implemented with the tangent hyperbolic function. Hence, a factor is multiplied on each of the pressure losses such that;

$$\frac{\Delta p}{L} = \frac{\Delta p_{\mathrm{L}}}{L} \frac{1 - \tanh\left(\frac{Re-2150}{50}\right)}{2} + \frac{\Delta p_{\mathrm{T}}}{L} \frac{\tanh\left(\frac{Re-2150}{50}\right) + 1}{2} \tag{A.23}$$

This is illustrated in Fig. A.5 for a hydraulic line with diameter 10 mm, where the blue line indicates the loss in a laminar regime whereas the red line is for the turbulent flow regime. The pressure loss used in the model is given by the black line.

The difference in the model for a hose and a pipe is that the bulk modulus of the fluid in the hoses is limited to 7000 bar which for the pipe model is limited to 15000 bar. Hence, the stiffness of the hoses and pipes are indirectly included in the effective bulk modulus. The length and diameter of each hose and pipe are given in table A.1 along with the friction factor for the fittings connecting the hose/pipe.

Pressure losses in fittings connecting hoses, tubes and valve blocks are model as:

$$\Delta p = \frac{\xi \rho_{\mathrm{fluid}} v_{\mathrm{hose}}^2}{2} \tag{A.24}$$

Where v_{hose} is the mean velocity of fluid flow through the fitting with the loss coefficient ξ, which is taken from table information.

	L[m]	d[in]	n	ξ_1	ξ_2
H_1	4.35	1.50	4	0.70/0.45	0.45
H_2	1.35	1.25	2	0.35	-
P_2	1.2	1.50	2	0.35	0.35
H_{3a}	1.69	1.25	3	0.45/0.35	0.35
P_{3a}	1.50	1.50	2	0.35	0.35/1.2
H_{3b}	1.49	1.27	3	0.45	0.35
P_{3b}	1.32	1.5	2	-	0.35/0.35
H_{idle}	2.70	1.25	-	-	
H_{L}	4.50	1.5	5	0.70/1.30	0.35
H_{M}	4.50	1.5	5	0.70/1.30	0.35
H_{H}	4.50	1.5	5	0.70/1.30	0.35

Table A.1: *Data for the hose in the PTO system.*

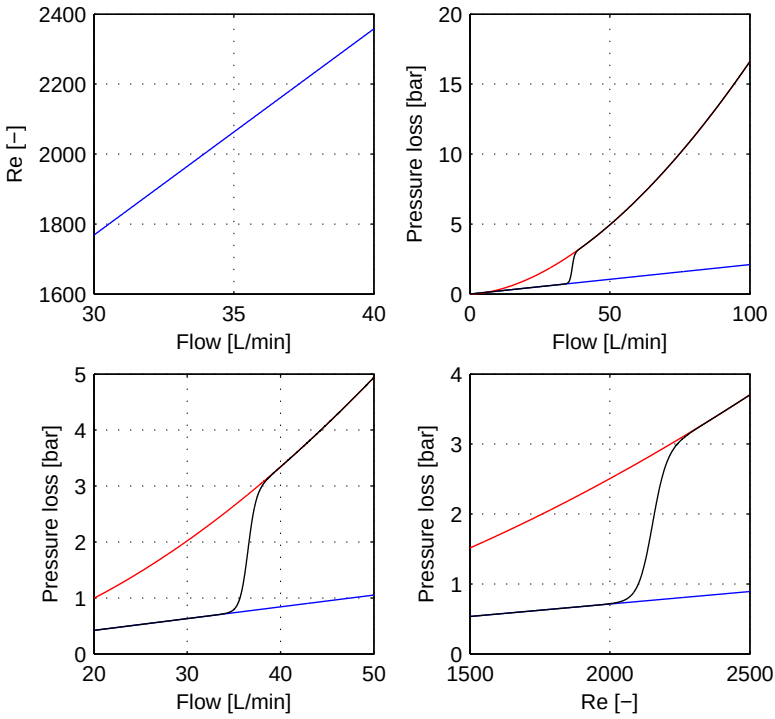

Figure A.5: *Friction model for transmission line. Upper left; Reynolds number based on flow. Upper right and lower left; Pressure loss based on flow. Lower right; Pressure loss based on Reynolds number.*

Accumulator models

The accumulator model utilised includes energy dissipation as heat diffusion from the gas through the wall to the surroundings. The volume of the gas is modelled temperature dependent as:

$$V_{\mathrm{g}} = \frac{p_{\mathrm{acc},0} V_{\mathrm{g},0}}{T_0} \frac{T}{p_{\mathrm{acc}}} \tag{A.25}$$

The gas volume gradient of the fluid is found based on the oil flow into the accumulator and the pressure gradient and the hydraulic capacitance.

$$\dot{V}_{\mathrm{g}} = \dot{p}_{\mathrm{acc}} \frac{V_{\mathrm{oil}}}{\beta_{\mathrm{v}}} - Q_{\mathrm{in}} \tag{A.26}$$

The volume of fluid in the accumulator is given as the difference in initial and gas volume.

$$V_{\mathrm{oil}} = (V_{\mathrm{acc}} + V_0) - V_{\mathrm{g}} \tag{A.27}$$

Here V_0 is the dead volume in the accumulator connection block. The temperature of the gas in the accumulator is found as;

$$\dot{T} = \frac{1}{\tau}(T_{\text{wall}} - T) - R\frac{T}{c_{\text{v}} V_{\text{g}}}\dot{V}_{\text{g}} \tag{A.28}$$

Where the first term is from heat diffusion through the wall and the second term is related to the ideal gas law. The pressure gradient in the fluid is given as;

$$\dot{p}_{\text{acc}} = \frac{Q_{\text{in}} + \frac{1}{1+\frac{R}{c_{\text{v}}}}\frac{V_{\text{g}}}{T}\frac{1}{\tau}(T_{\text{wall}} - T)}{\frac{V_{\text{oil}}}{\beta_{\text{v}}} + \frac{1}{1+\frac{R}{c_{\text{v}}}}\frac{V_{\text{g}}}{p_{\text{acc}}}} \tag{A.29}$$

Hence, it is seen that the oil flow into the accumulator is causing a pressure and temperature increase. The capacitance is here given in a fluid and gas part (first and second term in the denominator respectively). The heat exchange time constant, inlet diameter and wall temperature is set to $\tau = 18.95$, $D_{\text{inlet}} = 38.1$ mm and $T_{\text{wall}} = 50°\text{C}$ respectively for all accumulators. The size and pre-charge pressure of the accumulators are given in table A.2.

	V [L]	p_0 [bar]
acc_1	25.0	14
acc_2	25.0	50
acc_3	25.0	94
acc_4	3.8	14
acc_5	3.8	50
acc_6	3.8	94

Table A.2: *Data for the accumulators in the PTO-system, see Fig.A.1.*

A.2 Model Based Controller Design

A controller is designed based on the system model derived above. With a good system model at hand a controller cancelling most non-linearities and external load may be designed. However, for thus a controller to work properly the model must be relative precise and state measurements are often required.

A.2.1 Feedback Linearisation Controller

The controller type investigated is an input-output feedback linearisation controller, developed based on the system model on state space form:

$$\begin{aligned} \dot{\mathbf{x}}(t) &= \mathbf{f}(\mathbf{x}(t), u(t), t) \\ y(t) &= g(\mathbf{x}(t)) \end{aligned} \tag{A.30}$$

Where $\mathbf{x}(t)$ is the state vector, $u(t)$ is the input and $y(t)$ is the output. The system model is contained within the equations given in $\mathbf{f}(\mathbf{x}(t), u(t), t)$. Note that the system model is given as a single input single output model. For the given system the input

is the spool reference for the servo valve and the output is either the piston position or velocity depending on the objective for the controller to be designed. As for most systems the output function $g(\cdot)$ does not explicitly contain the input $u(t)$ for the current system. Therefore the output $y(t)$ is differentiated as many times as required until the input $u(t)$ explicitly appears in the derivatives of $g(\cdot)$.

With the input directly contained in the function,

$$y^{(n)} = G(\mathbf{x}(t), u(t), t) \tag{A.31}$$

a input $u(t)$ is chosen such that:

$$y^{(n)} = v(t) \tag{A.32}$$

Hence, $u(t) = H(\mathbf{x}(t), v(t), t)$ with a new "controller" input v which as clearly seen directly controls the n'th derivative of the output y. The task in the controller design thereby becomes; to identify the linearisation term $H(\mathbf{x}(t), v(t), t)$ which cancels the system dynamics (linear and non-linear) and identify the new control input $v(t)$ which leads to a desired system behaviour. A schematic overview of the feedback linearisation controller developed is given in Fig. A.6.

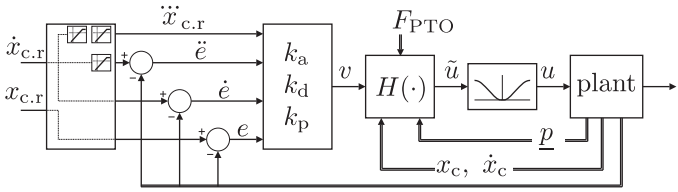

Figure A.6: *Illustration of the controller structure. The PTO force is seen as an external measured load.*

Here it is seen how measurements of the piston position, velocity and acceleration along with the cylinder chamber pressures are required in the feedback loops. The inner loop encountering $H(\cdot)$ is the linearisation term whereas the outer loop consists of a pole placement like linear controller.

Velocity control
Using the original state space model, however, with the assumption of the valve spool position to be the control input the model reduces to:

$$\begin{aligned}
\dot{x}_1 &= x_2 \\
\dot{x}_2 &= \tfrac{1}{M}\left(A_{\mathrm{ws}}x_3 - A_{\mathrm{ws}}x_4 - F_{\mathrm{Fric}}(x_2) + F_{\mathrm{PTO}}(t)\right) \\
\dot{x}_3 &= \tfrac{\beta_{\mathrm{eff}}(x_3)}{V_{\mathrm{A}0}+A_{\mathrm{ws}}x_1}\left(C_{\mathrm{d}}A_{\mathrm{d}}(u)\sqrt{\tfrac{2}{\rho}(p_{\mathrm{P}} - x_3)} - A_{\mathrm{ws}}x_2\right) \\
\dot{x}_4 &= \tfrac{\beta_{\mathrm{eff}}(x_4)}{V_{\mathrm{B}0}-A_{\mathrm{ws}}x_1}\left(A_{\mathrm{ws}}x_2 - C_{\mathrm{d}}A_{\mathrm{d}}(u)\sqrt{\tfrac{2}{\rho}(x_4 - p_{\mathrm{T}})}\right)
\end{aligned} \tag{A.33}$$

$$y = x_2$$

From the model the feedback linearisation input is obtained by taking the derivative of the output until the control input u appears in the equation:

$$\dot{y} = \frac{1}{M}\left(A_{\mathrm{ws}}x_3 - A_{\mathrm{ws}}x_4 - F_{\mathrm{Fric}}(x_2) + F_{\mathrm{PTO}}(t)\right) \tag{A.34}$$

$$\ddot{y} = \frac{1}{M}\left(A_{\mathrm{ws}}\dot{x}_3 - A_{\mathrm{ws}}\dot{x}_4 - \dot{F}_{\mathrm{Fric}}(x_2) + \dot{F}_{\mathrm{PTO}}(t)\right) \tag{A.35}$$

$$\begin{aligned}\ddot{y} =& \frac{A_{\mathrm{ws}}C_{\mathrm{d}}}{M}A_{\mathrm{d}}(u)\left(\frac{\beta_{\mathrm{A}}\sqrt{\frac{2}{\rho}(p_{\mathrm{P}} - x_3)}}{V_{\mathrm{A}}} + \frac{\beta_{\mathrm{B}}\sqrt{\frac{2}{\rho}(x_4 - p_{\mathrm{T}})}}{V_{\mathrm{B}}}\right) \\ &- \frac{A_{\mathrm{ws}}^2}{M}\left(\frac{\beta_{\mathrm{A}}}{V_{\mathrm{A}}} + \frac{\beta_{\mathrm{B}}}{V_{\mathrm{B}}}\right)x_2 \\ &- \frac{1}{M}\dot{F}_{\mathrm{Fric}}(x_2) + \frac{1}{M}\dot{F}_{\mathrm{PTO}}(t)\end{aligned} \tag{A.36}$$

To account for the area function of the servo valves the control input is defined as:

$$u = A_{\mathrm{d}}^{-1}(\tilde{u}) \tag{A.37}$$

This yields $A_{\mathrm{d}}(u) = \tilde{u}$ simplifying the derivation of the linearisation term. One may see that choosing $\tilde{u}$ as,

$$\begin{aligned}\tilde{u} =& \frac{M}{A_{\mathrm{ws}}C_{\mathrm{d}}\left(\frac{\beta_{\mathrm{A}}\sqrt{\frac{2}{\rho}(p_{\mathrm{P}} - x_3)}}{V_{\mathrm{A}}} + \frac{\beta_{\mathrm{B}}\sqrt{\frac{2}{\rho}(x_4 - p_{\mathrm{T}})}}{V_{\mathrm{B}}}\right)}(v \\ &+ \frac{A_{\mathrm{ws}}^2}{M}\left(\frac{\beta_{\mathrm{A}}}{V_{\mathrm{A}}} + \frac{\beta_{\mathrm{B}}}{V_{\mathrm{B}}}\right)x_2 \\ &+ \frac{1}{M}\dot{F}_{\mathrm{Fric}}(x_2) - \frac{1}{M}\dot{F}_{\mathrm{PTO}}(t)\Big)\end{aligned} \tag{A.38}$$

will yield the second derivative of the output, $\ddot{y}$ to be equal to the new input term v. Hence, the jerk in the system, is given as:

$$\ddot{y} = v \tag{A.39}$$

The new controller input v is set to:

$$v = \ddot{y}_{\mathrm{d}} + k_{\mathrm{a}}(\dot{y}_{\mathrm{d}} - \dot{y}) + k_{\mathrm{d}}(y_{\mathrm{d}} - y) \tag{A.40}$$

Recalling that y is the system output and noticing y_{d} as the reference request for the system output, Eq. (A.40) may be rewritten as an ordinary differential equation describing the dynamics of the error $e = y_{\mathrm{d}} - y$;

$$0 = \ddot{e} + k_{\mathrm{a}}\dot{e} + k_{\mathrm{d}}e \tag{A.41}$$

Recognising the error dynamics as a ordinary second order differential equation and recalling the output y as the velocity, the velocity error is exponential stable if the coefficients $k_{\mathrm{a}},\ k_{\mathrm{d}} > 0$:

$$e,\ \dot{e} \to 0\ ,\ t \to \infty \tag{A.42}$$

Hence, the velocity error and the acceleration error goes to zero as time goes to infinity.

Position control
A position controller may be designed based on the derivation of the velocity controller. Defining the position as output of the model, $y = x_1$, one will recognise the first derivative to be equal to the output in the velocity control problem. Hence, for the position controller the control law is given as:

$$\begin{aligned}\tilde{u} = & \frac{M}{A_{\mathrm{ws}} C_{\mathrm{d}} \left(\frac{\beta_{\mathrm{A}} \sqrt{\frac{2}{\rho}(p_{\mathrm{P}} - x_3)}}{V_{\mathrm{A}}} + \frac{\beta_{\mathrm{B}} \sqrt{\frac{2}{\rho}(x_4 - p_{\mathrm{T}})}}{V_{\mathrm{B}}} \right)} (v \\ & + \frac{A_{\mathrm{ws}}^2}{M} \left(\frac{\beta_{\mathrm{A}}}{V_{\mathrm{A}}} + \frac{\beta_{\mathrm{B}}}{V_{\mathrm{B}}} \right) x_2 \\ & + \frac{1}{M} \dot{F}_{\mathrm{Fric}}(x_2) - \frac{1}{M} \dot{F}_{\mathrm{PTO}}(t) \Big)\end{aligned} \tag{A.43}$$

$$\dddot{y} = v \tag{A.44}$$

$$v = \dddot{y}_{\mathrm{d}} + k_{\mathrm{a}}(\ddot{y}_{\mathrm{d}} - \ddot{y}) + k_{\mathrm{d}}(\dot{y}_{\mathrm{d}} - \dot{y}) + k_{\mathrm{a}}(y_{\mathrm{d}} - y) \tag{A.45}$$

Now, note that the output y is the piston position and that the position error dynamic is given as a third order ordinary differential equation:

$$0 = \dddot{e} + k_{\mathrm{a}}\ddot{e} + k_{\mathrm{d}}\dot{e} + k_{\mathrm{p}}e \tag{A.46}$$

To guarantee a stable behaviour of the position error the coefficients must obey:

$$\frac{k_{\mathrm{a}}k_{\mathrm{d}} - k_{\mathrm{p}}}{k_{\mathrm{a}}}, \; k_{\mathrm{p}} > 0 \tag{A.47}$$

Which is derived from the Routh-Hurwitz criterion.

A.2.2 Controller test

Simulation results with the designed feedback linearisation controller utilised are given in Fig. A.7. A sinus wave is applied as position reference while imposing a discrete force step every 2.5 s. The controller is tested with the model assuming no PTO force and friction, and with the model assuming no PTO force, and lastly as shown in the controller design.

Measurements of piston velocity and position is seen in Fig. A.8 for the test-bench when imposing the feedback linearisation controller.

It is clearly seen that unwanted velocity oscillation are present even though the position measurements might look smooth. The velocity oscillations may partly be imposed due to controller input, this is due to the fact that the control law utilises the acceleration as feedback. The acceleration feedback is currently performed by differentiation of the velocity measurements and as evident from any practically engineering experience this may lead to problems. Hence, to enable control by feedback linearisation an accelerometer is to be installed or other options as state estimation may be imposed.

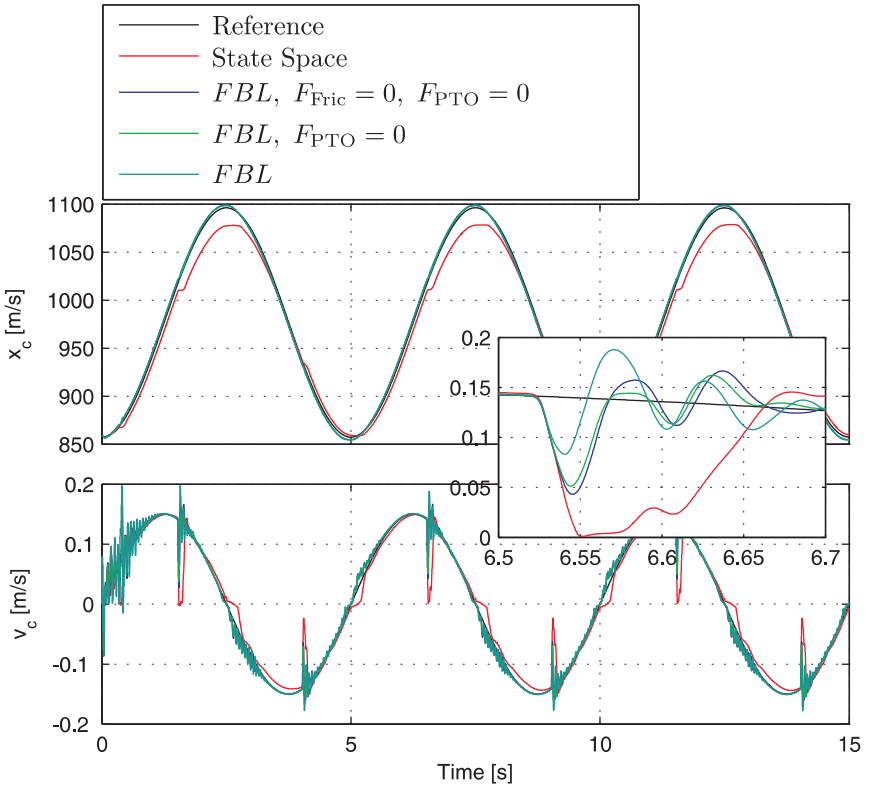

Figure A.7: *Piston velocity and position simulation results while utilising feedback linearisation controller.*

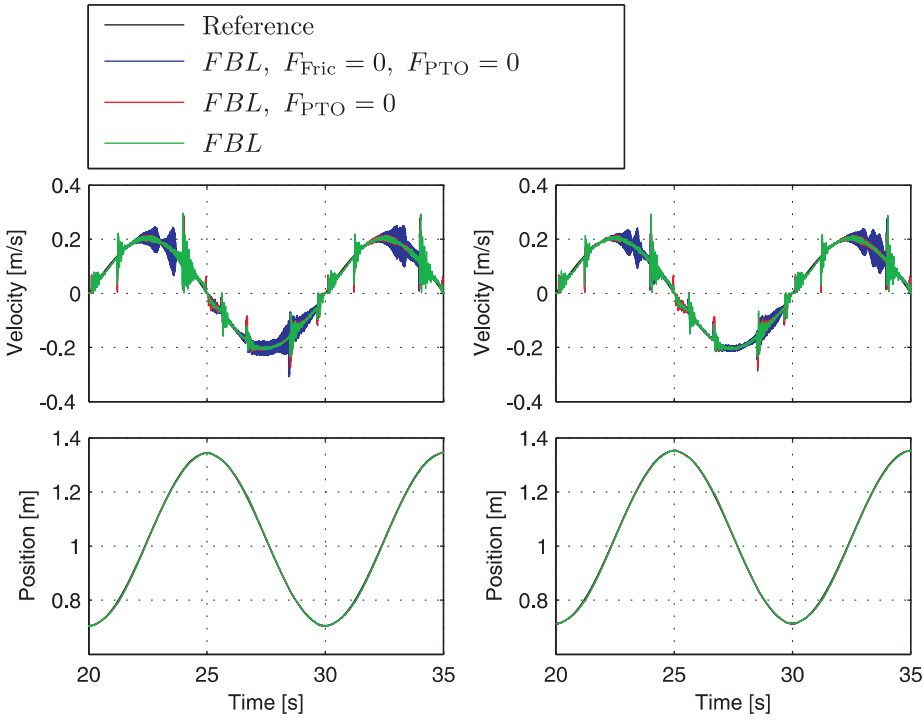

Figure A.8: *Piston velocity and position measurements while utilising feedback linearisation controller.*